

Louisiana Tech University

Louisiana Tech Digital Commons

Doctoral Dissertations

Graduate School

Spring 5-2020

Stress Analysis of Operating Gas Pipeline Installed by Horizontal Directional Drilling and Pullback Force Prediction During Installation

Hongfang Lu

Follow this and additional works at: <https://digitalcommons.latech.edu/dissertations>

**STRESS ANALYSIS OF OPERATING GAS PIPELINE INSTALLED
BY HORIZONTAL DIRECTIONAL DRILLING AND PULLBACK
FORCE PREDICTION DURING INSTALLATION**

by

Hongfang Lu, B.S., M.S.

A Dissertation Presented in Partial Fulfillment
of the Requirements of the Degree
Doctor of Philosophy

COLLEGE OF ENGINEERING AND SCIENCE
LOUISIANA TECH UNIVERSITY

May 2020

LOUISIANA TECH UNIVERSITY

GRADUATE SCHOOL

November 7, 2019

Date of dissertation defense

We hereby recommend that the dissertation prepared by

Hongfang Lu

entitled **STRESS ANALYSIS OF OPERATING GAS PIPELINE INSTALLED
BY HORIZONTAL DIRECTIONAL DRILLING AND PULLBACK FORCE
PREDICTION DURING INSTALLATION**

be accepted in partial fulfillment of the requirements for the degree of

Doctor of Philosophy in Engineering, Materials & Infrastructure Systems Conc.



David (Thomas) Iseley, Supervisor of Dissertation Research

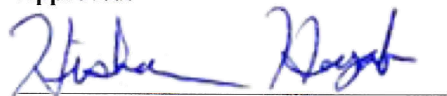


Xingran (Jay) Wang,
Head of Engineering

Members of the Doctoral Committee:

David (Thomas) Iseley
Arun Jaganathan
Xingran (Jay) Wang
John Matthews
Shaurav Alam

Approved:



Hisham Hegab
Dean of Engineering & Science

Approved:



Ramu Ramachandran
Dean of the Graduate School

ABSTRACT

With the development of the natural gas industry, the demand for pipeline construction has also increased. In the context of advocating green construction, horizontal directional drilling (HDD), as one of the most widely utilized trenchless methods for pipeline installation, has received extensive attention in industry and academia in recent years. The safety of natural gas pipeline is very important in the process of construction and operation. It is necessary to conduct in-depth study on the safety of the pipeline installed by HDD method.

In this dissertation, motivated by the following considerations, two aspects of HDD installation are studied. First, through the literature review, one issue that has not received much attention so far is the presence of stress problem during the operation condition. Thus, two chapters (Chapters 3 and 4) in this dissertation are related to the pipe stress analysis during the operation. Regarding this problem, two cases are considered according to the fluidity of drilling fluid. The more dangerous situation is determined by comparing the pipeline stress in the two working conditions. The stress of pipeline installed by HDD method and open-cut method is also compared, and it indicates that the stress of pipeline installed by HDD method is lower. Moreover, through the analysis of influence factors and stress sensitivity, the influence degree of different parameters on pipeline stress is obtained.

Secondly, literature review indicates that the accurate prediction of pullback force in HDD construction is of great significance to construction safety and construction success. However, the accuracy of current analytical methods is not high. In the context of machine learning and big data, three new hybrid data-driven models are proposed in this dissertation (Chapter 5) for near real-time pullback force prediction, including radial basis function neural network with complete ensemble empirical mode decomposition with adaptive noise (CEEMDAN-RBFNN), support vector machine using whale optimization algorithm with CEEMDAN (CEEMDAN-WOA-SVM), and a hybrid model combines random forest (RF) and CEEMDAN. Three novel models have been verified in two projects in China. It is found that the prediction accuracy is dramatically improved compared with the original analytical models (or empirical models). In addition, through the feasibility analysis, the great potential of machine learning model in near real-time prediction is proved.

At the end of this dissertation, in addition to summarizing the primary conclusions, three future research directions are also pointed out: (1) stress analysis of pipelines installed by HDD in more complex situations; (2) stress analysis of pipeline during HDD construction; (3) database establishment in HDD engineering.

APPROVAL FOR SCHOLARLY DISSEMINATION

The author grants to the Prescott Memorial Library of Louisiana Tech University the right to reproduce, by appropriate methods, upon request, any or all portions of this Dissertation. It is understood that “proper request” consists of the agreement, on the part of the requesting party, that said reproduction is for his personal use and that subsequent reproduction will not occur without written approval of the author of this Dissertation. Further, any portions of the Dissertation used in books, papers, and other works must be appropriately referenced to this Dissertation.

Finally, the author of this Dissertation reserves the right to publish freely, in the literature, at any time, any or all portions of this Dissertation.

Author _____

Date _____

DEDICATION

This dissertation is dedicated to my dear parents and my beloved motherland—the People’s Republic of China. Without your support, my dissertation could not be completed.

TABLE OF CONTENTS

ABSTRACT.....	iii
APPROVAL FOR SCHOLARLY DISSEMINATION	v
DEDICATION	vi
LIST OF FIGURES	x
LIST OF TABLES	xiii
ACKNOWLEDGMENTS	xv
CHAPTER 1 INTRODUCTION	1
1.1 Research Background	1
1.1.1 Oil and Gas System.....	1
1.1.2 Oil and Gas Pipeline Construction.....	3
1.1.3 Pipeline Installation Methods	5
1.1.4 Oil and Gas Pipeline Safety	11
1.2 Objectives	12
1.3 Literature Review	12
1.3.1 Theoretical Advances in Pipeline Stress Analysis.....	13
1.3.2 Pipeline Stress Analysis.....	15
1.3.3 Pullback Force Prediction During HDD Construction	19
1.4 Dissertation Organization	21
1.5 Contributions	22
CHAPTER 2 HDD TECHNIQUE INTRODUCTION.....	23
2.1 Foreword.....	23

2.2	HDD Technology Introduction	23
2.3	HDD System	26
2.3.1	Drilling Rig System	26
2.3.2	Direction Control and Deflecting System.....	27
2.3.3	Drilling Tools.....	28
2.3.4	Mud System	28
2.3.5	Reaming and Pullback System.....	29
2.3.6	Power and Auxiliary System	30
2.4	HDD Construction Requirement	30
CHAPTER 3 FINITE ELEMENT METHOD AND MODEL VERIFICATION		32
3.1	Foreword.....	32
3.2	Finite Element Analysis Theory	32
3.2.1	Commercial Software for Pipeline Stress Analysis	35
3.2.2	ANSYS Workbench Software Introduction.....	36
3.3	Yield Criterion	37
3.4	Finite Element Method Verification	39
3.4.1	Existing Case Overview.....	40
3.4.2	Finite Element Analysis	41
3.5	Summary	51
CHAPTER 4 STRESS ANALYSIS OF THE OPERATING GAS PIPELINE INSTALLED BY HDD		52
4.1	Foreword.....	52
4.2	Project Overview	52
4.3	Preliminary Analysis of the Project After Construction.....	53
4.4	Finite Element Analysis.....	55
4.4.1	Case 1	55

4.4.2	Case 2.....	69
4.5	Discussions	73
4.5.1	Comparison of Case 1 and Case 2	74
4.5.2	Comparison of HDD Method and Open-cut Method	74
4.5.3	Influencing Factors Analysis	77
4.5.4	Stress Sensitivity Analysis.....	83
4.6	Summary.....	85
CHAPTER 5 NEAR REAL-TIME PULLBACK FORCE PREDICTION DURING HDD CONSTRUCTION		86
5.1	Foreword.....	86
5.2	Theories	86
5.2.1	Data Denoising Method--CEEMDAN.....	87
5.2.2	Prediction Models	89
5.3	Applications	97
5.3.1	Project Overview and Data Description	97
5.3.2	Prediction Steps	99
5.3.3	Results and Discussions.....	103
5.3.4	Feasibility of Near Real-time Prediction	114
5.4	Summary.....	115
CHAPTER 6 CONCLUSIONS AND FUTURE WORKS.....		117
6.1	Conclusions.....	117
6.2	Future Works	118
APPENDIX A PROGRAM FOR DRUCKER-PRAGER MODEL IN WORKBENCH.....		119
BIBLIOGRAPHY.....		121

LIST OF FIGURES

Figure 1-1: Oil and gas systems (Lu et al., 2020a).....	2
Figure 1-2: Global transmission oil and gas pipeline length.	4
Figure 1-3: HDD machines manufactured and sold in United States (1992–2018).....	7
Figure 1-4: Accident statistics of hazardous liquid pipeline and gas pipeline in the United States (Data source: PHMSA).....	11
Figure 2-1: Schematic diagram of Hong Kong International Airport HDD project.....	25
Figure 2-2: Drilling rig system.	26
Figure 2-3: Reamers. (a) barrel reamer; (b) flying reamer; (c) rock reamer; (d) plate reamer.	29
Figure 2-4: HDD construction process.	30
Figure 3-1: Steps of stress analysis using ANSYS Workbench software.....	37
Figure 3-2: The geometric model of the pipeline in the case of foundation settlement. (a) axial view along the pipe; (b) longitudinal profile view.	42
Figure 3-3: The geometric model of the pipeline in the case of foundation settlement. (a) axial view along the pipe; (b) longitudinal profile view.	42
Figure 3-4: Commonly used two-dimensional and three-dimensional meshes.	45
Figure 3-5: Three kinds of meshes.	45
Figure 3-6: The mesh results of this case using Workbench software.	48
Figure 3-7: Boundary conditions and loads.....	49
Figure 3-8: Simulation results. (a) soil deformation; (b) soil stress; (c) pipe deformation; (d) pipe stress.	51
Figure 4-1: Construction site of Yangtze River main channel crossing project.....	53
Figure 4-2: The crossing path of main channel crossing project.	53
Figure 4-3: Physical model of Case 1.....	54
Figure 4-4: Physical model of Case 2.....	55

Figure 4-5: Pipeline-soil geometric model (Case 1) established by DesignModeler software.....	56
Figure 4-6: Contact between the inner wall of the borehole and the outer wall of the pipe. (a) contact body; (b) target body.....	59
Figure 4-7: Direction of action of internal pressure on pipeline.....	59
Figure 4-8: Total pressure of static liquid on curved surface.	60
Figure 4-9: The hydrostatic pressure acting on the borehole wall and the outer wall of the pipe. (a) borehole wall; (b) outer wall of the pipe.	62
Figure 4-10: Loads for Case 1.	62
Figure 4-11: Von Mises stress along the pipeline axial with three boundary conditions.....	63
Figure 4-12: Equivalent stress nephogram of pipeline under three boundary conditions. (a) free boundary; (b) fixed boundary; (c) horizontal displacement limited boundary.	64
Figure 4-13: Boundary conditions of the pipeline-soil system.....	65
Figure 4-14: Generated mesh (Case 1).	66
Figure 4-15: The results of mesh independent study (Case 1).	67
Figure 4-16: Analysis results of stress and deformation of pipe. (a) stress (overall view); (b) stress (partial view); (c) deformation (overall view); (d) deformation (side view).	68
Figure 4-17: Pipeline-soil geometric model (Case2) established by DesignModeler software.....	69
Figure 4-18: Contact between the inner wall of the borehole and the mud cake. (a) contact body; (b) target body.	71
Figure 4-19: Generated mesh (Case 2).	72
Figure 4-20: Analysis results of stress and deformation of pipe. (a) stress (overall view); (b) stress (partial view); (c) deformation (side view).	73
Figure 4-21: Pipe-soil system of the open-cut method.	75
Figure 4-22: Stress and deformation of the pipe installed by traditional open-cut method. (a) stress; (b) deformation.	76
Figure 4-23: Curve of maximum pipe stress and pipe diameter.....	77

Figure 4-24: Curve of maximum pipe stress and pipe thickness.	78
Figure 4-25: Curve of maximum pipe stress and buried depth.....	79
Figure 4-26: Curve of maximum pipe stress and pressure.	79
Figure 4-27: Influence of soil parameters on maximum stress of pipeline. (a) elastic modulus; (b) Poisson’s ratio; (c) soil density; (d) cohesion; (e) inner friction angle; (f) dilatancy angle.	82
Figure 4-28: Sensitivity coefficient curve of pipeline stress.	84
Figure 5-1: Prediction process based on CEEMDAN (Lu et al., 2020c).....	89
Figure 5-2: The architecture of the RBFNN (Lu et al., 2020d).	90
Figure 5-3: Support vector machine.	93
Figure 5-4: Flow chart of WOA-SVM.	95
Figure 5-5: Basic flowchart of RF (Safari et al., 2017).	97
Figure 5-6: Design crossing curves for two HDD projects.	98
Figure 5-7: Decomposition of raw data by CEEMDAN. (a) Project 1; (b) Project 2. ..	100
Figure 5-8: Normalized data. (a) Project 1; (b) Project 2.	101
Figure 5-9: Predictive sliding window schematic.....	101
Figure 5-10: Data denoising and prediction processes.	102
Figure 5-11: Prediction results by RBFNN-based models. (a) Project 1; (b) Project 2.	106
Figure 5-12: Prediction results by WOA-SVM-based models. (a) Project 1; (b) Project 2.	109
Figure 5-13: Percentage error at each prediction point. (a) Project 1; (b) Project 2.....	112
Figure 5-14: Standard deviation of the percentage error of two models in Project 1 and Project 2.	113

LIST OF TABLES

Table 1-1: Characteristics of different types of pipes.	3
Table 1-2: Large oil and gas long-distance pipeline projects in recent years.	5
Table 1-3: Characteristics of trenchless technologies and the open-cut method (Najafi, 2010).	6
Table 1-4: Characteristics and application scope of various trenchless installation methods (Ma, 2014; Najafi, 2013; Bennett et al., 1995).....	8
Table 1-5: Considerations of research target in this dissertation.	12
Table 2-1: Classification of HDD method (Iseley and Gokhale, 1997).....	24
Table 3-1: The advantages of various finite element analysis software.	36
Table 3-2: Characteristics and applicability of five common yield criteria.....	38
Table 3-3: Advantages and disadvantages of five conventional yield criteria.	39
Table 3-4: Reference information for FEA verification.	40
Table 3-5: Parameters of the plastic pipe.....	43
Table 3-6: Parameters of the soil.	43
Table 4-1: Parameters of the steel pipe.....	57
Table 4-2: Parameters of the soil.	57
Table 4-3: Five contact types in ANSYS Workbench.	58
Table 4-4: The results of mesh independent study (Case 1).	66
Table 4-5: Parameters of the mud cake.....	70
Table 4-6: The results of mesh independent study (Case 2).	72
Table 4-7: Stress and deformation comparison of Case 1 and Case 2.	74
Table 4-8: Pipeline stress corresponding to different mud densities.	80

Table 4-9: Soil parameters.	81
Table 4-10: Interval of sensitivity coefficient of each factor.	84
Table 5-1: Design parameters of two HDD projects.	99
Table 5-2: The prediction errors of CEEMDAN-RBFNN and RBFNN in the two HDD projects.	107
Table 5-3: The prediction errors of CEEMDAN-WOA-SVM and WOA-SVM in the two HDD projects.	110
Table 5-4: The prediction errors of CEEMDAN-RF and RF in the two HDD projects.	111
Table 5-5: The prediction MAPEs of test sets corresponding to different sliding window lengths.	114

ACKNOWLEDGMENTS

I would like to thank my research advisor, Dr. Tom Iseley, for his guidance in academic, career and life. In the past three years, he not only supported the research I wanted to do, but also taught me how to connect theory with practice. I am very glad to be able to work with him. I would like to specially thank Ms. Xiaonan Wu for her help and support. Although she is my research advisor in my master's degree, she has been guiding me since I knew her. I would also like to thank Dr. Mohammadamin Azimi for his academic guidance and help.

I would like to thank Dr. John Matthews, Dr. Sharav Alam, Dr. Jay Wang and Dr. Arun Jaganathan for their valuable comments on my dissertation. I would like to sincerely thank Dr. Collin Wick, Fredda Wagner, Kimlin Hall, Amy Bell, Diana Bryan and Saleh Behbahani for the support and help in my doctoral program. I would also like to thank Professor Kun Huang, Professor Shanbi Peng, Professor Enbin Liu, Professor Guoguang Ma, and Dr. Xin Ma for the help and support.

I would like to thank my friends for their friendship, support, help and encouragement. Thank you to Shijuan Wu for the consistent support. Thanks to Fan Li for the help and support over the past three years. I would like to thank my friend, Dr. Kenny Crump, who not only gave me academic advice, but also let me know to be a person with broad interests and persistence. I would like to thank Xiaoyu Han, Zilin Liu, Lingdi Fu, Yuxin Xie, Feifei Cheng, and Gang Hu for the friendship.

I would like to thank Mr. Houming Ni, Mr. Jiang Peng, and Dr. Lijun Guo for their help and guidance in my career and personal development.

I would like to thank Taylor Swift for her music that encourages me to be fearless.

I would like to thank the following organizations or scholarships for their support during my doctoral program:

China Scholarship Council (CSC);

National Association of Sewer Service Companies (NASSCO);

Heather Berry Scholarship;

Tullis Endowed Scholarship;

North American Society for Trenchless Technology (NASTT);

China Petroleum & Chemical Corporation;

Southwest Petroleum University.

CHAPTER 1

INTRODUCTION

1.1 Research Background

1.1.1 Oil and Gas System

Despite the rapid development of new energy (such as wind energy, geothermal energy, and solar photovoltaic) in recent years, oil and gas resources still occupy the main energy market. According to the World Energy Outlook released by British Petroleum (BP) in 2019 (BP, 2019), the demand of petroleum will continue to rise in the next 20 years, but at a much slower rate than in the past. Natural gas is the fastest-growing energy source besides renewable energy, increasing by nearly 50% by 2040 (Lu et al., 2020a). The rising demand of oil and gas resources means that more transportation infrastructure is needed. The pipeline is the most significant way to transport oil and gas resources, and it is also the most economical method. Therefore, the pipeline can be said to be the lifeline of industrial and economic development. In different scenarios, there are different types of pipes, as shown in **Figure 1-1**. Pipelines can be divided into gathering pipelines, transmission pipelines, and distribution pipelines. Note that distribution pipelines are only applicable to gas system (USGA Office, 2014). Their functions and features are shown in **Table 1-1**. It reveals that the distance of the transmission pipeline is much longer than that of the gathering pipeline and distribution pipeline. Moreover, the diameter of the transmission pipeline is large, and the pressure is high. Although the transmission

pipeline may cause fewer casualties in the event of an accident than distribution pipeline (because it is usually far away from densely populated areas), its economic losses and environmental damage may be the greatest, so its safety problems should not be underestimated.

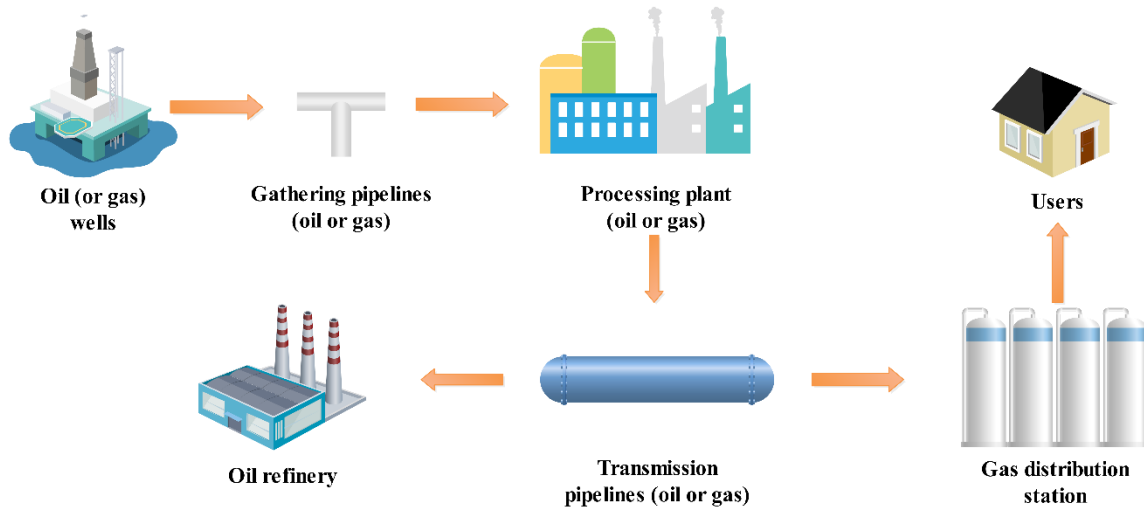


Figure 1-1: Oil and gas systems (Lu et al., 2020a).

Table 1-1: Characteristics of different types of pipes.

Pipe type	Gathering	Transmission	Distribution
Function	Transport fluid from the wells to the processing plant or storage tank	Transport fluid over long distances across states, countries and continents	Deliver gas to the user
Diameter (mm)	Under 450 for gas, 50–200 for crude oil	Usually 500–1200	Under 900 for main pipelines, less than 50 for service pipelines
Length (m)	Approximately 200	Up to thousands of kilometers	—
Medium	Natural gas, crude oil, natural gas liquids	Natural gas, crude oil, natural gas liquids and refined products	Natural gas
Pressure (MPa)	Under 5 for gas	1.5–8.5	Up to 1.5 for main pipelines, around 0.05 for service pipelines
Material	Steel	Steel	Steel, cast iron, plastic, and copper

1.1.2 Oil and Gas Pipeline Construction

As of 2017, there are approximately 3800 transmission oil and gas pipelines worldwide with a total length of approximately one million two hundred and ten thousand miles. By region, global oil and gas pipelines are mainly distributed in Asia Pacific, Russia and Central Asia, Europe, North America, Latin America, Middle East, and Africa (Zhu et al., 2017). As shown in **Figure 1-2**, the total length of oil and gas pipelines in North America accounts for about 43% of the world.

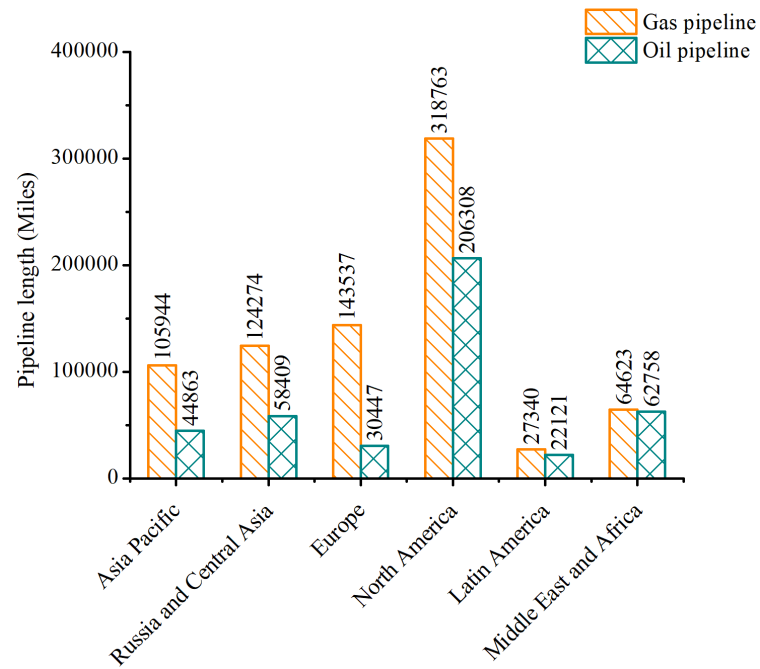


Figure 1-2: Global transmission oil and gas pipeline length.

Due to the impact of oil and gas prices and the economy, investment in oil and gas pipeline construction has entered a decline period since 2016, from 166 billion dollars in 2016 to 106 billion dollars in 2018 (Zhu et al., 2017). The new pipeline is mainly concentrated on gas pipelines and submarine pipelines, with the most substantial investment in North America and the Asia Pacific, followed by the Middle East and Latin America. **Table 1-2** lists the large-scale oil and gas long-distance pipeline projects in recent years.

Table 1-2: Large oil and gas long-distance pipeline projects in recent years.

Project	Medium	Length (km)	Diameter (mm)	Transport capacity¹
Central Asia–China gas pipeline	Gas	1833	1067	55 billion m ³ /a
Nord Stream	Gas	1222	1220	55 billion m ³ /a
Polarled Gas Pipeline	Gas	482	914	70 million m ³ /d
TurkStream	Gas	930	813	31.5 billion m ³ /a
Sino-Myanmar Gas Pipeline	Gas	793	1016	12 billion m ³ /a
Sino-Myanmar Crude Oil Pipeline	Crude oil	771	813	12 million t/a

1.1.3 Pipeline Installation Methods

From **Table 1-2**, it can be known that the construction of long-distance pipelines is still playing a pivotal role in global energy allocation. Thus, how to efficiently install pipelines is an essential issue. The traditional pipeline installation method requires trenching, installing, and backfilling soil, which is not only time-consuming, but also affects traffic and environment. Later, trenchless technology emerged, which can install pipes with minimum excavation (Lu et al., 2020f). **Table 1-3** lists the characteristics of trenchless technologies and traditional open-cut method. It reveals that the trenchless construction has many advantages such as environmental protection and quicker, so the

¹ The unit is not uniform because the annual operating days may be different, and the measurement units for natural gas and crude oil are different.

utilization is increasing. At present, trenchless installation technologies suitable for oil and gas pipelines include horizontal auger boring (HAB), horizontal directional drilling (HDD), pipe jacking (PJ), microtunneling (MT), impact moling (IM), pipe ramming (PR), and direct pipe (DP). They have advantages and disadvantages, as shown in **Table 1-4**.

Table 1-3: Characteristics of trenchless technologies and the open-cut method (Najafi, 2010).

Pipe installation method	Trenchless method	Open-cut method
Construction cost	Low	High
Road surface excavation	Very small	Yes
Carbon emission	Low	High
Noise	Low	High
Construction speed	Fast	Slow
Impact on traffic	No	Yes

According to the “21st annual directional drilling survey” (Underground Construction, 2019), in 2019, about 38% of contracts performed HDD work worth up to \$1 million, while about 60% of contracts performed HDD work valued at more than \$1 million, and many contractors’ work exceeded \$10 million in value. HDD will remain strong in trenchless installations; contractors expect HDD construction to account for roughly 47% of their work in 2020, and it will grow to 51% by 2024. As shown in **Figure 1-3**, since 1992, there have been three rapid growth periods in the manufacture and sale of HDD machines. Through investigation, it is also known that HDD is mostly used in the construction of long-distance oil and gas pipelines in the case of crossing rivers and

highways. Therefore, in this dissertation, gas pipeline installed by HDD is taken as the research object.

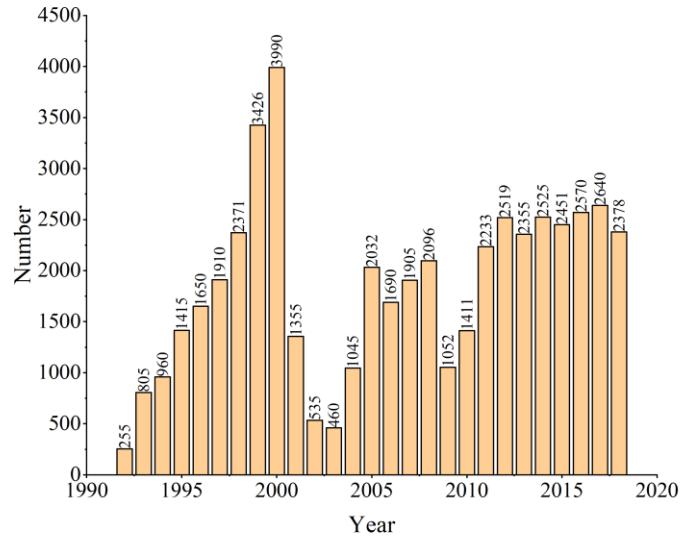


Figure 1-3: HDD machines manufactured and sold in United States (1992–2018).

Table 1-4: Characteristics and application scope of various trenchless installation methods (Ma, 2014; Najafi, 2013; Bennett et al., 1995).

Installation method	Advantage	Limitation	Applications	
			Length (m)	Diameter (mm)
HAB	Little or no impact on the formation	<ol style="list-style-type: none"> 1. Generally, the pipe laying direction cannot be controlled, and the construction accuracy is limited 2. It is challenging to construct in large gravel or very soft soil layers 	30–100 (more than 200 for equipment with high capacity)	100–1500
HDD	<ol style="list-style-type: none"> 1. Economical, efficient, and environmentally friendly 2. The excavation volume of earthwork is small 	<ol style="list-style-type: none"> 1. Larger requirements on the construction site 2. Not applicable to sand or gravel formations 3. Underground pipelines need to be identified before construction 	50–3000	200–2000
PJ	<ol style="list-style-type: none"> 1. Economical, efficient, and environmentally friendly 2. The excavation volume of earthwork is small 	<ol style="list-style-type: none"> 1. Difficult to construct when the radius of curvature is small or there are multiple curves 2. Deviation and uneven settlement are likely to occur in the soft soil layer 	>500	330–4000

Table 1-4: Continued.

Installation method	Advantage	Limitation	Applications	
			Length (m)	Diameter (mm)
MT	<ol style="list-style-type: none"> 1. When the buried depth of the pipeline is large, the construction cost is lower than the traditional construction method 2. The direction of the pipe can be precisely controlled 3. It can work under harsh geological conditions 	<ol style="list-style-type: none"> 1. Detailed surveys of geological conditions are required 2. The equipment investment is large, and the technical and experience of the construction personnel are high 3. Two working pits need to be excavated 	>500	>1900
IM	<ol style="list-style-type: none"> 1. The supporting equipment is simple, convenient for transportation, installation and maintenance 2. The operation is simple, the construction cost is low, and the pipe laying speed is fast 	<ol style="list-style-type: none"> 1. It is easy to deviate from the direction when the formation conditions change or encounter obstacles 2. It is not suitable for hard soil, large gravelly soil and water-rich soil 3. The accuracy of pipe laying is low 	50	30–250

Table 1-4: Continued.

Installation method	Advantage	Limitation	Applications	
			Length (m)	Diameter (mm)
PR	<ol style="list-style-type: none"> 1. Geological adaptability is strong 2. Strong construction capacity, good quality and high efficiency 	<ol style="list-style-type: none"> 1. Both material and wall thickness are specifically required 2. The direction is not controllable 	10–100	50–2000 (the maximum diameter can reach 4000)
DP	<ol style="list-style-type: none"> 1. The equipment occupies less land, the construction period is short, and the complex geological adaptability is strong 2. Drilling and pipe installation are completed at the same time, and the operation is simple and continuous 3. Accurate directional control is possible 4. The optimum solution for access only from one side 5. No costly and time-consuming shaft construction 	There are no construction standards for the time being	>1500	750–1500

1.1.4 Oil and Gas Pipeline Safety

After the pipeline construction, its safe operation is of great significance for energy transportation. The pipeline failure modes during operation are corrosion, stress exceeding the limit, third-party damage, and other reasons. In the United States, some pipeline accident statistics can be obtained from Pipeline and Hazardous Materials Safety Administration (PHMSA), as shown in **Figure 1-4**; the accident rate for oil and gas pipelines in the United States has two peak periods in the last 20 years: 2000–2005 and 2010–2015. Therefore, considering the reasons shown in **Table 1-5**, the stress analysis of the operating gas pipeline installed by HDD is necessary.

On the other hand, in the construction process, although the pipeline pullback is the last step, its safe operation is crucial. In this process, the calculation and prediction of the pullback force is the key to the success of the construction. Therefore, the prediction of pullback force in HDD construction process is also one of the research objects in this dissertation.

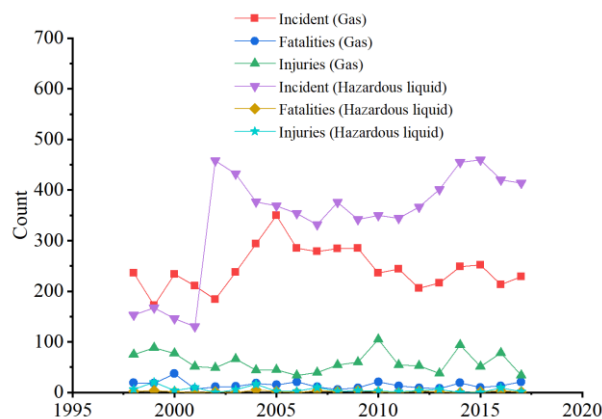


Figure 1-4: Accident statistics of hazardous liquid pipeline and gas pipeline in the United States (Data source: PHMSA).

Table 1-5: Considerations of research target in this dissertation.

Considerations	Selection result
Trenchless installation technologies have higher potential and utilization value than the traditional open-cut method	Research on trenchless installation technology
HDD has the largest market in all trenchless installation technologies	Research on HDD in the installation technologies
There are many stress analysis studies on pipelines, but there are few stress analyses on pipelines installed by trenchless methods	Stress analysis on the pipeline installed by trenchless technology
Natural gas pipelines have higher pressure than crude oil pipelines, the failure risk is higher, and the accident consequences are more serious	Research on gas pipelines

1.2 Objectives

There are two objectives in this dissertation. One objective is to conduct a detailed stress analysis of operating gas pipeline installed by HDD method; another one is to apply machine learning models to the pullback force prediction during installation process. Stress analysis of operating gas pipelines installed by HDD method can provide reference for pipeline managers and designers. The use of machine learning models to predict the pullback force during construction can help construction personnel know the pullback force in advance to reduce the risk.

1.3 Literature Review

The literature review of this dissertation is based on research objectives. First, **Section 1.3.1** reviews some theoretical studies of pipeline stress in the field of trenchless installation. **Sections 1.3.2** reviews various application scenarios and findings of pipeline

stress analysis, and **Section 1.3.3** reviews the research of pullback force prediction during HDD construction.

1.3.1 Theoretical Advances in Pipeline Stress Analysis

Based on Marston trench load theory, the earth pressure analysis of pipelines using open-cut method and trenchless method is carried out by Zhao and Doherty (2003). They concluded that the earth pressure on the pipeline installed by open-cut method is much higher than that of the trenchless method, and the earth pressure on the pipeline installed by open-cut is more sensitive to surface overload than that of the trenchless methods. Sun (2006) used ANSYS software to carry out stress analysis on the construction process of drainage pipe installed by PJ method. Through finite element analysis (FEA), the section deformation diagram and internal force diagram of the pipe are obtained. In addition, he also analyzed some influencing factors such as deformation modulus of soil and elastic modulus of the pipeline, and concluded that the release of initial ground stress in each construction stage is the primary factor affecting the stress and deformation of pipeline. Adedapo (2007) compared the effects of HDD and open-cut installation on pavement deterioration and polyethylene (PE) pipe behavior through numerical simulation and field experiments. Among them, the FLAC3D software is used in the numerical simulation, and the Mohr-Coulomb failure criterion is adopted. In the field experiment, two 200 mm SDR-17² DIPS³ high-density polyethylene (HDPE) pipes were buried 1.5 m underground. The experimental results show that the pipe installed by HDD method has smaller annular deflection and strain during installation. Cousens and

² SDR denotes standard dimension ratio.

³ DIPS denotes ductile iron pipe size.

Jandu (2008) summarized the calculation methods of the loads, stresses and deflections of natural gas pipelines using HAB and HDD methods. The loads include soil loads, traffic loads, settlement loads, and construction loads. The stresses include circumferential bending stress, axial membrane stress, axial bending stress, and combined stress. Zhou et al. (2015) conducted a comparative study on the calculation model of earth pressure for pipelines installed by trenchless methods provided by different standards. The comparison criteria include GB 50332 in China, ASTM F1962 in North America and BS EN 1594 in Europe. They found that the calculation model of GB 50332 is simple, but the cohesion of the soil is neglected, and the influence of the friction angle of the soil on the soil arch coefficient is not fully considered. A preliminary study was conducted by Zheng et al. (2016) to explore the effect of soil pressure on pipelines installed by trenchless method and open-cut method. They used PLAXIS software to simulate the HDPE pipeline in Waterloo, Canada. They compared the simulation results with the field data and proved that the PLAXIS software had a higher accuracy and the error was less than 5%. In addition, they concluded that the maximum pressure and deformation of pipelines installed by open-cut method are much greater than those installed by trenchless method under the same conditions. The maximum pressure of pipeline using open-cut method is 2.66–11.65 times greater than pipeline installed by trenchless method, and the deformation is 3.96–11.95 times greater than pipeline using trenchless method. Tsung et al. (2016) conducted a comparative study of the soil pressure and deformation of pipes constructed by open-cut method and trenchless method. Through numerical simulation and field experiments, they concluded that under the same conditions, the maximum soil pressure and vertical deflection of the pipe installed by

open-cut method is much larger than that of the trenchless method. Moreover, they also concluded that regardless of the construction method, the soil pressure and deformation of the underground pipeline are not evenly distributed. The maximum soil pressure can usually be found on both sides of the pipeline, and the minimum soil pressure can be found at the bottom of the pipeline. Sun (2017) used ANSYS software to establish the finite element model of a river-crossing pipeline installed by HDD method, and obtained the relationship between the pipeline length and maximum stress. In addition, he also concluded that the changes of equivalent stress and pullback force of the pipeline obey the polynomial law under the same soil condition. Moreover, on the basis of satisfying the construction conditions, it is suggested that the small entry angle and exit angle should be chosen as far as possible. Díaz-Díaz et al. (2018) used RS² to perform two-dimensional FEA on pipelines installed by PJ method. They performed axisymmetric and plane strain analysis to obtain stress distribution and displacement of the pipeline. In addition, the paper also provides a nephogram of bending moments and shear forces along concrete pipes. Zhao (2018) theoretically analyzed the ground surface and excavation surface deformation caused by soil stress release during pipe jacking. ABAQUS software was used to simulate the pipe jacking process, and the ground surface deformation law during jacking was obtained.

1.3.2 Pipeline Stress Analysis

According to the application of the pipeline, this section reviews the research of pipeline stress analysis from three aspects.

1.3.2.1 *River-crossing pipe*

There have been many studies on the stress of river-crossing pipelines, which can be divided into large excavation crossing, trenchless crossing and suspended crossing. Li et al. (2014) used CAESAR II software to analyze the stress of a river-crossing gas pipeline. They considered not only the hydrostatic pressure, but also the seismic load. Lan et al. (2014) considered the influence of river erosion on the crossing pipeline. They used ABAQUS software to analyze the stress of two river-crossing pipelines installed by HDD method. Yao et al. (2015) carried out stress analysis on the river-crossing pipeline by suspended method. They used Fluent software to simulate the effect of the fluid and utilized ANSYS software to carry out mechanical analysis. In this study, they also discussed the relationship between critical suspended length and flow velocity (or wall thickness). Wu et al. (2017) conducted a stress analysis on the river-crossing oil pipelines installed by large excavation method. Through engineering examples, they concluded that the temperature difference has a greater influence on the pipeline stress than the pressure for oil pipelines. Liu et al. (2018) used ABAQUS software to analyze the stress of the river-crossing pipeline. During the analysis, they used beam model to simulate the pipeline and casing. It can be seen from the literature review that the river-crossing pipeline installed by suspension is the research focus in recent years, and many scholars focus on the study of suspended length. At the same time, there are few studies on the stress of river-crossing pipeline installed by HDD method. However, when using the HDD method, the stress problem of the pipeline is worthy of further study due to the application of mud involved in the construction process and the change of the mud from liquid to solid.

1.3.2.2 *Highway-crossing pipe*

Noor and Dhar (2003) established a three-dimensional pipe-soil finite element model and simplified the vehicle load to a moving load. The results show that when the pipe depth is 1.5 times the pipe diameter, the vehicle load has little effect on the pipe stress. Wang (2006) used a quarter-vehicle vibration model to analyze the stress of pipeline under vehicle load, and discussed the influences of dynamic vehicle load, dynamic load coefficient, vehicle speed and other factors on the pipe stress. Zhang and Shao (2007) used the finite element numerical method based on u-p format to analyze the dynamic response of pipelines in saturated soil under traffic load. Considering the influences of inertial force, water-soil coupling, and pipe-soil interaction, the governing equation is adopted. The standard Galerkin discretization method and Newmark- β method are used to establish the finite element dynamic equation, and the transmission boundary conditions are introduced to simulate the infiniteness of the horizontal direction of the soil. Goltabar and Shekarchi (2010) carried out stress analysis of buried pipeline under traffic load. In the study, they used Plaxis-3D software to carry out stress analysis and conducted field experiments, which show that the FEA method is effective. In addition, they also analyzed the influence of different factors on the pipeline stress. Lan et al. (2012) used ANSYS software to perform stress analysis on highway-crossing buried pipelines. They simplified the weight of the vehicle to point loads and applied to the road surface. They concluded that the stress at the center of the pipe increases as the weight of the vehicle increases. Fan et al. (2019) used ABAQUS software to analyze the dynamic response of the buried pipeline under the multi wheel load, and obtained the stress distribution of the inner and outer walls of the pipeline. Through literature review,

it can be known that the stress analysis of pipeline under traffic load is limited to buried pipeline, and the traffic load is usually simplified as point pressure or wheel area pressure.

1.3.2.3 Seismic zone-crossing pipe

O'Rourke's research shows that the seismic level usually needs to reach 6–6.5 to destroy the pipeline (O'Rourke and Liu, 1999). Kershenbaum et al. (2000) analyzed the stress of non-buried pipelines in seismic fault zones. The results show that the longitudinal seismic faults have less influence on straight pipes than snaked pipe. Vazouras et al. (2010) analyzed the stresses and strains of steel pipes that traversed the strike-slip tectonic faults. They considered the large deformation problem in the model and discussed the effects of soil and pipe parameters on the stress. Wu et al. (2015) used CAESAR II software to analyze the stress of the oil pipeline under earthquake action. The spectrum analysis method was used in the analysis process to obtain the maximum stress along the axial direction of the pipeline. Banushi and Weidlich (2018) analyzed the stress of the district heating pipeline. The analysis results show that the heating pipeline usually has stress concentration due to greater flexibility. Alzabeebee (2019) used a developed finite element software to conduct seismic analysis of concrete pipelines and studied the comprehensive effects of factors such as diameter and depth. The results show that seismic vibration can significantly increase the maximum bending moment. Literature review indicates that the stress analysis of pipelines under earthquake action can be divided into static analysis and dynamic analysis. Static analysis can show the maximum stress of the pipeline, while dynamic analysis can get the seismic behavior of the pipeline more carefully. In dynamic analysis, spectrum analysis and time history

analysis are the most popular methods. Time history analysis is closer to reality, but seismic data need to be obtained specially.

1.3.3 Pullback Force Prediction During HDD Construction

The software Phillips Driscopipe's method for calculating the pullback force of the PE pipe is called the Driscopipe model (Driscopipe 1993). In this method, the length and inclination of each pipe are calculated, and the whole crossing curve is simplified as a straight-line section of one-time connection. At the same time, the weight, buoyancy, and friction between the pipe and soil are considered. Huey et al. (1996) proposed a model called PRCI, which assumes that the pilot hole curve consists of a series of curved segments and straight segments, and the pilot hole is filled with the mud. The model considers that the maximum pullback force occurs when the last section of the pipe is pulled into the pilot hole, and this method does not consider the frictional resistance between the pipe and soil. Baumert and Allouche (2002) evaluated three methods for calculating tensile loads for HDD applications and applied them to steel and PE pipes. They concluded that the tensile load is very sensitive to mud weight and mud resistance. Francis et al. (2004) evaluated the pullback force calculation method based on the data of five actual projects. The analysis results show that the relative error is in the range of -240% to 73%. ASTM (2011) proposed a calculation method for the pullback force in the HDD construction, which assumes that the middle section of the crossing curve is a horizontal straight line and the heights of the entrance and exit points are the same. Besides, the influence of the bending stiffness of the pipeline is ignored in the model. Cai et al. (2012) studied the variables related to the pullback force and analyzed three components of the pullback resistance (the friction caused by the pipe quality, the

resistance caused by the resistance effect of the bending section, and the mud drag resistance). The analysis results show that these three resistances all have higher contribution weights in the pullback force, and the contribution weights show dynamic changes during the pullback process. Yang et al. (2014) considered that the HDD pullback process is a complex dynamic problem and proposed a dynamic model for simulating the pipe pullback process. The pipe is modeled by a three-dimensional Euler-Bernoulli flexible beam element, and the interaction between the pipe and the borehole is described by the nonlinear Hertz contact theory. Rabiei et al. (2016) proposed a method for calculating the pullback force of a PE pipe in HDD construction. In this method, the geometry of the pilot hole can be ignored. The case study shows that the method is more accurate than the ASTM method and the PRCI method. Xu et al. (2018) proposed that the original methods of predicting the pullback force did not consider the interaction between the soil and the pipe. Therefore, they used ANSYS software to simulate an HDD project. The results show that the model considering the wedging effect can effectively improve the prediction accuracy (an increase of 7.7% in the example). Cai and Polak (2019) improved the HDD pullback prediction model proposed by Polak in 2007. They used the Winkler model to describe the surrounding soil, considered the non-Newtonian properties of the mud and considered the resistance exerted on the drill string. They also applied this method to two plastic pipes tested at University of Waterloo in 2001. The results show that the new method can accurately predict the pullback force in the overall trend.

According to the literature review, it indicates that there are many calculation theories of pullback force prediction in HDD construction recently, and it is continuously developing. Many scholars updated the analytical model by considering more factors to

achieve higher precision. Although the prediction accuracy has been improved, the error is still significant. Driven by machine learning, many projects have used data-driven models to solve problems in recent years, not only using empirical models and analytical models. Therefore, several machine learning models are used to predict the pullback force during HDD construction in this dissertation. Different from traditional methods, these models need real-time data on the field to make predictions. Therefore, as a near real-time prediction method, it has the following application prospects: (1) the model can be trained based on a small amount of data and then predict subsequent pullback forces, which can better guide the project and ensure construction safety and reliability. (2) In the context of big data, a variety of engineering monitoring data can be imported into the model for training, so that the trained model can obtain higher prediction accuracy in the practical engineering.

1.4 Dissertation Organization

This dissertation is divided into six chapters: (1) Introduction; (2) HDD introduction; (3) Finite element method and model verification; (4) Stress analysis of the operating gas pipeline installed by HDD; (5) Near real-time pullback force prediction during HDD construction; (6) Conclusions and future works.

Chapter 2 introduces the basic theory related to HDD construction, including the composition of the HDD system and some conventional construction procedures and requirements. Chapter 3 briefly introduces the relevant theory of FEA and the features of some widely used software. Moreover, the feasibility of finite element simulation is proved by an example. In Chapter 4, the finite element method is utilized to analyze the stress of the river-crossing pipeline installed by HDD, the stress sensitivity of different

factors is also analyzed. In Chapter 5, three novel hybrid models for near real-time pullback force prediction are proposed. Chapter 6 summarizes the main conclusions of this dissertation and future works.

1.5 Contributions

The main contributions of this dissertation are as follows:

1. In this dissertation, the stress of the operating gas pipeline installed by HDD method is analyzed, which can provide reference for pipeline management. The influence factors and stress sensitivity analysis are carried out, which can provide basis for design.
2. The traditional pullback force predictions during HDD construction are based on the analytic methods. In this dissertation, several data-driven models are adopted. These models can play an auxiliary role in the actual HDD construction.

CHAPTER 2

HDD TECHNIQUE INTRODUCTION

2.1 Foreword

Since the research objects of this dissertation are related to pipelines installed by HDD, it is a prerequisite to understand the construction process, system and construction requirements of HDD thoroughly. This chapter provides a brief introduction to the HDD construction.

2.2 HDD Technology Introduction

HDD is a technique used to drill a tunnel under a waterway or other designated area to pull a pipe or other facility through a drilled underground tunnel (ASCE, 2017). It began in the mid-1940s and was used to lay large-diameter, long-distance oil and sewage pipelines. It was developed rapidly in the United States after 1980s. According to the pipe diameter and length of the laying pipeline, the HDD method is divided into three categories: mini HDD, midi HDD, and maxi HDD, and their features and applications are shown in **Table 2-1**. For oil and gas pipelines, it is usually used for transmission pipeline crossing projects (such as rivers, highways, etc.) outside cities.

Table 2-1: Classification of HDD method (Iseley and Gokhale, 1997).

Type	Diameter range (mm)	Crossing length (km)	Pulling force ($\times 10^3$ N)	Machine weight (t)	Applications
Mini	50–300	≤ 0.18	<89	≤ 9	Distribution pipelines
Midi	300–600	≤ 0.27	89–445	≤ 18	Transmission pipelines
Maxi	600–1500	≤ 3.0	≤ 445	≤ 30	Transmission pipelines

The construction sequence of pipe laying using HDD is as follows: (1) geological prospecting; (2) underground pipeline detection; (3) drilling trajectory design; (4) slurry preparation; (5) drilling and anchoring; (6) pilot-hole drilling; (7) prereaming, and product pipe pullback (Zayed and Mahmoud, 2013; Yan et al., 2018).

On May 18, 2018, Hong Kong International Airport completed the installation of two 5.2-km submarine oil pipelines using HDD technology (constructed by China Langfang Huayuan Mechanical and Electrical Engineering Co., Ltd., China), as shown in **Figure 2-1**. The pipes are 508 mm in diameter, and the pipes are located 130 m below sea level. Drilling was done in the opposite direction of the airport island and Sha Chou, to a distance of 3.7 km and 1.5 km, respectively. The geological conditions are also very complex, and the level of difficulty from an engineering perspective is the highest in the world.

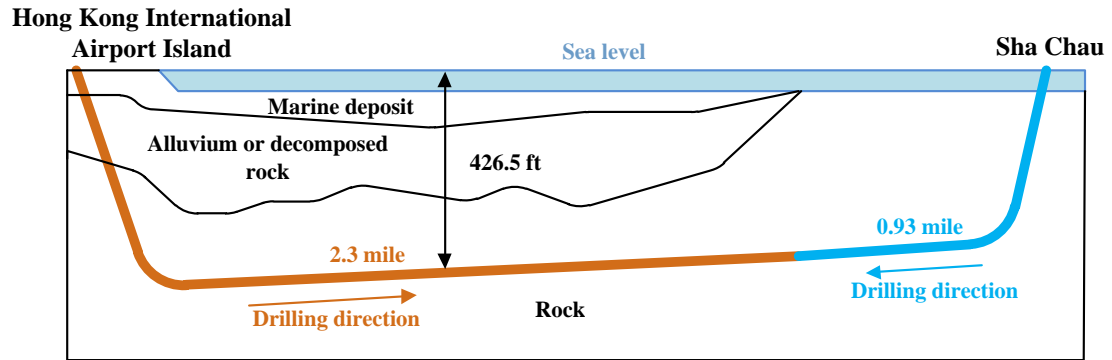


Figure 2-1: Schematic diagram of Hong Kong International Airport HDD project.

Herrenknecht (Schwanau, Germany) is one of the global market leaders in mechanized tunneling technology. To meet the requirements of extremely long and large crossing projects, the company developed a pipe thruster (PT), which can provide up to 750 t of extra thrust at exits when pipe is installed.

For HDD construction of oil and gas pipelines, current major challenge is the lack of skilled labor, and many projects lack sufficient geotechnical information and drillable profiles. In addition, HDD is also faced with the problem of reducing noise and design horizontal and compound curves in densely populated areas. On the other hand, in the past few years, HDD technology has made great progress with respect to mud cleaning, recycling systems, and the use of larger drill pipe, enabling HDD to better meet engineering requirements. In addition, improvements in drill pipe handling equipment have made HDD construction safer and faster (Bradley, 2016).

2.3 HDD System

HDD system is generally composed of drilling rig system, direction control and deflecting system, drilling tools, mud system, pullback system, power system, and auxiliary system (Sinopec, 2010).

2.3.1 Drilling Rig System

The drilling rig system is the core of the whole HDD system. It mainly consists of a base, a rig frame, a movable chuck, and a control room, as shown in **Figure 2-2**⁴.



Figure 2-2: Drilling rig system.

The functions of these main equipment are as follows:

(1) The base of the rig frame is generally divided into two sections, which are connected during use. It has rack tracks, sidewalks, handrails, and so on. There are support legs at the back and bottom of the base, the upper end is connected with the hinge of the base, and the lower end is connected with the steel cushion block. The cushion block is located on the ground or fixed on the special trailer. The base is equipped with

⁴ Figures 2-2, 2-3, 4-1, 4-2 and 5-6 are from reference (Sinopec, 2010).

two hydraulic pipe clamps (chucks), one fixed at the front end of the base, and the other can move back and forth along the slides, thus realizing the thread connection and disassembly of the drill pipe. The height of the rear support leg can be adjusted to change the entry angle.

(2) Rig frame, with travel drive system, is meshed by gears and racks on the inside of the rig base. It is driven by a hydraulic motor through a gear pair and moves forward and backward on the base. The main function of the rig frame is to provide jacking force for boreholes and pulling force for pipeline pullback.

(3) The movable chuck is installed at the front end of the rig frame, it can make the drill pipe produce different rotational speeds and torques.

(4) The control room has a variety of control instruments, display instruments, and computer systems to control the speed and direction of the rig frame and turntable.

2.3.2 Direction Control and Deflecting System

HDD direction control can be divided into wired direction control and wireless direction control. Wireless direction control is only suitable for short-distance and shallow crossing. It is used with small and medium-sized drilling rigs. It is characterized by convenient and accurate direction control, but it is used rarely because of the limitation of the crossing depth and terrain. Wired direction control is suitable for long-distance and deep crossing, and is used with large drilling rigs.

The deflecting system is a technical measure taken when the actual drilling curve deviates from the theoretical curve. The deflecting system and the deviation rectification are realized by the deviation tool. When drilling, as long as the drill pipe is driven into the borehole without rotation, the reaction force acting on the deflecting short joint

changes the direction of the bit and realizes the diagonal drilling; if the deflecting short joint is fed and rotated at the same time, the directionality of the deflecting short joint neutralized, the straight drilling can be realized.

2.3.3 Drilling Tools

Commonly used drilling tools include drill bits, mud motors, and drill pipes. Frequently-used HDD drill bits include a milling bit, a roller bit, and a diamond bit. In rock formations, the use of a mud motor can effectively reduce the required thrust to advance the bit.

For different geological conditions, different drill combinations can be used when drilling the pilot holes. When the length of the drill pipe is very long and a large thrust is required, the drill pipe is easily destabilized under pressure, and it is particularly important to properly combine the drill.

2.3.4 Mud System

In the crossing construction, the mud is mainly used for borehole wall protection, sand carrying and lubrication to ensure the normal and smooth construction. A large amount of mud is used during the HDD crossing process for hydraulic jet cutting, providing energy to the mud motor, lubricating the drill bit, and carrying the cuttings to the ground.

The mud demand for HDD crossing construction is large. Under normal conditions, the mud discharge is twice the amount of solid phase cutting. However, for some complicated and difficult geological conditions, the mud displacement may exceed 264.17 m³/min. The configuration speed of the on-site mud cannot keep up with the need of mud discharge (Sinopec, 2010).

2.3.5 Reaming and Pullback System

Pullback is the last step in the construction of pipeline crossing. Mud, reaming diameter, and reaming wall conditions must be fully considered, and the pullback force should be scientifically set. Especially in the case of large caliber and large dip pipe crossing, a reasonable pullback tool and pullback assist system must be established. Reaming is done by a reamer, commonly used reamers include barrel reamers, barrel reamers with diversion grooves, plate reamers, and flying reamers (see **Figure 2-3**). Pullback is carried out immediately after reaming. Under the pulling force of the drilling rig and the lubrication of the mud, the main pipe is towed back from the borehole along one bank to the other bank.

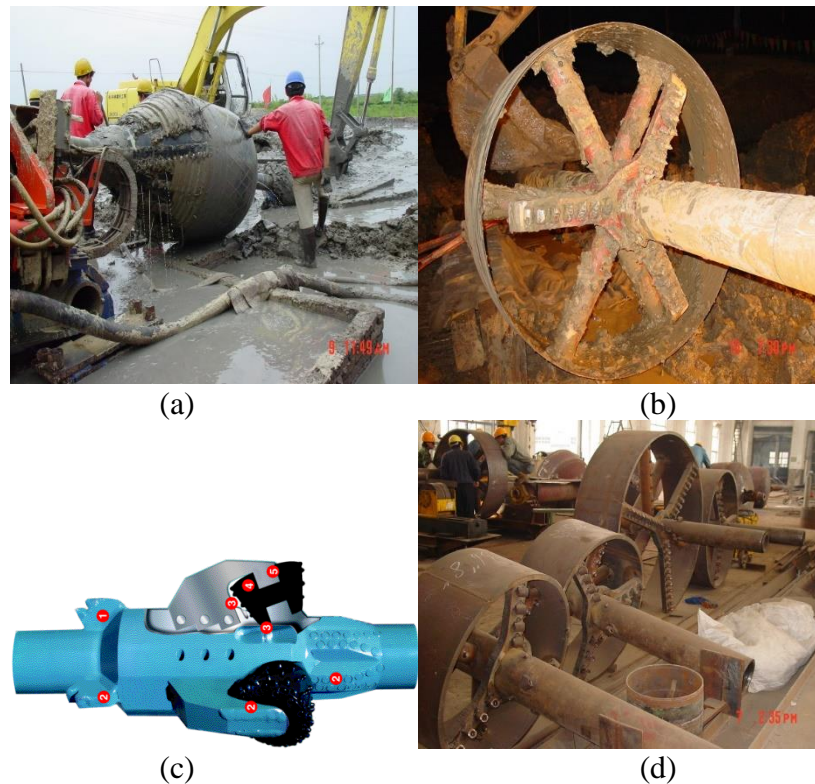


Figure 2-3: Reamers. (a) barrel reamer; (b) flying reamer; (c) rock reamer; (d) plate reamer.

2.3.6 Power and Auxiliary System

Power source generally consists of diesel engine, hydraulic pump, and generator. Its main function is to provide high-pressure oil for drilling rigs and mud pumps to drive hydraulic motors of various parts, and to supply power for computers, lighting and air conditioning equipment. The main auxiliary equipment is crane, single bucket excavator, bulldozer, and pipeline construction equipment.

2.4 HDD Construction Requirement

Figure 2-4 presents the whole process of HDD construction. In addition to the simple information on HDD construction described in **Section 2.2**, some considerations are listed below (Sinopec, 2010).

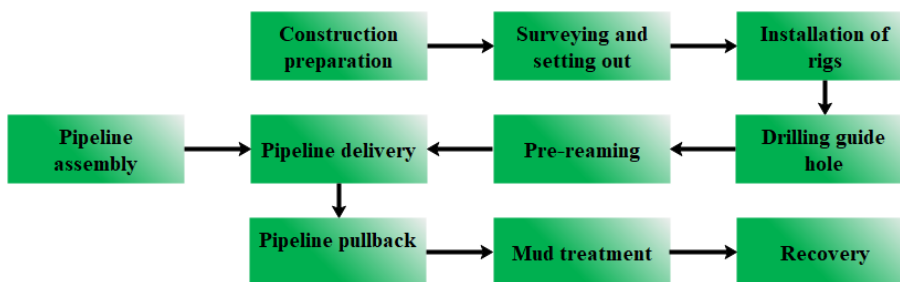


Figure 2-4: HDD construction process.

(1) The geological conditions that HDD is suitable for crossing include clay, mild clay, well-forming sand, and soft rock.

(2) The vertical distance between the center line of the pipeline and the underground pipeline, communication line or power cable (using wire direction control system) should be greater than 15 m. This is to avoid the magnetic field generated by underground pipelines and cables interfering with the sensors of underground instrument units.

(3) The curvature radius of the pipeline should be as large as possible, so as to avoid the increase of pullback resistance. The selection of curvature radius should consider the factors such as buried depth of pipeline, diameter of pipeline and existence of river embankment in the crossing area.

(4) The entrance and exit angles should be determined according to the topography, geological conditions and the diameter of the pipeline. Generally, the entrance angle should be controlled at 8 to 18 degrees and the exit angle should be controlled at 4 to 12 degrees. At present, the maximum entrance angle can reach 28 degrees and the exit angle can reach 15 degrees.

(5) Before HDD construction, geological detailed survey report should provide at least the following information: plane map, geological profile, sampling depth, water content, saturation, granularity, standard penetration number, liquid index, plastic index, liquid limit, plastic limit.

CHAPTER 3

FINITE ELEMENT METHOD AND MODEL VERIFICATION

3.1 Foreword

One of the primary studies in this dissertation is the stress analysis of the operating pipeline, which can usually be analyzed by experiment or simulation. Both methods have their pros and cons. The results of experiment analysis are close to the real state, and it is also the fastest and most effective way. However, experiments usually require special sites and equipment, which are expensive. In addition, it is difficult to repeat the experiment when the parameters need to be changed. On the contrary, the simulation analysis is less expensive, safe and reproducible, and can view the mechanical state of any position without restricting the position and number of sensors. In this dissertation, the finite element method (FEM) is used to simulate the stress of the pipeline under operating conditions. Before simulation, it is necessary to understand the relevant theory and software of the FEM. In addition to introducing the basic theory, in this chapter, an existing study is used as the analysis object to prove the reliability of the FEM.

3.2 Finite Element Analysis Theory

The basic idea of the FEM is to simplify the complex problems, solve the simple problems one by one, and finally combine the solutions of the simple problems organically. Its idea comes from the development of the matrix structure method in solid

mechanics and the intuitive judgment of engineers on structural similarity. The FEM divides the solution domain into many interrelated sub-domains. First, approximate solutions are obtained for each sub-domain, and then the solutions of these sub-domains are further solved to satisfy and approximate the general conditions. Although the solution obtained in this way is not absolutely accurate, it is also a solution very close to the exact solution. Because there are many factors to be considered in the engineering practice, it is difficult to obtain accurate solutions. Therefore, relatively speaking, the FEM not only has high calculation accuracy, but also considers the impact of various complex factors on the project more comprehensively.

In the FEM, the continuum studied is represented as a set of small parts. These elements can be considered to be connected to each other at specified junctions (nodes). These nodes are usually placed on the boundaries of elements, and the adjacent elements are considered to be connected to them. Because the real change of field variables in continuum is unknown, the change of field variables in FEM can be approximated by a simple function. These approximate functions (or interpolation functions) can be determined by the values of field variables at the nodes. When the field functions are written for the whole continuum medium, the new unknown quantity is the node value of the field variable. Solving the field functions is to get the node values of the field variables. Once these node values are known, the field variables of the whole set of elements can be determined by approximate functions. When solving general continuum problems by FEM, it always carried out step by step (Zienkiewicz et al., 1977):

- (1) Discrete structure or solution domain. The solution domain is divided into many small parts, and the number, type, size and layout of elements are determined.

(2) Choose the appropriate interpolation mode.

(3) Element analysis. According to the assumed interpolation model, the stiffness matrix and the load vector of the element are derived by using equilibrium conditions or appropriate variational principles, and the element equilibrium equation can be formed.

(4) Overall synthesis. Set the element equations to get the total equilibrium equation. Since the structure is composed of several elements, the stiffness matrix and load vector of each element should be aggregated in an appropriate way to establish the total equilibrium equation

$$M_s V_{np} = V_{nl} \quad \text{Eq. 3-1}$$

where M_s represents the overall stiffness matrix; V_{np} represents node parameter vectors of the whole structure; V_{nl} represents the nodal load vector.

(5) Introduce constraints. Based on the overall equilibrium equation, the total equilibrium equation is modified according to the boundary conditions. After considering the boundary conditions, the equilibrium equation can be expressed as

$$\bar{M}_s V_{np} = \bar{V}_{nl} \quad \text{Eq. 3-2}$$

where \bar{M}_s represents the overall stiffness matrix with boundary conditions; \bar{V}_{nl} represents the nodal load vector with boundary conditions.

(6) Solve the function. The linear problem can easily solve the vector V_{np} . For the non-linear problem, the stiffness matrix M_s and the load vector V_{nl} need to be corrected in each step.

(7) Calculate other parameters. After calculating the node variables, other parameters can be calculated.

3.2.1 Commercial Software for Pipeline Stress Analysis

With the wide application of computer in engineering design, there are many kinds of stress analysis software on the market. According to their functions, they can be divided into two types: general software and professional software. Commonly used large-scale general FEA software includes SAP5, ADINA (ADINAT), MSC/NASTRAN, ALGOR, HKS/ABAQUS, ANSYS, ANSYS/LS-DYNA, etc. Large-scale professional pipeline stress analysis software includes CAESAR II, AutoPIPE, etc.

The core of SAP-5 software is a general program for calculating linear elasticity of structures, which can be used for stress calculation of various structures. Equivalent stiffness method stress analysis program is also an early application of pipeline stress calculation, which can be used to calculate the stress and displacement caused by internal pressure, dead weight, thermal expansion, end displacement, and other loads. SIMFLEX-II pipeline stress analysis program developed by PENG Engineering Company in the United States has compact structure and strong database functions. At the same time, many American chemical pipeline standards such as API-610 and API-661 are solidified in this program. CAESAR II is a professional pipeline stress analysis software developed by COADE Company in the United States. It was acquired by INTERGRAPH Company and became one of its main products. In addition to dynamic and static analysis, it can also carry out seismic analysis, local stress analysis and so on. The calculation results are accurate and have been widely used in the design of petrochemical pipelines. ANSYS, a software developed by ANSYS Company in the United States, can solve the stress-strain relationship in real environment by modeling. ANSYS can be used to analyze the static, dynamic and non-linear stress and strain of pipeline structure. ABAQUS software was

introduced by HKS in 1979, which is one of the early finite element programs. At present, ABAQUS and ANSYS software are the two most used FEA software. The difference is that ABAQUS has very strong nonlinear computing power. The advantages of various FEA software are shown in the **Table 3-1**. According to the software license of Louisiana Tech University, ANSYS Workbench software is used in this dissertation.

Table 3-1: The advantages of various finite element analysis software.

Software	Core model	Advantages
SAP-5	Structural linear elastic model	Suitable for a variety of structures
SIMFLEX-II	Elastic beam model	(1) Compact structure; (2) Programmed solidification of various American chemical pipeline standards; (3) Good calculation accuracy
CAESAR II	Elastic beam model	(1) Wide range of applications; (2) Accurate; (3) There are many standards and material parameters
ANSYS	Multivariate finite element model	Various element types, abundant computational models and high calculation accuracy
ABAQUS	Multivariate finite element model	(1) Various element types, abundant computational models and high calculation accuracy; (2) It has very powerful non-linear computing ability

3.2.2 ANSYS Workbench Software Introduction

Workbench is an integrated environment software released by ANSYS in 2002 when ANSYS 7.0 was introduced. Because it is more friendly than the ANSYS software interface, it is very popular among designers and researchers. Workbench not only inherits all the functions of ANSYS classic platform in FEA, but also integrates the powerful geometric modeling functions of computer-aided design (CAD) software such

as UG, PRO/E and ISIGHT. The advantage is that the product design, simulation and optimization functions are truly integrated, which can help technicians to complete all the work in the product development process under the same software environment.

In the Workbench software, the following steps are required to perform FEA: (1) Engineering data; (2) Geometry; (3) Model; (4) Setup; (5) Solution; (6) Results. The content of each step is shown in **Figure 3-1**.

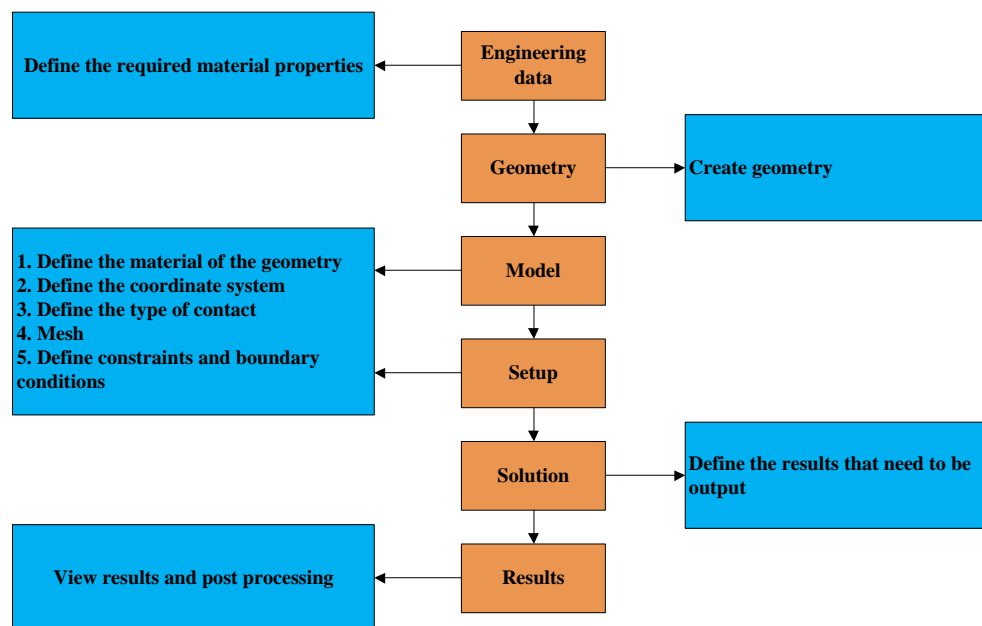


Figure 3-1: Steps of stress analysis using ANSYS Workbench software.

3.3 Yield Criterion

Yield criterion is the condition to judge whether the material begins to yield. There are five conventional yield criteria: the Tresca criterion, the Von-Mises criterion, the Mohr-Coulomb criterion, the Drucker-Prager criterion, and the Zienkiewicz-Pande criterion. Their characteristics and applicability are shown in **Table 3-2**, and their advantages and disadvantages are shown in **Table 3-3**.

Table 3-2: Characteristics and applicability of five common yield criteria.

Yield criterion	Feature	Applications
Tresca criterion (Matsuoka and Nakai, 1985)	When the maximum shear stress in the deformed body or particle reaches a certain value, the material yields. It has nothing to do with hydrostatic pressure and does not consider the influence of intermediate stress	Metallic materials
Von-Mises criterion (Eraslan, 2002)	When the distortion energy corresponding to the stress state of a point in the object reaches a certain limit value, the point will yield	Metallic materials
Mohr-Coulomb criterion (Bai and Wierzbicki, 2010)	When the shear stress in a plane reaches a certain limit value, the material yields	Rock, soil, concrete materials
Drucker-Prager criterion (Alejano and Bobet, 2012)	It includes an additional term in the Von Mises expression	Concrete, rock, soil and other granular materials
Zienkiewicz-Pande criterion	It is an improvement of Mohr-Coulomb criterion	Rock, soil, concrete materials

Table 3-3: Advantages and disadvantages of five conventional yield criteria.

Yield criterion	Advantage	Disadvantage
Tresca criterion (Matsuoka and Nakai, 1985)	When the order of the principal stresses is known, the application is simple	The effect of normal stress and hydrostatic pressure on yield is not considered; The yield surface has a turning point
Von-Mises criterion (Eraslan, 2002)	The effects of medium principal stress on yield and failure are considered; The parameters are easy to determine experimentally; The yield surface is smooth and has no edges	The effect of hydrostatic pressure on yielding is not considered
Mohr-Coulomb criterion (Bai and Wierzbicki, 2010)	Simple and practical; It reflects the effect of three-way isobaric pressure of hydrostatic pressure	The effects of medium principal stress on yield and failure are not considered
Drucker-Prager criterion (Alejano and Bobet, 2012)	The effects of medium principal stress on yield and failure are considered; More practical, it considers the effect of hydrostatic pressure on yield	The influence of pure hydrostatic pressure on the yield of geotechnical materials and the nonlinear characteristics of yield and failure are not considered
Zienkiewicz-Pande criterion	Conducive to numerical calculations, the nonlinear relationship between yield curve and hydrostatic pressure is considered to a certain extent	—

3.4 Finite Element Method Verification

In fact, the FEA is based on some reasonable assumptions and simplification. It is very important whether the established model conforms to reality to a large extent. At the same time, to verify the accuracy of the model, field experiments are usually needed.

However, the site and conditions for field experiments are limited, so an indirect way is adopted in this dissertation. Indirect verification method refers to using the proposed model to simulate a problem in existing literature and comparing their results. If the error is small, the reliability of the proposed model is higher.

Through literature review, it can be found that the mechanical analysis of HDD is usually focused on the pullback force simulation, and there is no stress monitoring data. Therefore, in this dissertation, a more complex pipeline stress analysis case is selected from the existing literature (Luo et al., 2015). The basic information of this relevant article is shown in **Table 3-4**.

Table 3-4: Reference information for FEA verification.

Information	Content
Title	Numerical simulation of strength failure of buried polyethylene pipe under foundation settlement
Publication year	2015
Journal name	Engineering Failure Analysis

Note that there are several reasons to choose this article: (1) In this paper, the pipeline stress analysis involves the soil model, which is similar to the case of stress analysis in the subsequent chapter. (2) Ground settlement involves large deformation problem and is more complicated than conventional stress analysis problems.

3.4.1 Existing Case Overview

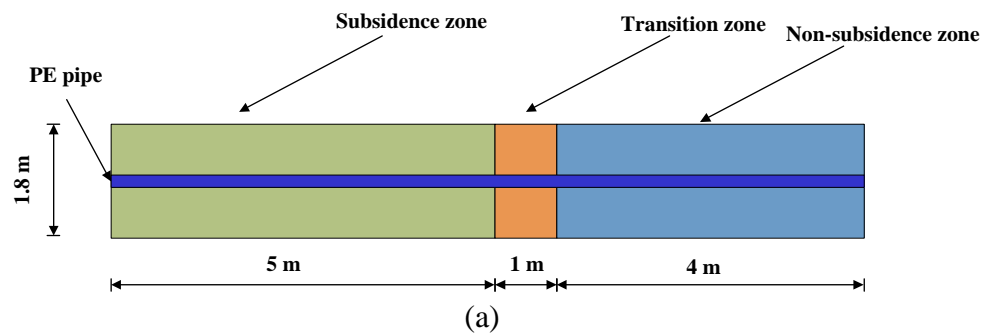
In the literature of (Luo et al., 2015), the authors' research object is the stress analysis of plastic pipes under foundation settlement. They divided the whole model into

three zones along the axis direction of the pipeline: subsidence zone (5 m), transition zone (1 m), and non-subsidence zone (4 m). The soil in the subsidence area has a settlement of 0.5 m along the gravity direction. At a position of approximately 1 m below the ground surface, there is a PE pipe with an outer diameter of 110 mm and an internal pressure of 0.4 MPa.

3.4.2 Finite Element Analysis

3.4.2.1 Geometric model

As shown in **Figure 3-2**, based on the data and conditions, in this dissertation, the geometric model of FEA is established. The entire pipe-soil system along the axial direction of the pipe is divided into three zones: subsidence zone, transition zone, and non-subsidence zone, their lengths are 5 m, 1 m, and 4 m, respectively. Geometric dimensions of soils are 3 m × 1.8 m × 10 m (width × height × length). A PE pipe with an outer diameter of 110 mm and a wall thickness of 10 mm is buried in the center of the soil body. Since the model is symmetrical in geometric shape, only need to build half of the model for saving calculations, that is, the soil size is 1.5 m × 1.8 m × 10 m (width × height × length). Therefore, the geometric model established by the SpaceClaim software⁵ is shown in **Figure 3-3**.



⁵ SpaceClaim is a software for sketching, which is embedded in ANSYS 2019.

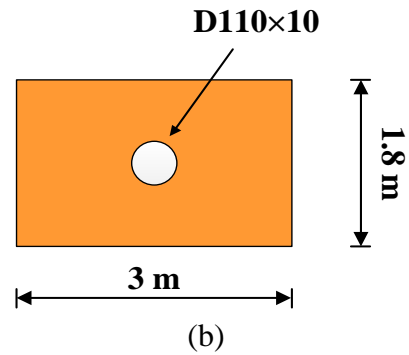


Figure 3-2: The geometric model of the pipeline in the case of foundation settlement. (a) axial view along the pipe; (b) longitudinal profile view.

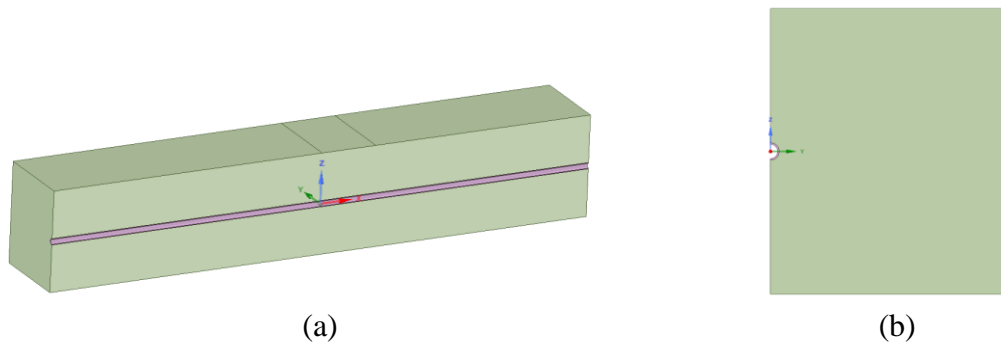


Figure 3-3: The geometric model of the pipeline in the case of foundation settlement. (a) axial view along the pipe; (b) longitudinal profile view.

3.4.2.2 Material properties

The materials required for FEA include two types, one is soil material and the other is pipeline material. The properties of the soil are shown in **Table 3-5**, the geometry and material properties of PE pipe are shown in **Table 3-6**.

Table 3-5: Parameters of the plastic pipe.

Parameter	Value
Pipe size (diameter×thickness)	110 mm × 10 mm
Material	PE80
Elastic modulus	1115 MPa
Yield tensile strength	15.4 MPa
Poisson's ratio	0.45
Density	951 kg/m ³

Table 3-6: Parameters of the soil.

Properties	Value
Deformation modulus	0.2 MPa
Poisson's ratio	0.40
Internal friction angle for Drucker–Prager criterion	28.7°
Dilatancy angle of soil	0°
Internal friction angle	18.4°
Cohesion	29300 Pa
Density	1867.3 kg/m ³

3.4.2.3 Soil model: Drucker-Prager model

As mentioned in **Section 3.3**, in soil mechanics, two commonly used yield criteria are Drucker-Prager yield criterion and Mohr-Coulomb yield criterion (Alejano and Bobet, 2012). The practice proves that the Drucker-Prager yield criterion is more suitable for the soil model. It can be expressed as

$$\sqrt{J_2} - \lambda I_1' + \kappa = 0 \quad \text{Eq. 3-3}$$

where λ and κ denote material constants; I_1' denotes the first invariant of the stress tensor; J_2 denotes the second invariant of the stress deviator tensor.

$$I_1' = \sigma_1' + \sigma_2' + \sigma_3' \quad \text{Eq. 3-4}$$

$$J_2 = \frac{1}{6} [(\sigma_1' - \sigma_2')^2 + (\sigma_1' - \sigma_3')^2 + (\sigma_3' - \sigma_1')^2] \quad \text{Eq. 3-5}$$

where σ_1' , σ_2' and σ_3' denote the principal effective stresses.

When expressed by octahedral shear stress τ_{oct} and octahedral normal stress σ'_{oct} , the form of the criterion is

$$\tau = \sqrt{\frac{2}{3}} (3\lambda\sigma'_{oct} + \kappa) \quad \text{Eq. 3-6}$$

where $\sigma'_{oct} = \frac{1}{3}I_1'$ and $\tau_{oct} = \frac{\sqrt{6}}{3}\sqrt{J_2}$.

According to the data in the literature, the soil uses the Drucker-Prager criterion, which needs to be implemented by the command stream in the ANSYS Workbench software. The input command stream is shown in **Appendix 1**.

3.4.2.4 Mesh type

Typical meshes include two-dimensional meshes and three-dimensional meshes, as shown in **Figure 3-4**. Two-dimensional meshes can be divided into triangular meshes

and quadrilateral meshes. Three-dimensional meshes can be divided into tetrahedron, hexahedron, pyramid and prism (Lyu, 2012).

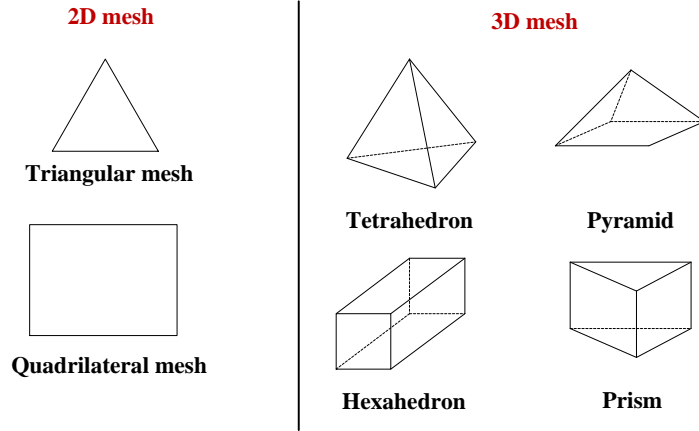


Figure 3-4: Commonly used two-dimensional and three-dimensional meshes.

Three-dimensional models are established in this dissertation, so this section focuses on the three-dimensional meshes. Tetrahedral mesh is unstructured mesh, hexahedral mesh is usually structured mesh, pyramid is the transition between tetrahedron and hexahedral, prism is usually formed by stretching tetrahedron mesh. In this section, two kinds of tetrahedral meshes and one kind of hexahedral mesh are introduced, as shown in **Figure 3-5**.

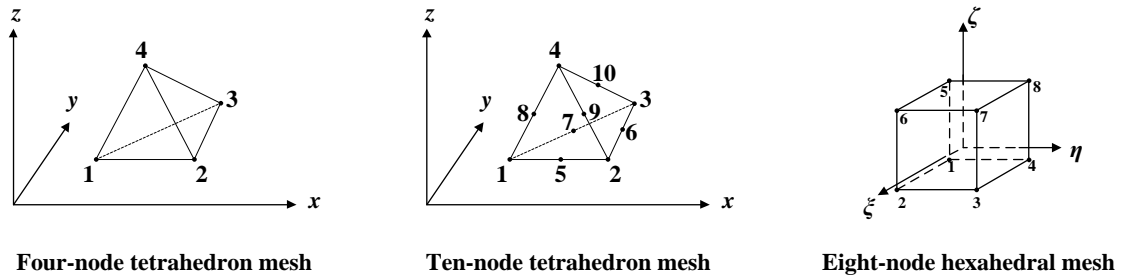


Figure 3-5: Three kinds of meshes.

(1) Four-node tetrahedron mesh

The displacement modes of each node in four-node tetrahedral element are as follows

$$\begin{cases} u = a_1 + a_2x + a_3y + a_4z \\ v = b_1 + b_2x + b_3y + b_4z \\ w = c_1 + c_2x + c_3y + c_4z \end{cases} \quad \text{Eq. 3-7}$$

The shape function is

$$N_i = \frac{1}{6V}(a_1 + b_ix + c_iy + d_iz), i = 1, \dots, 4 \quad \text{Eq. 3-8}$$

where V represents element volume.

(2) Ten-node tetrahedron mesh (Wang et al., 2018)

The displacement modes of each node in ten-node tetrahedral element are as follows

$$\begin{cases} u = a_1 + a_2x + a_3y + a_4z + a_5xy + a_6yz + \\ \quad a_7xz + a_8x^2 + a_9y^2 + a_{10}z^2 \\ v = b_1 + b_2x + b_3y + b_4z + b_5xy + b_6yz + \\ \quad b_7xz + b_8x^2 + b_9y^2 + b_{10}z^2 \\ w = c_1 + c_2x + c_3y + c_4z + c_5xy + c_6yz + \\ \quad c_7xz + c_8x^2 + c_9y^2 + c_{10}z^2 \end{cases} \quad \text{Eq. 3-9}$$

The shape function based on natural coordinate system is

$$N_i = (2L_i - 1)L_i, i = 1, \dots, 4 \quad \text{Eq. 3-10}$$

(3) Eight-node hexahedral mesh

The displacement modes of each node in eight-node hexahedral element are as follows

$$\begin{cases} u = a_1 + a_2x + a_3y + a_4z + a_5xy + a_6yz + a_7xz + a_8xyz \\ v = b_1 + b_2x + b_3y + b_4z + b_5xy + b_6yz + b_7xz + b_8xyz \\ w = c_1 + c_2x + c_3y + c_4z + c_5xy + c_6yz + c_7xz + c_8xyz \end{cases} \quad \text{Eq. 3-11}$$

The shape function is

$$\begin{cases} N_i = 0.125(1 + \xi_0)(1 + \eta_0)(1 + \zeta_0) \\ \xi_0 = \xi_i\xi, \eta_0 = \eta_i\eta, \zeta_0 = \zeta_i\zeta, i = 1, \dots, 8 \end{cases} \quad \text{Eq. 3-12}$$

where ξ_i , η_i and ζ_i represent unit coordinates of eight nodes.

Tetrahedral and hexahedral meshes belong to solid elements, they have first and second order elements. Tetrahedral mesh has good adaptability to complex geometry, it is mostly used for free mesh generation and can generate meshes quickly. However, under the same size, the accuracy of the results is worse than that of the hexahedron, so higher-order elements are needed, which leads to a larger amount of calculation. Hexahedral meshes are usually used for dynamic analysis because of their relatively small computational scale. However, this requires more time for geometric simplification and cutting, resulting in a longer generation time.

In this dissertation, solid models are used for soil and pipeline. To ensure the accuracy of calculation, most of the meshes are hexahedron meshes. Therefore, in the early stage, it is necessary to set the size of the meshes and refine the meshes around the pipelines, as shown in **Figure 3-6**. The mesh uses first-order linear element, the overall model has a total of 9366 nodes and 7346 elements.

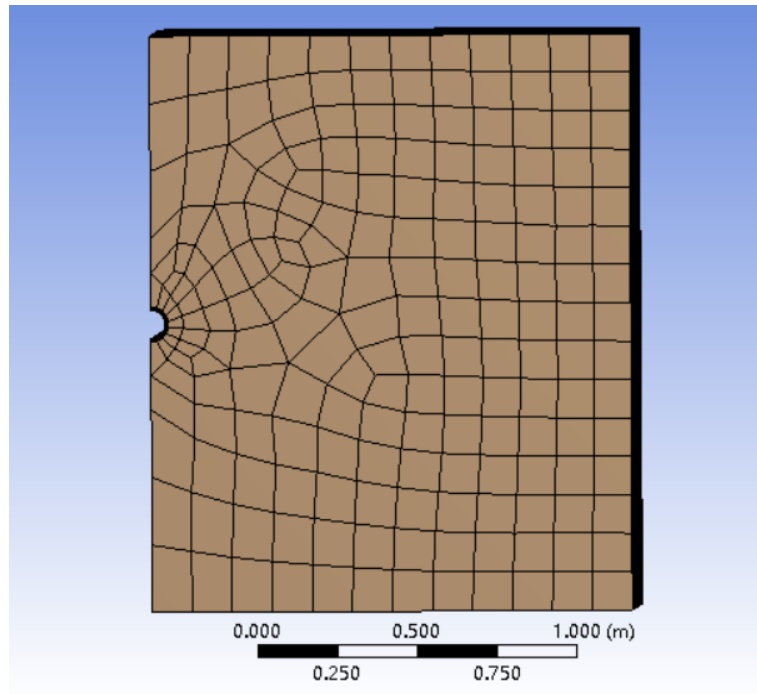


Figure 3-6: The mesh results of this case using Workbench software.

3.4.2.5 Load and boundary conditions

According to the data in the literature (Luo et al., 2015), the upper part of the soil is free boundary, the vertical surface and the bottom surface of the non-subsidence zone are fixed constraints, and the other surfaces are constrained in the horizontal direction, as shown in **Figure 3-7**. In addition, the soil in the subsidence zone has a remote displacement vertically downward with a displacement of 0.5 m. The inner wall of the pipe is subjected to a pressure of 0.4 MPa, and the overall model is subjected to gravity (the gravitational acceleration is 9.8066 m/s^2).

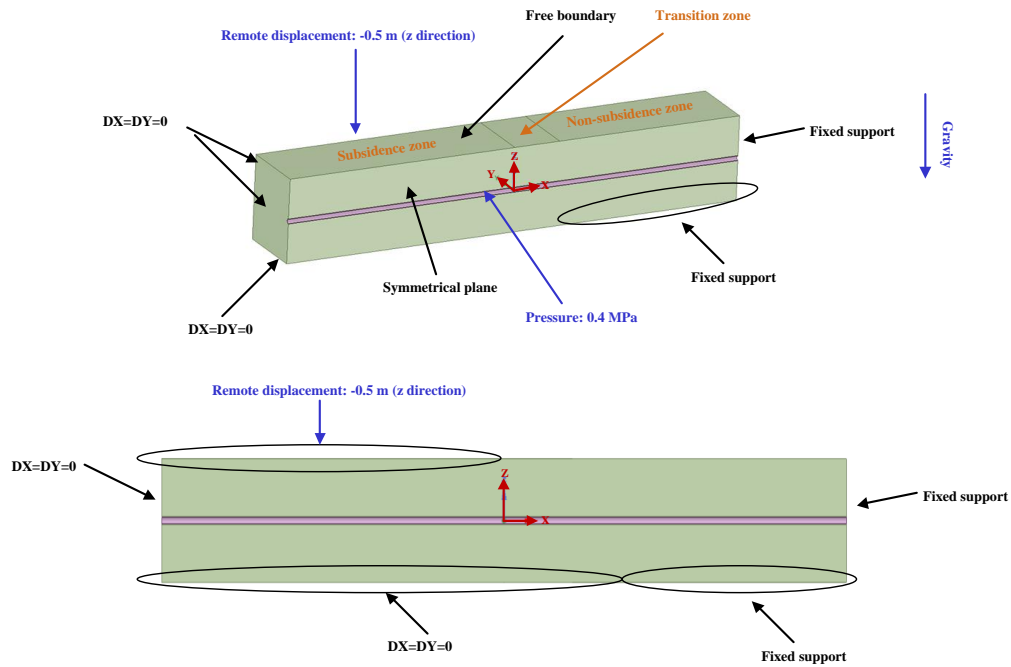
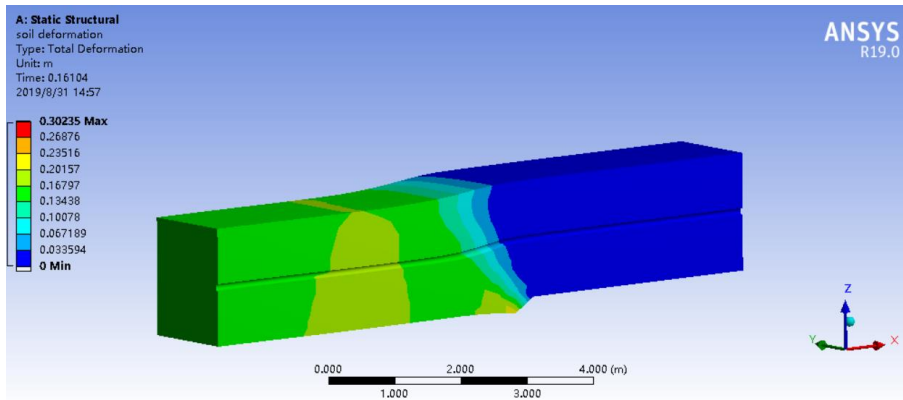


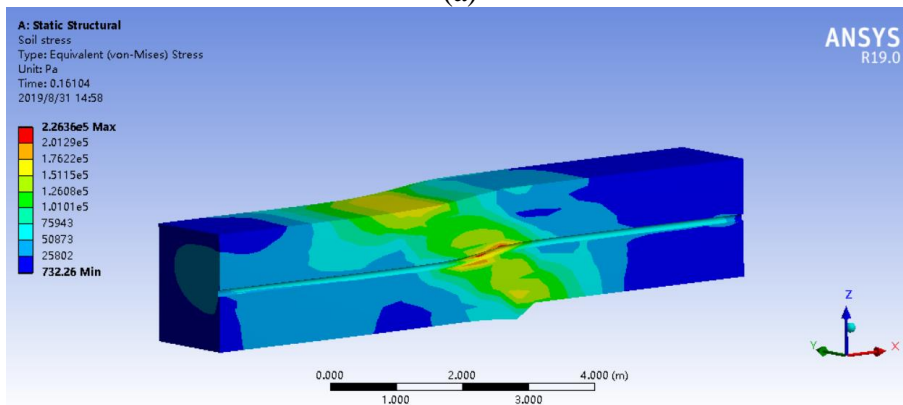
Figure 3-7: Boundary conditions and loads.

3.4.2.6 Results and comparison

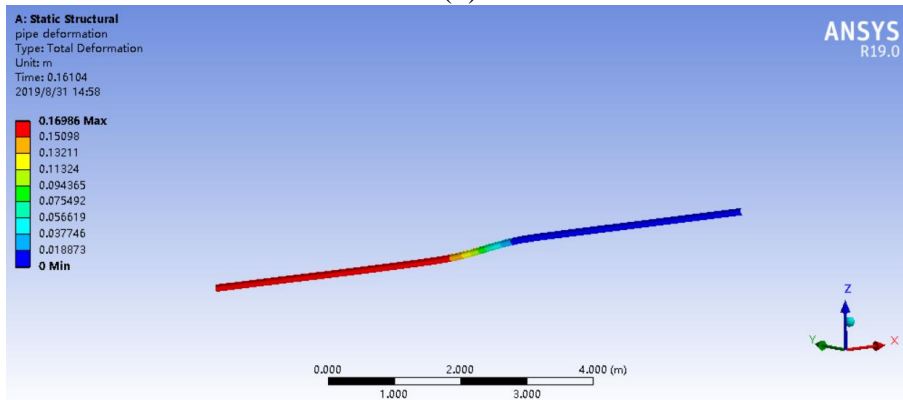
After all the settings are completed, four results are output: deformation and stress of the soil and deformation and stress of the pipe, as shown in **Figure 3-8**. It reveals that the maximum deformation of the soil is 0.30235 m, the maximum deformation of the pipeline is 0.16986 m, the maximum stress of the soil is 0.22636 MPa, and the maximum stress of the pipeline is 14.094 MPa. In the literature (Luo et al., 2015), when the settlement is 0.5 m, the maximum stress of the pipeline obtained by the authors is about 14 MPa (there is no specific value in the paper, only a broken line diagram). Therefore, it can be concluded that although a different meshing method and a different geometric model are adopted compared with the published paper, the results of the model established by ANSYS Workbench software have a high reliability.



(a)



(b)



(c)

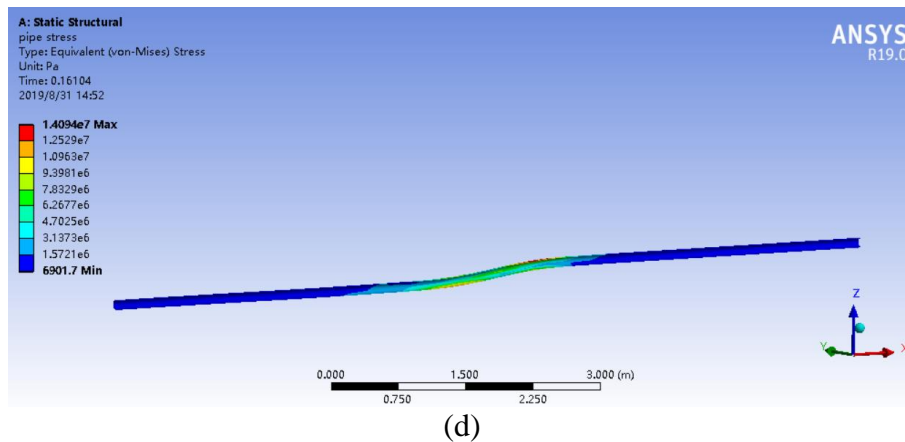


Figure 3-8: Simulation results. (a) soil deformation; (b) soil stress; (c) pipe deformation; (d) pipe stress.

3.5 Summary

In this chapter, the theory of FEA is briefly introduced, and the ANSYS Workbench software is selected as the tool for simulation. In order to verify the reliability of the pipeline stress analysis model, ANSYS Workbench software is used to simulate the relevant research in the existing paper (a pipeline stress analysis case under foundation settlement condition). The geometric model, material property, soil model, mesh, boundary condition, and load are introduced in detail. The simulation results are very little different from those in the literature. It shows that the model established by ANSYS Workbench software has high reliability. Therefore, similar methods will be used in the follow-up studies in this dissertation.

CHAPTER 4

STRESS ANALYSIS OF THE OPERATING GAS PIPELINE INSTALLED BY HDD

4.1 Foreword

In this chapter, the stress of an operating gas pipeline installed by HDD is studied. Firstly, the basic information of an HDD project crosses the Yangtze River in China is introduced. Then, the geometric model is established, and the stress analysis is carried out with Workbench software. In addition, by adjusting the design parameters of the pipeline and the soil, the sensitivity of each parameter is analyzed.

4.2 Project Overview

The real project studied in this dissertation is in China. The Yangtze River crossing area of Nanjing Branch of Sichuan-East Gas Pipeline Project is from the Sanjiangkou of Jing'an Town, Qixia District, Nanjing to the south of Qingshan Town, Yizheng City (see **Figure 4-1**). The main pipeline adopts longitudinal submerged arc welded (LSAW) steel pipe with 813 mm diameter and 15.9 mm wall thickness. The transmission pressure of the pipeline is 6.4 MPa. The soil of the main channel crossing project is mainly silty sand, and the crossing length is 1809.8 m (the crossing path is shown in **Figure 4-2**).



Figure 4-1: Construction site of Yangtze River main channel crossing project.

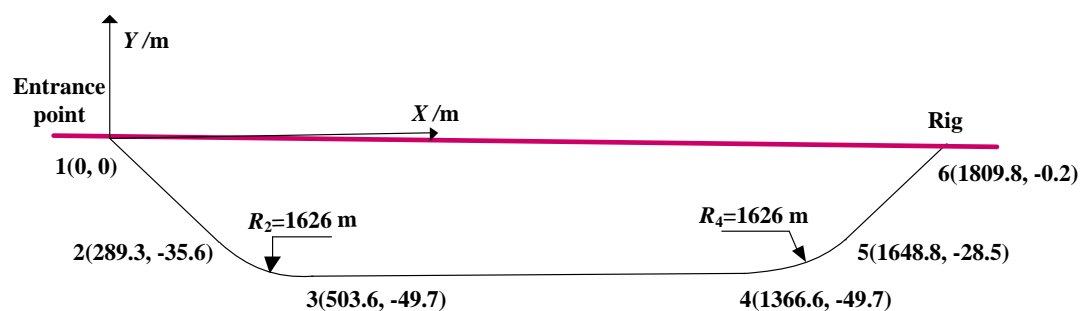


Figure 4-2: The crossing path of main channel crossing project.

4.3 Preliminary Analysis of the Project After Construction

When installing pipelines by HDD method, to ensure the smooth pulling of pipelines, the diameter of boreholes is usually larger than that of pipelines, and it is about 1.2–1.5 times of the pipeline diameter. Therefore, after the pipeline installation, an annulus will be formed between the borehole wall and the pipeline. The annulus is filled with a mixture of mud (drilling fluid) and drilling cuttings. It has the characteristics of high water content and high sediment (solids) content, and its strength is much smaller

than the surrounding soil. At this time, the mud has fluidity, and will generate hydrostatic pressure on the pipeline and borehole wall (Case 1). However, after a certain period of time, the mud will gradually dry up, that is, lose liquidity. At this point, the pipeline is no longer subject to hydrostatic pressure, and the bottom of the pipeline will closely adhere to the bottom of the borehole. In addition, a layer of mud cake will be formed around the borehole wall, which can increase the stability of the borehole wall (Case 2). In fact, the situation after HDD project construction is very complex. If the borehole wall is unstable, it will lead to other situations, for example, if a borehole collapses, the soil in the upper part will squeeze the pipe. It is assumed that the stability of the borehole wall is high and there is no other complex situation in this dissertation. Therefore, in this chapter, the stress of the pipeline is analyzed for these two cases. **Figure 4-3** and **Figure 4-4** present the physical models of these two cases.

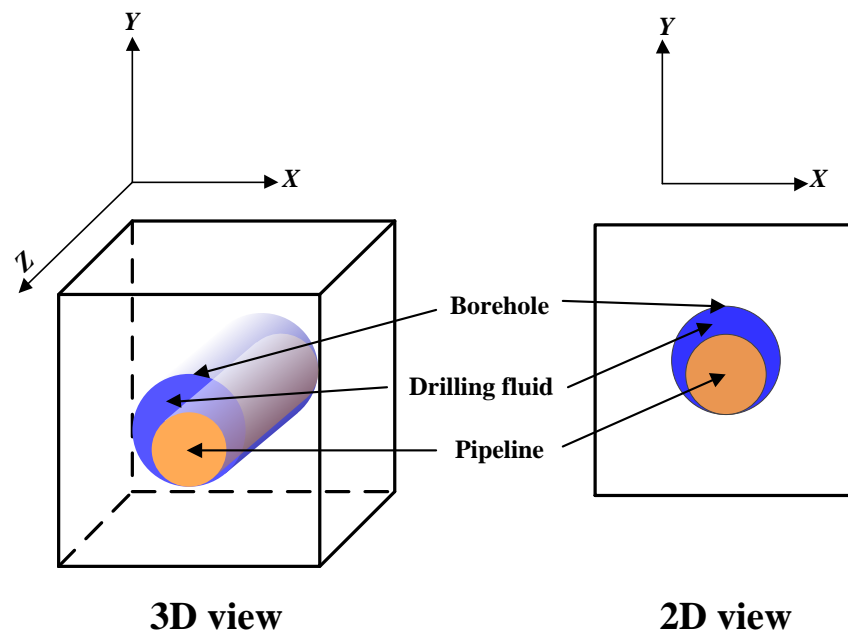


Figure 4-3: Physical model of Case 1.

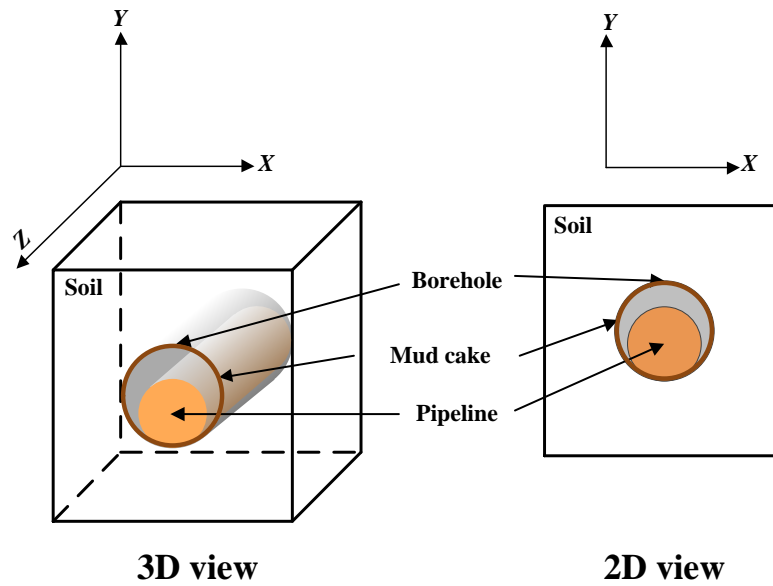


Figure 4-4: Physical model of Case 2.

4.4 Finite Element Analysis

In this section, the pipe stress under two cases is analyzed, and the more dangerous case can be determined by comparing the results.

4.4.1 Case 1

4.4.1.1 Geometric model

The establishment of geometric model is the basis of FEA. The principle of its establishment is the same as the reality as far as possible, but sometimes it needs to simplify the model for reducing the calculation. In this case, the size of the pipe is 813 mm \times 15.9 mm (diameter \times thickness), and the diameter of the borehole is 1219.5 mm. According to Saint Venant's principle (Toupin, 1965), the soil far away from the object has little influence on the analysis, so the width and height of the soil are set at about 11 times the diameter of the borehole, which is 14 m. According to **Figure 4-3** or **Figure 4-4**, it can be implied that the analysis object is symmetrical on the X -axis. In order to save

computing power, only half of the models for soil and pipeline are needed. In addition, the length of the pipe is taken as 10 m in this dissertation. Therefore, the size of the whole model is 7 m \times 10 m \times 14 m (width \times length \times height). The geometric model built with DesignModeler⁶ software is shown in **Figure 4-5**.

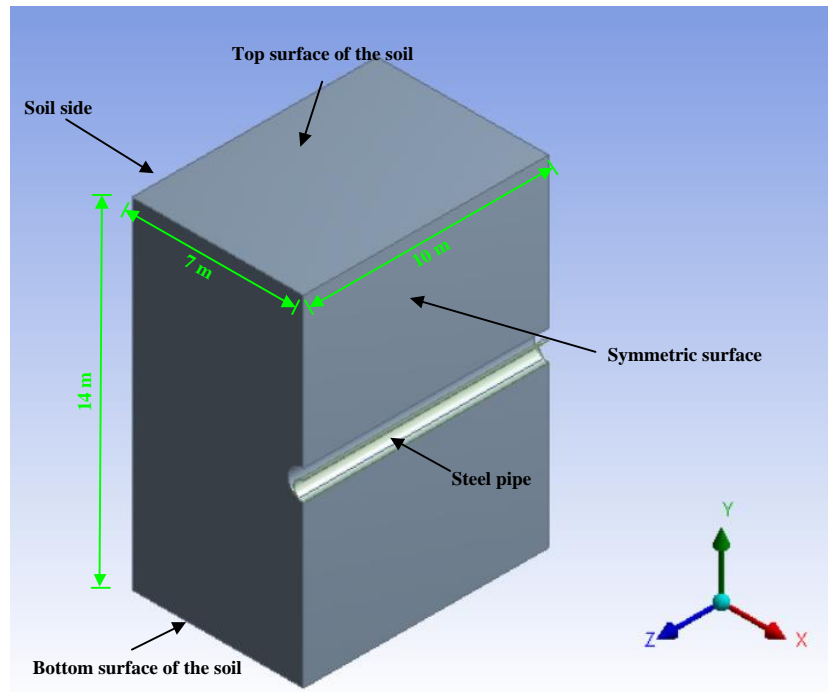


Figure 4-5: Pipeline-soil geometric model (Case 1) established by DesignModeler software.

4.4.1.2 *Material properties*

In Case 1, mechanical properties of pipe and soil need to be set, as shown in **Table 4-1** and **Table 4-2**, respectively. Drucker-Prager model is used for soil, which can be closer to the actual situation.

⁶ DesignModeler is a software for sketching, which is embedded in ANSYS 2019.

Table 4-1: Parameters of the steel pipe.

Parameter	Value
Outer diameter (OD)	813 mm
Wall thickness	15.9 mm
Material	LSAW steel
Elastic modulus	210 GPa
Bulk modulus	175 GPa
Shear modulus	80.769 GPa
Poisson's ratio	0.3
Density	7850 kg/m ³

Table 4-2: Parameters of the soil.

Properties	Value
Poisson's ratio	0.2
Elastic modulus	42 MPa
Dilatancy angle of soil	4.83°
Internal friction angle	9.65°
Density	2500 kg/m ³
Cohesion of soil	12.94 kPa

4.4.1.3 Contact model

In ANSYS Workbench, there are five types of contact, including bonded, no separation, frictionless, rough, and frictional (özgün, 2018). Their characteristics and applications are shown in **Table 4-3**.

Table 4-3: Five contact types in ANSYS Workbench.

Contact type	Feature	Applications
Bonded	There is no tangential sliding and normal separation between the contact surfaces	Suitable for all contact areas
No separation	There is no normal separation between the contact surfaces, and there may be a small amount of frictionless sliding	Similar with bonded contact
Frictionless	When tangential relative slip occurs, there is no friction	Similar with bonded contact
Rough	There can only be static friction and no sliding	Very rough contact
Frictional	The two contact surfaces can be either normal separation or tangent sliding	Frictional contact

In Case 1, there is only one contact involved in the model: contact between the inner wall of the borehole and the outer wall of the pipe. Since the bottom of the pipe is in contact with the bottom of the borehole, that is, the normal direction is not separated, the tangential direction may have a small sliding, so that the “frictional” contact is used,

as shown in **Figure 4-6**. According to actual engineering data, the coefficient of friction between the pipeline and the soil is 0.24.

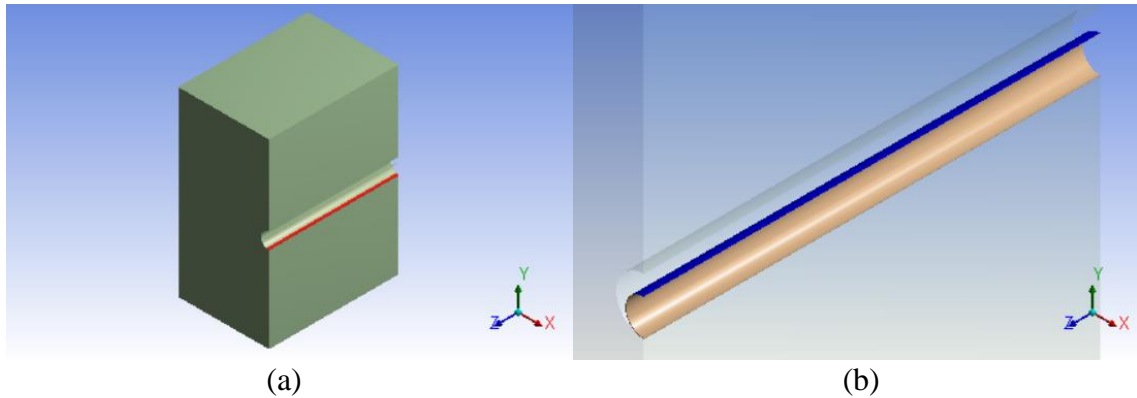


Figure 4-6: Contact between the inner wall of the borehole and the outer wall of the pipe. (a) contact body; (b) target body.

4.4.1.4 *Loads*

In Case 1, there are three types of loads. First, the entire pipeline-soil system is subject to gravity. The direction of gravity acceleration is vertical downward ($-Y$), and the acceleration of gravity is 9.8066 m/s^2 . Second, according to the engineering data, the inner wall of the pipeline is subject to a pressure of 6.4 MPa. For a pipe with a circular cross section, the direction of pressure is from the center of the circle to the inner wall surface of the pipe, as shown in **Figure 4-7**.

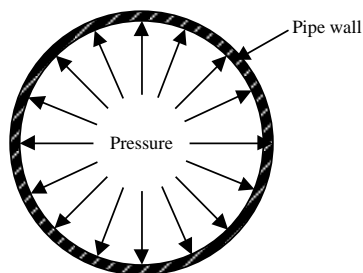


Figure 4-7: Direction of action of internal pressure on pipeline.

Finally, since the gap between the borehole and the pipeline is filled with drilling fluid, the outer surface of the pipeline and the borehole wall are also subject to hydrostatic pressure. Because both the borehole wall and the pipe wall are curved surfaces, it is necessary to use the theory of fluid mechanics to calculate the pressure of the curved surface. The calculation principle can be found in literature (Chen, 2015):

Suppose there is a curved surface ABCD under liquid pressure, and its area is S , as shown in **Figure 4-8**.

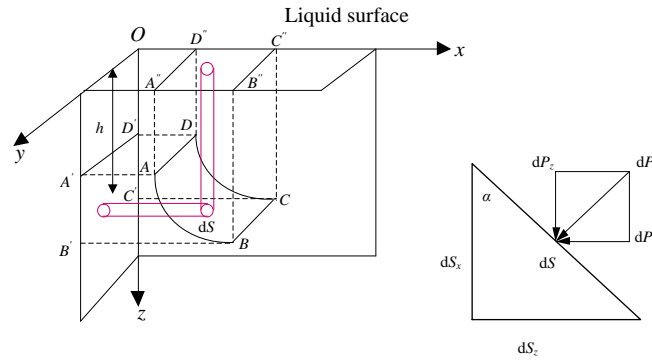


Figure 4-8: Total pressure of static liquid on curved surface.

At the depth of h , take the area dS of the microelement on the surface, and assume that the pressure on the micro area is p , then the pressure of the liquid acting on the dS is: $dP = p dS = \rho_l g h dS$ (ρ_l represents liquid density). Since the directions of the forces acting on different areas of microelements are different, the action forces can be decomposed into horizontal and vertical component forces, and the two component forces can be integrated over the entire area to obtain the total pressure.

The horizontal component force of the microelement is

$$dP_x = \rho_l g h dS \cos \alpha = \rho_l g h dS_x \quad \text{Eq. 4-1}$$

The horizontal component force of the total pressure is

$$P_x = \rho_l g h \int_S dS_x \quad \text{Eq. 4-2}$$

Similarly, the vertical component of the total pressure is

$$P_z = \rho_l g h \int_S dS_z \quad \text{Eq. 4-3}$$

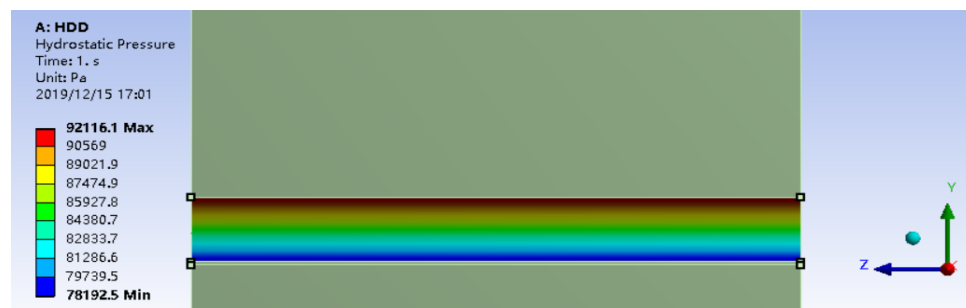
The total pressure is

$$P = (P_x^2 + P_z^2)^{0.5} \quad \text{Eq. 4-4}$$

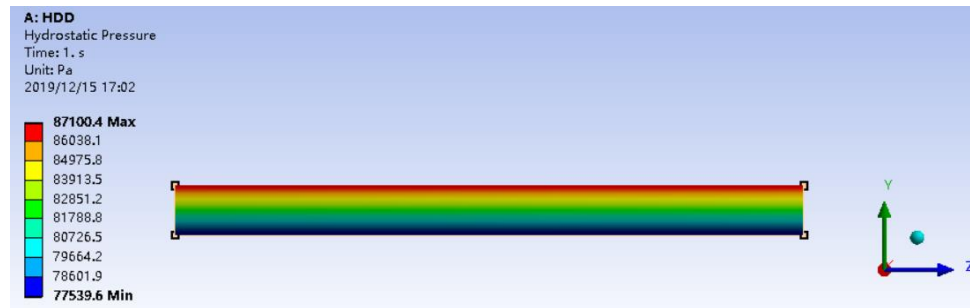
Its direction is

$$\theta = \arctan \frac{P_x}{P_z} \quad \text{Eq. 4-5}$$

In Workbench, the hydrostatic pressure of a curved surface can be calculated automatically. When the density of drilling fluid is 1200 kg/m^3 , the calculation results of the hydrostatic pressure acting on the borehole wall and the outer wall of the pipeline are shown in **Figure 4-9**. It shows that the hydrostatic pressure on the upper part of the pipeline is greater than that on the lower part. Based on the above analysis, all loads in this case are shown in **Figure 4-10**.



(a)



(b)

Figure 4-9: The hydrostatic pressure acting on the borehole wall and the outer wall of the pipe. (a) borehole wall; (b) outer wall of the pipe.

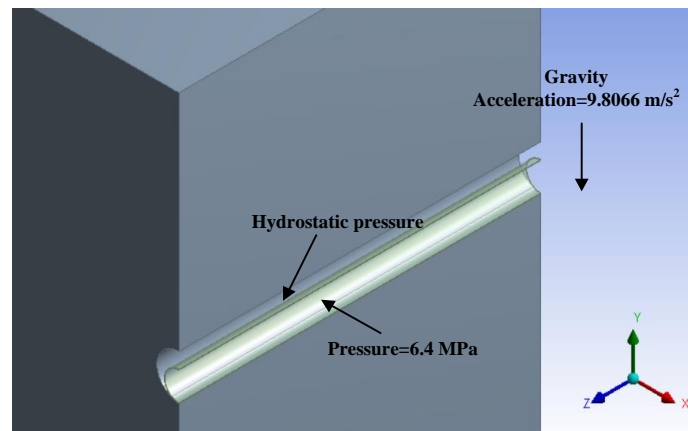


Figure 4-10: Loads for Case 1.

4.4.1.5 Boundary conditions

In Case 1, the setting of boundary conditions can be divided into two modules. First, through the literature review, the boundary conditions of the soil are similar to buried pipelines, that is, horizontal displacement constraints are added to the side of the soil, fixed constraints are added to the bottom surface, and the upper surface is a free boundary.

Secondly, special attention needs to be paid to the boundary conditions of the pipeline. The boundary conditions may be different depending on the position of the

analysis target in the entire pipeline. In this dissertation, a river-crossing pipe section is analyzed. In fact, the length of the pipe is thousands of kilometers, it is especially important to set reasonable boundary conditions. Three kinds of boundary conditions are considered: (1) completely free boundary; (2) fixed boundary; (3) horizontal displacement limited boundary. The Von-Mises stress (see **Figure 4-11**) of the pipeline is extracted along the axial direction of the pipeline, it can be seen that under fixed boundary condition and horizontal displacement limited boundary, the stress at the ends of the pipeline has a sudden change trend.

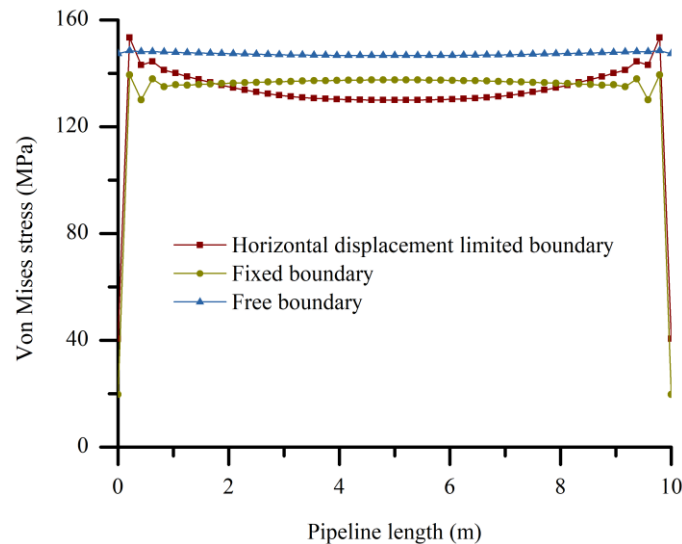


Figure 4-11: Von Mises stress along the pipeline axial with three boundary conditions.

However, it can also be seen in **Figure 4-12** that when the boundary condition is a fixed boundary, there is a significant stress concentration at both ends of the pipe. When the horizontal displacement limited boundary is utilized, stress concentration also occurs near the two ends of the pipe. Obviously, this phenomenon is not consistent with the

actual situation. Therefore, it is reasonable to use free boundaries at both ends of the pipeline. The boundary conditions of the pipe-soil system are shown in **Figure 4-13**.

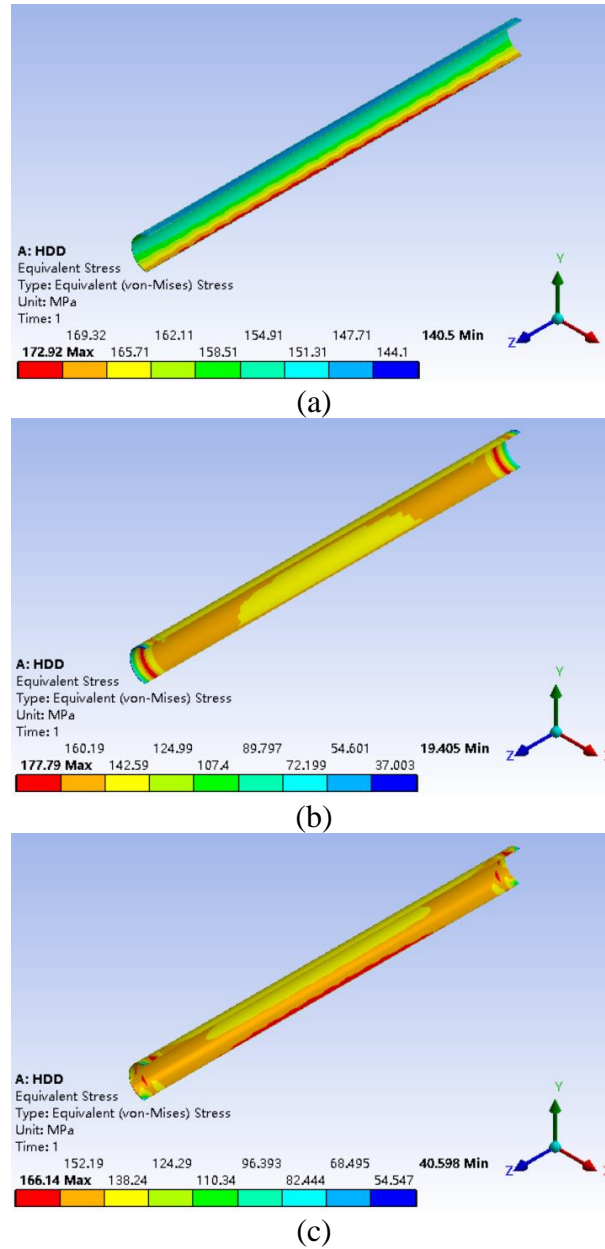


Figure 4-12: Equivalent stress nephogram of pipeline under three boundary conditions. (a) free boundary; (b) fixed boundary; (c) horizontal displacement limited boundary.

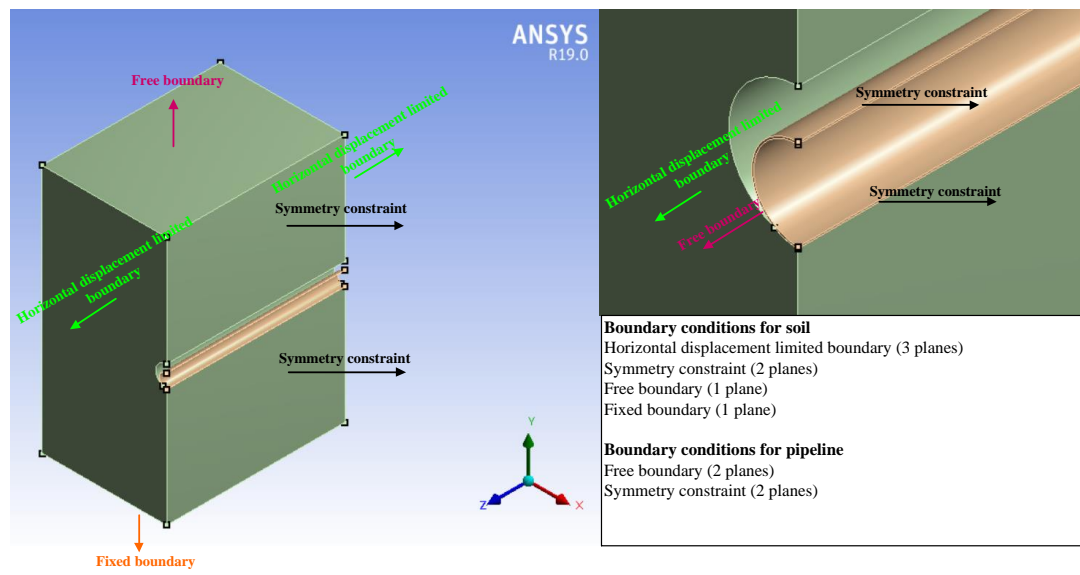


Figure 4-13: Boundary conditions of the pipeline-soil system.

4.4.1.6 Mesh and mesh independent study

It can be known from **Section 3.4.2.4** that for the FEA of pipeline engineering, it is necessary to refine the mesh around the pipeline to improve accuracy, and it is similar for borehole. **Figure 4-14** illustrates that the generated mesh is mainly hexahedron mesh, and the mesh near the pipeline and borehole is relatively dense, which shows that the quality of the mesh is high. In addition, when performing FEA, it is necessary to reduce the calculation amount under the premise of ensuring the calculation accuracy. Therefore, mesh independence study is needed. Mesh independent solution refers to the solution in which the calculation result does not change significantly when the mesh is continuously refined. In Case 1, five mesh numbers are adopted, and their calculation results are shown in **Table 4-4** and **Figure 4-15**. It implies that when the number of mesh is greater than 10000, the maximum stress of the pipeline does not change significantly, indicating that when the number of mesh is 13430, the requirements of calculation accuracy can be satisfied for Case 1.

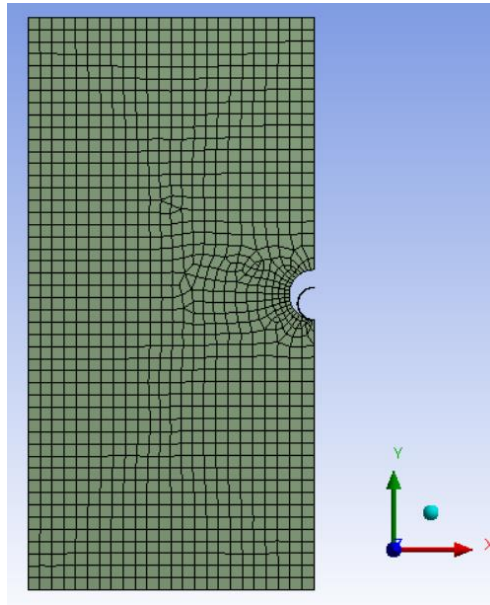


Figure 4-14: Generated mesh (Case 1).

Table 4-4: The results of mesh independent study (Case 1).

Total mesh number	Maximum stress of pipe (MPa)
7738	168.14
9390	172.67
13430	172.92
27770	173.45
48550	174.24

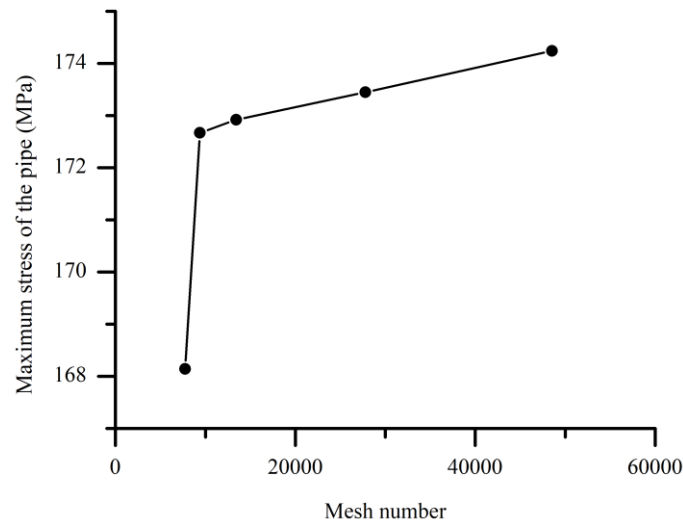


Figure 4-15: The results of mesh independent study (Case 1).

4.4.1.7 Simulation results

Figure 4-16 shows the analysis results of stress and deformation of the pipeline. Through the overall view, it reveals that the maximum stress and the minimum stress of the pipeline appear at the bottom of the pipeline, which are 172.92 MPa and 140.5 MPa, respectively. The side view shows that the stress value of the pipeline in the wall thickness direction has a large difference, and the stress of the inner wall is larger. The maximum deformation of the pipe is 34.473 mm, which appears near the contact surface between soil and pipeline. The minimum deformation is 34.098 mm, which appears in the upper half of the pipe. Thus, there is little difference between them.

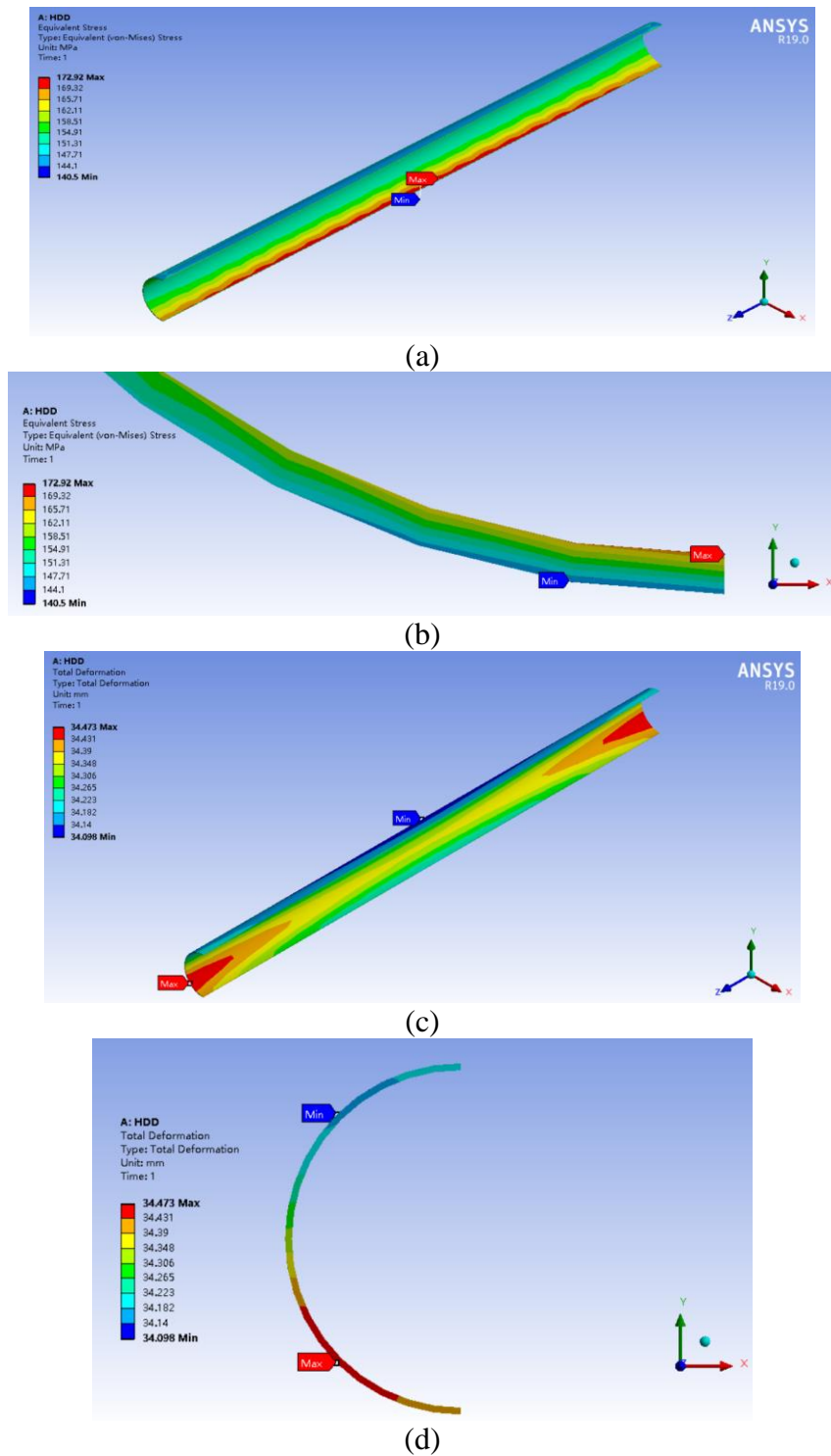


Figure 4-16: Analysis results of stress and deformation of pipe. (a) stress (overall view); (b) stress (partial view); (c) deformation (overall view); (d) deformation (side view).

4.4.2 Case 2

4.4.2.1 Geometric model

According to the same method as Case 1, the physical model of Case 2 is established. The model is slightly different from Case 1. Because the mud loses its fluidity, a mud cake is formed on the inner wall of the borehole, and its thickness is about 2 cm. There is also a large part of the drilling fluid that will seep into the crevices of the soil. Therefore, mud cake close to the borehole wall is added to the model, as shown in **Figure 4-17**. In this model, the diameter of the borehole is 1219.5 mm, the mud cake is a ring, and its outer circular surface fits snugly against the inner wall of the borehole. That is, the outer ring has a diameter of 1219.5 mm and the inner ring has a diameter of 1179.5 mm. Considering that the mud cake will be squeezed by the pipeline under gravity and the area of the pipeline bottom contacting the drilling fluid is less during the construction process, the thickness of the mud cake at the pipe bottom is 1 cm (50% thinner than elsewhere). The pipe size is same with Case 1, which is 813 mm \times 15.9 mm (diameter \times wall thickness).

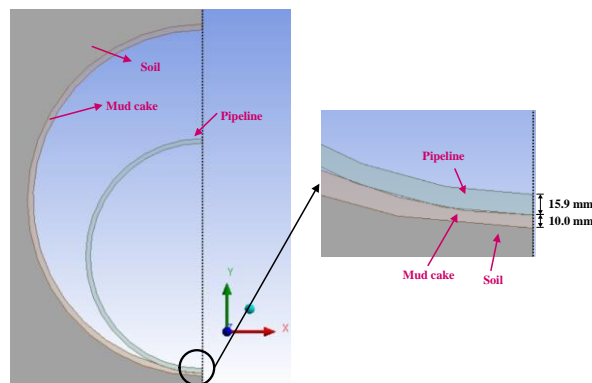


Figure 4-17: Pipeline-soil geometric model (Case2) established by DesignModeler software.

4.4.2.2 *Material properties*

In Case 2, in addition to pipeline and soil materials, mud cake materials need to be collected. Pipeline materials and soil materials are the same as Case 1 (see **Section 4.4.1.2**). The parameters of the mud cake are shown in **Table 4-5**.

Table 4-5: Parameters of the mud cake.

Parameter	Value
Outer diameter (OD)	1219.5 mm
Thickness	20 mm
Material	Mixture of mud and drilling cuttings
Elastic modulus	720 MPa
Bulk modulus	400 MPa
Shear modulus	300 MPa
Poisson's ratio	0.2
Density	1200 kg/m ³

4.4.2.3 *Contact model*

In Case 2, there are two contacts involved in the model: 1) contact between the inner wall of the borehole and the outer wall of the mud cake; 2) contact between the bottom of the pipe and the bottom of the mud cake. Since the mud cake fits snugly against the inner wall of the borehole, the contact between the inner wall of the borehole and the mud cake is set to bonded contact, as shown in **Figure 4-18**. The contact between

the mud cake and the pipe is similar to Case 1, using “frictional” contact with a friction coefficient of 0.24.

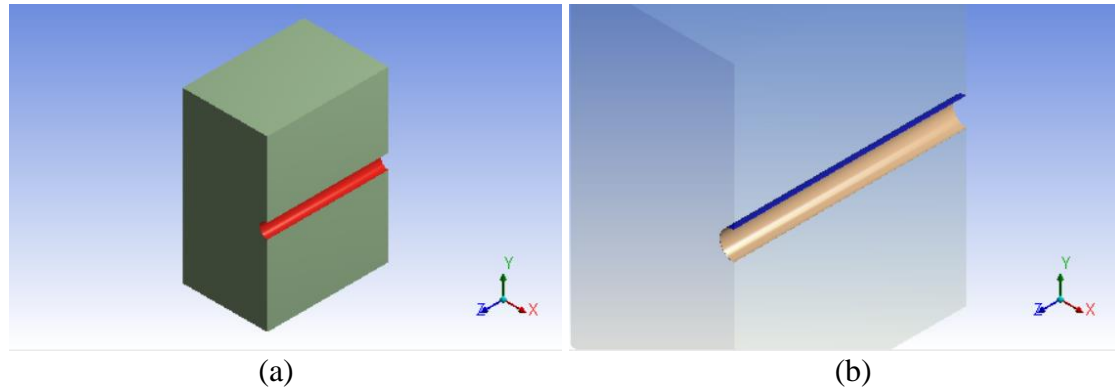


Figure 4-18: Contact between the inner wall of the borehole and the mud cake. (a) contact body; (b) target body.

4.4.2.4 *Loads and boundary conditions*

In Case 2, there are only two types of loads on the pipeline-soil system: the inner wall of the pipeline is subjected to a pressure of 6.4 MPa, and the entire system is subjected to gravity. The boundary conditions are similar to Case 1. The difference is that due to the addition of mud cake, additional symmetry constraints need to be established.

4.4.2.5 *Mesh and mesh independent study*

The mesh generation method is the same as Case 1 (see **Figure 4-19**), the mesh independent study results are shown in **Table 4-6**. It reveals that there is no significant difference in the maximum stress of the pipeline under different mesh density. In this dissertation, the model with 13675 meshes is selected.

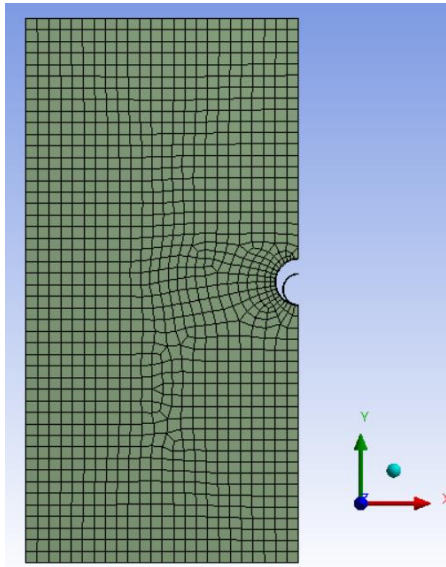


Figure 4-19: Generated mesh (Case 2).

Table 4-6: The results of mesh independent study (Case 2).

Total mesh number	Maximum stress of pipe (MPa)
10346	167.44
13675	167.84
14489	167.33
19740	167.39

4.4.2.6 Simulation results

Figure 4-20 shows the stress and deformation for the pipe. The maximum stress of the pipe is 167.84 MPa, it appears on the inside of the pipe bottom. The maximum deformation is 35.386 mm, it appears at the bottom of the pipe.

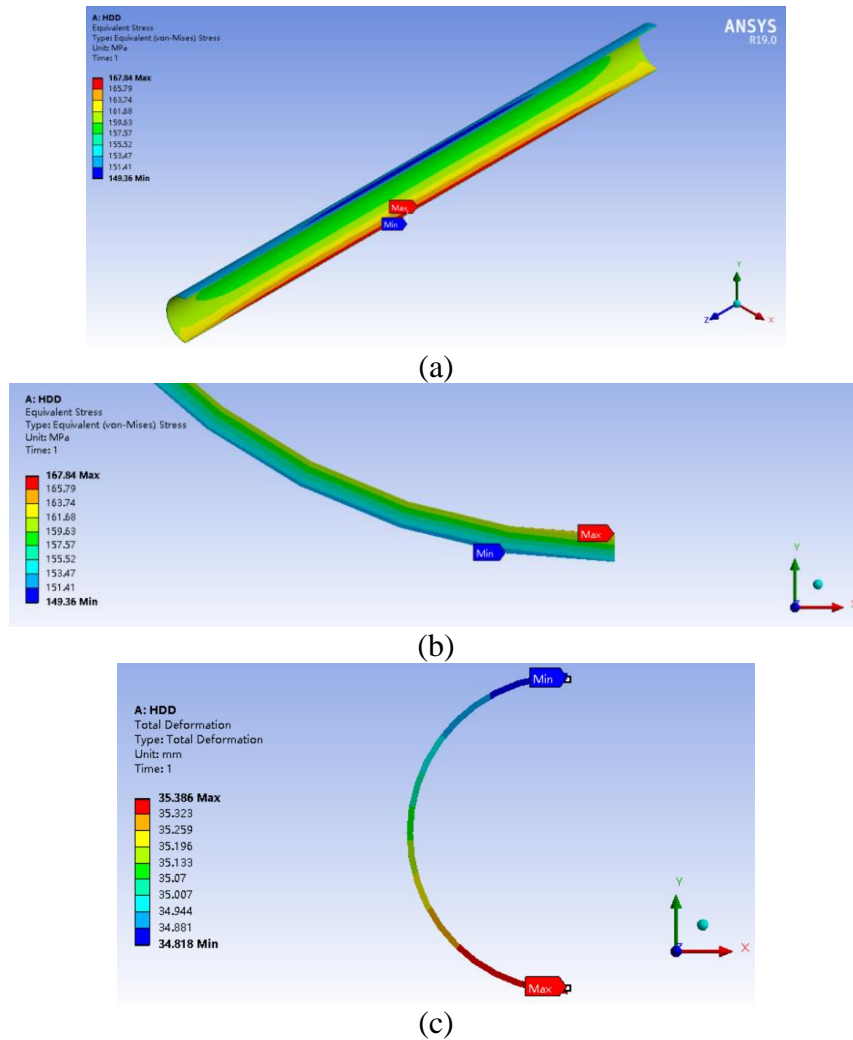


Figure 4-20: Analysis results of stress and deformation of pipe. (a) stress (overall view); (b) stress (partial view); (c) deformation (side view).

4.5 Discussions

The discussion of this chapter includes four aspects. (1) two cases in **Section 4.4** are compared; (2) the stress of pipeline installed by HDD method and open-cut method is compared; (3) the parameters of various design factors of pipeline are analyzed; (4) the stress sensitivity of pipeline installed by HDD method is analyzed.

4.5.1 Comparison of Case 1 and Case 2

Table 4-7 summarizes the maximum stress and maximum deformation of pipe in Case 1 and Case 2. It reveals that the maximum stress of the pipeline in Case 1 is higher than that in Case 2, but the maximum deformation is slightly smaller than that in Case 2. It shows that when the annulus is filled with drilling fluid (that is, shortly after the completion of the pipeline construction), the pipeline operation is more dangerous. Therefore, Case 1 is used as a prototype in the subsequent influencing factors analysis. The deformation of the pipeline in Case 1 is slightly smaller than that in Case 2. This may be because the hydrostatic pressure and buoyancy of the drilling fluid in the annulus reduce the influence of gravity on the deformation of the pipeline.

Table 4-7: Stress and deformation comparison of Case 1 and Case 2.

Case	Description	Maximum stress of the pipe (MPa)	Maximum deformation of the pipe (mm)
1	The annulus between the borehole and the pipe is filled with drilling fluid	172.92	34.473
2	There is a layer of mud cake on the inner wall of the borehole	167.84	35.386

4.5.2 Comparison of HDD Method and Open-cut Method

In addition to the HDD method, river-crossing pipeline construction can also be carried out by open-cut method. Open-cut method for pipeline installation across rivers requires cofferdam diversion, drainage and silt removal, trench excavation, backfilling and other operations. It not only has huge workload and more carbon emissions, but also destroys the original balance of the formation, making the external load of the pipeline

more uneven. Therefore, in order to highlight the advantages of the HDD method in mechanical design over the traditional open-cut method, in this dissertation, the stresses of the pipes installed by the HDD method and the open-cut method are compared. Unlike HDD method, the borehole diameter is equal to the outer diameter of the pipeline for open-cut method. That is, the inner wall of the borehole is closely connected with the outer wall of the pipeline (see **Figure 4-21**).

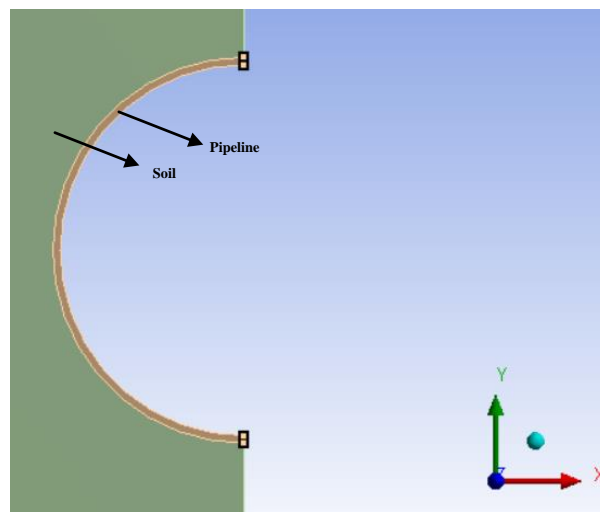


Figure 4-21: Pipe-soil system of the open-cut method.

According to **Figure 4-22**, it reveals that the stress distribution of the pipeline installed by the open-cut method is similar to that of the pipeline installed by the HDD method, but the maximum stress is 197.84 MPa. In addition, it can be known from the stress nephogram that the fluctuation range of stress is large. However, under the same conditions, the maximum stress of the pipeline installed by HDD method is 172.92 MPa, which is relatively reduced by 12.6%.

The maximum deformation of the pipeline installed by the open-cut method is 39.318 mm, which appears at the top of the pipeline, which is different from that of the

pipeline installed by the HDD method. The maximum deformation of the pipeline installed by HDD method is 35.386 mm, which is 10% lower than that of open-cut method.

In conclusion, the stress distribution law of the pipeline installed by HDD method is similar to that of open-cut method, but the deformation law is different, which may be due to the large squeezing effect of the soil on the upper part of the pipeline in open-cut method. Moreover, the stress and deformation of the pipeline installed by HDD method are less than that of open-cut method, which proves that the pipeline installed by HDD method is safer in operation.

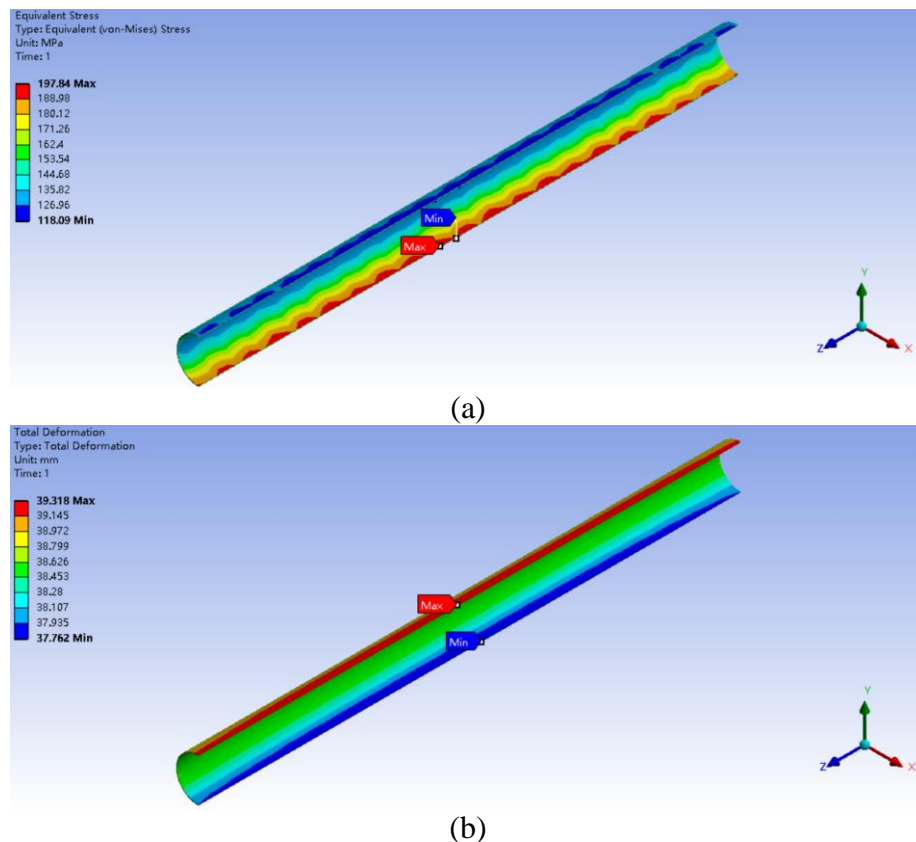


Figure 4-22: Stress and deformation of the pipe installed by traditional open-cut method. (a) stress; (b) deformation.

4.5.3 Influencing Factors Analysis

In this section, the influencing factors of the pipeline stress are analyzed, so as to provide the basis for the pipeline design. Six influencing factors are considered: pipe diameter, wall thickness, buried depth, pressure, soil type, and drilling fluid density. Among them, the factors of soil type, such as internal friction angle and density, need to be considered. Because Case 1 is more dangerous than Case 2, the pipeline of Case 1 is used as the analysis object.

4.5.3.1 Diameter

To keep other conditions of the pipeline unchanged, pipes with diameters from 660 mm to 1168 mm are selected as the analysis object according to the steel pipe standard (China National Petroleum Corporation, 1997). The simulation results are shown in **Figure 4-23**. It reveals that the maximum stress of the pipeline and the diameter of the pipeline basically increase linearly.

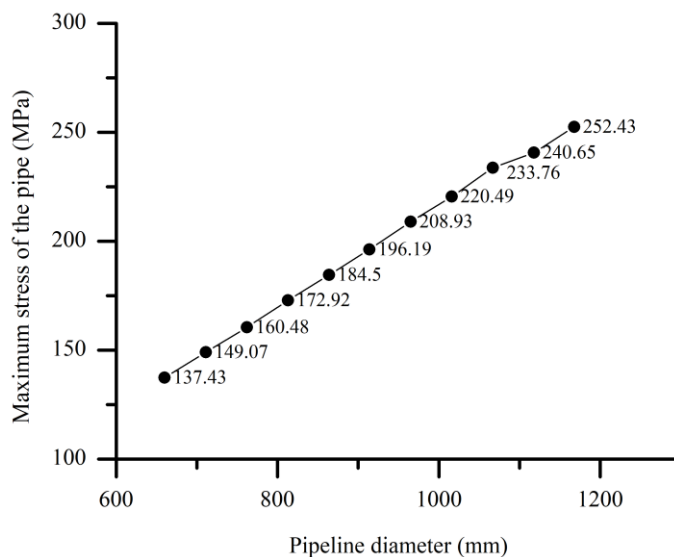


Figure 4-23: Curve of maximum pipe stress and pipe diameter.

4.5.3.2 Thickness

Keeping other conditions unchanged, pipes with different wall thicknesses are selected as analysis objects, and the wall thickness range is from 11.1 mm to 19.1 mm. The simulation results are shown in **Figure 4-24**. It can be seen that as the wall thickness increases, the maximum stress of the pipeline decreases. However, they are not linearly related.

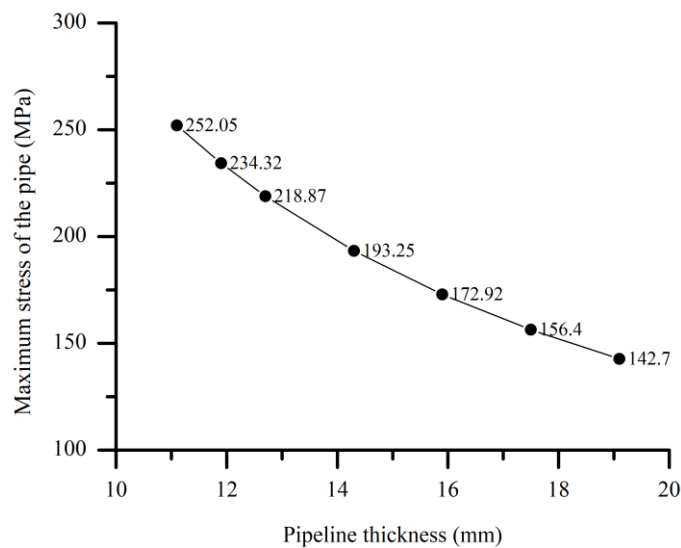


Figure 4-24: Curve of maximum pipe stress and pipe thickness.

4.5.3.3 Buried depth

In this section, the depth of the pipeline is adjusted, and stress analysis is performed. As shown in **Figure 4-25**, the maximum stress of the pipeline is on the rise as a whole with the increase of the depth, but in some positions, the maximum stress is slightly decreased with the increase of the depth.

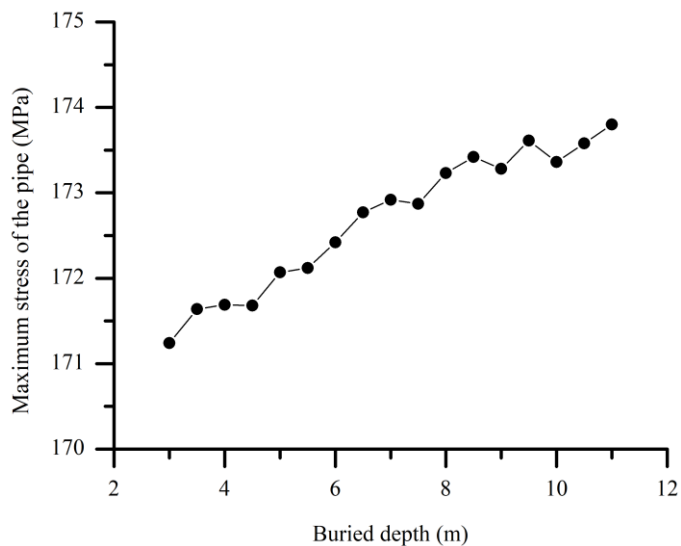


Figure 4-25: Curve of maximum pipe stress and buried depth.

4.5.3.4 Pressure

Figure 4-26 reveals that with the increase of pressure, the maximum stress of the pipeline shows an upward trend, and the pressure is basically linearly related to the maximum stress.

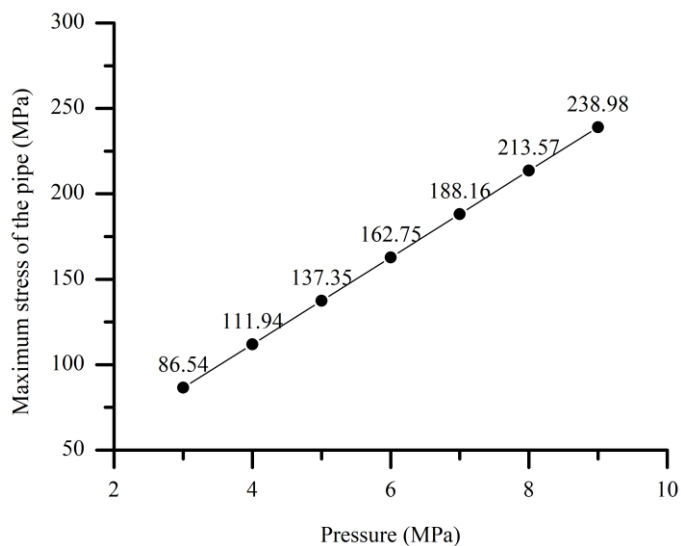


Figure 4-26: Curve of maximum pipe stress and pressure.

4.5.3.5 *Drilling fluid density*

The relative density of slurry used in HDD projects is usually from 1.1 to 1.2. In the engineering design data, drilling fluid density is 1200 kg/m³. In this dissertation, the stress of pipeline with drilling fluid density in the range of 1050 kg/m³ to 1300 kg/m³ is analyzed. It can be seen from **Table 4-8** that with the increase of drilling fluid density, the maximum stress of the pipeline generally shows an upward trend, but the change is very small.

Table 4-8: Pipeline stress corresponding to different mud densities.

Drilling fluid density (kg/m³)	Maximum stress of the pipe (MPa)
1050	172.53
1100	172.80
1150	173.10
1200	172.92
1250	173.57
1300	174.27

4.5.3.6 *Soil type*

There are many parameters that affect soil properties, such as internal friction angle and density. In the Drucker-Prager model, the definition of the parameters of soil density, elastic modulus, Poisson's ratio, cohesion, internal friction angle, and dilatancy angle is very important. Therefore, in this dissertation, only these parameters are used as the basis for soil classification. The data of soil parameters are from the literature (Tang

and Li, 2006), as shown in **Table 4-9**. As the influencing factor analysis in this dissertation is a single factor analysis, when analyzing one of the parameters, the remaining factors take the baseline value.

Table 4-9: Soil parameters.

Soil parameter	Value range	Baseline value
Elastic modulus (MPa)	From 29 to 34	32
Poisson's ratio	From 0.29 to 0.46	0.37
Density (kg/m³)	From 1700 to 1850	1750
Cohesion (kPa)	From 12 to 15	13
Friction angle (degree)	From 12 to 18	15
Dilatancy angle (degree)	From 10 to 12	11

The analysis results (**Figure 4-27**) indicate the following conclusions: (1) With the increase of soil elastic modulus and Poisson's ratio, the maximum stress of the pipeline decreases. Compared with the elastic modulus, the maximum stress of the pipe is more affected by Poisson's ratio. (2) With the increase of soil density, the maximum stress of the pipeline presents an upward trend, however, the upward trend is not obvious. (3) With the increase of cohesion, inner friction angle and dilatancy angle, the maximum stress of the pipeline has not changed. It can be considered that in the pipeline engineering installed by HDD method, the maximum stress of the pipeline is not affected by these three parameters. This may be due to the small contact area between the pipeline and the soil in the HDD projects.

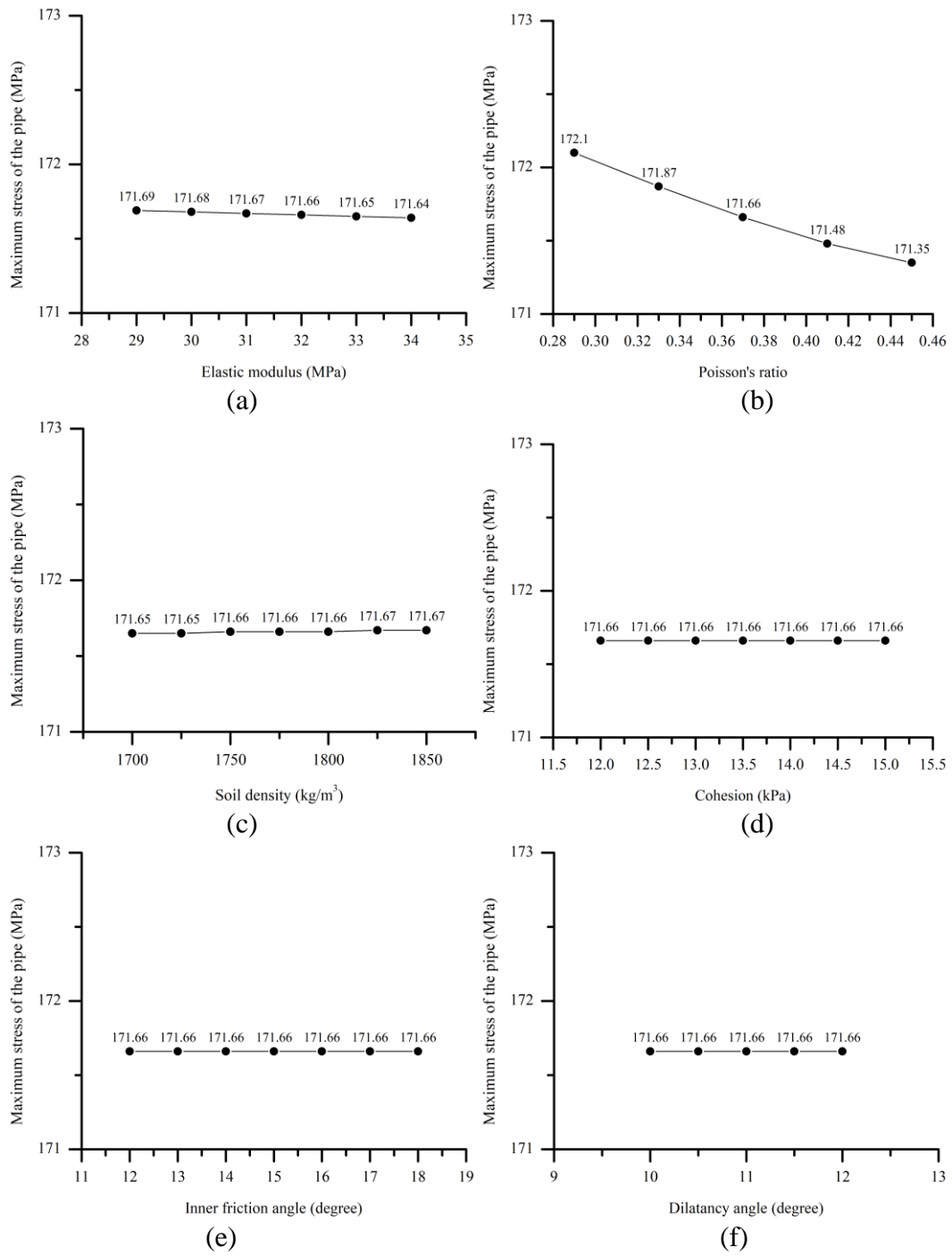


Figure 4-27: Influence of soil parameters on maximum stress of pipeline. (a) elastic modulus; (b) Poisson's ratio; (c) soil density; (d) cohesion; (e) inner friction angle; (f) dilatancy angle.

4.5.4 Stress Sensitivity Analysis

It is very important to understand the influence of a certain factor on the pipeline stress in the design of pipeline engineering. In fact, by observing the trend of the pipeline's stress by adjusting the parameters, the influence of a certain factor on the stress of the pipeline can also be obtained. However, in the comparison process, different factors may have different data dimensions, and there are different steps in the parameter adjustment. The stress sensitivity analysis can eliminate the data dimension of different factors, so as to make better comparison. The calculation equation of the sensitivity coefficient can be expressed as (Lu et al., 2020b)

$$SC = \frac{(\sigma_b - \sigma_t) \times F_b}{\sigma_b \times (F_b - F_t)} \quad \text{Eq. 4-6}$$

where σ_b represents the base value of pipe stress; σ_t represents pipeline stress; F_b represents the base value of the influencing factor; F_t represents the value of influencing factor; SC represents the sensitivity coefficient. If SC is greater than 0, the stress is positively correlated with the influencing factor; if SC is less than 0, the stress is negatively correlated with the influencing factor. The larger the absolute value of SC , the higher the influence of the factor on the stress.

Figure 4-28 and **Table 4-10** show the trend of the sensitivity coefficient of each influencing factor. It implies that the pipeline stress is not sensitive to changes in the buried depth and drilling fluid density, pipe stress is more sensitive to changes in pipe diameter and wall thickness. Therefore, the sensitivity order (from high to low) of these five factors to pipeline stress is as follows: diameter, thickness, pressure, drilling fluid density, buried depth.

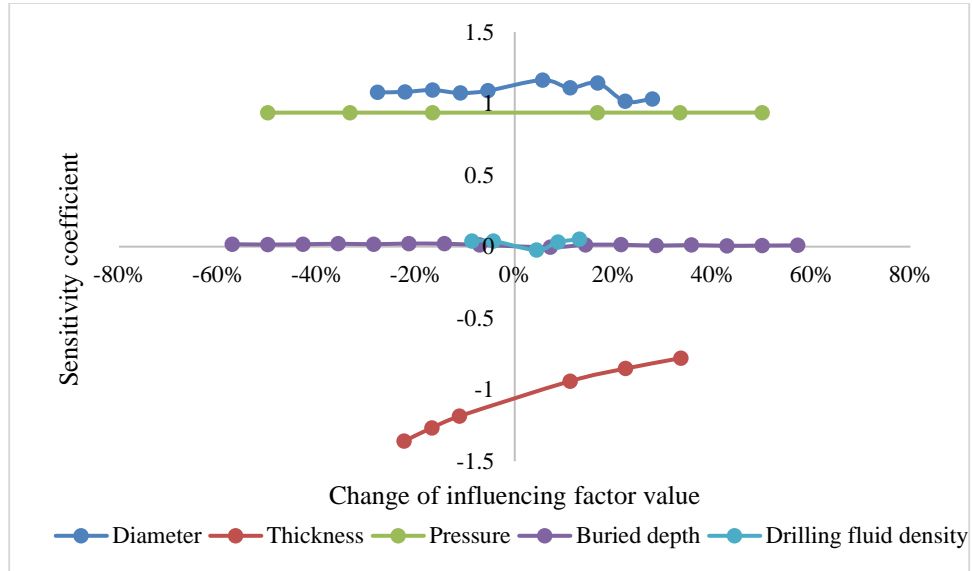


Figure 4-28: Sensitivity coefficient curve of pipeline stress.

Table 4-10: Interval of sensitivity coefficient of each factor.

Influencing factor	Sensitivity coefficient interval	Average of the absolute value of the sensitivity coefficient
Diameter	(1.015,1.164)	1.088
Thickness	(-0.779,-1.360)	1.064
Pressure	(0.9364,0.9368)	0.9366
Buried depth	(-0.004,0.022)	0.013
Drilling fluid density	(-0.024,0.052)	0.037

4.6 Summary

In this chapter, the stress of pipeline installed by HDD method is analyzed. First of all, the operation condition of the pipeline is divided into two cases according to the state of drilling fluid. Through the simulation in ANSYS Workbench software, it is concluded that Case 1 (the annulus between the borehole and the pipeline is filled with drilling fluid) is more dangerous.

Secondly, comparing the stress of the pipeline installed by the open-cut method and the HDD method under the same conditions, it is concluded that the stress of the pipeline installed by HDD method is lower, which highlights the advantages of the HDD method in the gas pipeline project.

Finally, through the influencing factor analysis and stress sensitivity analysis, it implies that: (1) In addition to the soil, the sensitivity order (from high to low) of these five factors to pipeline stress is as follows: diameter, thickness, pressure, drilling fluid density, buried depth; (2) The change of soil parameters has little effect on the stress of the pipeline. Among them, it can be considered that the cohesion, inner friction angle, and dilatancy angle have no effect on the stress of the pipeline.

CHAPTER 5

NEAR REAL-TIME PULLBACK FORCE PREDICTION DURING HDD CONSTRUCTION

5.1 Foreword

The prediction of pullback force is an important research field because it is the basis for choosing the type of drill rig and evaluating the dynamic stability of the pipeline in the pullback process. Pullback force refers to the force provided by the rig during the pullback process to overcome the resistance of the pipe to the soil and mud. It is affected by various factors such as length, soil properties, and mud rheology. Although there are some theoretical methods for calculating the pullback force, the calculated results are quite different from the actual values. Therefore, in recent years, many scholars have used various methods and theories to improve the accuracy of the pullback force prediction results. In this dissertation, a more intelligent approach is taken. Several machine learning-based models are utilized to realize the near real-time pullback force prediction during HDD construction.

5.2 Theories

Three hybrid models proposed in this dissertation introduce the complete ensemble empirical mode decomposition with adaptive noise (CEEMDAN) method into the original models. These three original models are radial basis function neural network (RBFNN), support vector machine using whale optimization algorithm (WOA-SVM),

and random forest (RF). They belong to neural network-based model, SVM-based model and decision tree-based model, respectively. CEEMDAN is used to denoise the original data, while these three basic models are used to train and predict the pullback force.

5.2.1 Data Denoising Method--CEEMDAN

The pullback force is often changed by the influence of mud, crossing length and other factors, so that the data will have large fluctuations and exhibit a high degree of nonlinear characteristics, which undoubtedly increases the difficulty of prediction. Therefore, many scholars use empirical mode decomposition (EMD), singular value decomposition (SVD), ensemble empirical mode decomposition (EEMD), wavelet decomposition (WD), and other methods to denoise the data. Although these methods can improve prediction accuracy to some extent, they all have some limitations. For example, mode mixing⁷ is easy to occur during EMD decomposition. EEMD eliminates mode mixing by adding white noise based on EMD, but the distribution of white noise is random, and the number of integrations is limited, the reconstructed signal after decomposition still has residual noise. The effect of WD may not be ideal in the case of white noise in practical problems (Song et al., 2018).

CEEMDAN is a non-linear, non-stationary data processing method based on EMD and EEMD approaches, with the characteristics of fast calculation speed and small reconstruction error (Lu et al., 2020e; Torres et al., 2011; Zhou et al., 2019). The

⁷ “Mode mixing” is defined as a single Intrinsic Mode Function (IMF) either consisting of signals of widely disparate scales, or a signal of a similar scale residing in different IMF components (Wu and Huang, 2009).

prediction process of CEEMDAN is shown in **Figure 5-1**. The execution process of CEEMDAN is described as follows (Torres et al., 2011; Lu et al., 2020c):

Let $d(t)$ be the original signal, by adding $wn^i(t)$ with a standard normal distribution, the i -th signal sequence is

$$d^i(t) = d(t) + \varepsilon_0 wn^i(t), i = 1, 2, \dots, I \quad \text{Eq. 5-1}$$

where $wn^i(t)$ represents white Gaussian noise; $d^i(t)$ represents the i -th signal sequence; ε represents noise standard deviation; I represents number of tests.

Then the EMD decomposition is performed on the signal after the first test, and the components obtained by the decomposition are averaged, that is, the first modal component is

$$\overline{IMF}_1(t) = I^{-1} \sum_{i=1}^I IMF_1^i(t) \quad \text{Eq. 5-2}$$

where $IMFs$ represent intrinsic mode functions; \overline{IMF}_k represents the k -th modal component.

The margin signal of the first stage ($k = 1$) is given as: $r_1(t) = d(t) - \overline{IMF}_1(t)$. Then the signal $r_1(t) + \varepsilon_1 E_1[wn^i(t)]$ can be further decomposed to obtain the second modal component

$$\overline{IMF}_2(t) = I^{-1} \sum_{i=1}^I E_1\{r_1(t) + \varepsilon_1 E_1[wn^i(t)]\} \quad \text{Eq. 5-3}$$

where $E_k(\cdot)$ represents the k -th modal component obtained by EMD decomposition; r represents residue.

In the following stages, the k -th margin signal can be calculated as

$$r_k(t) = r_{k-1}(t) - \overline{IMF}_k(t) \quad \text{Eq. 5-4}$$

The $(k + 1)$ -th modal component is computed as

$$\overline{IMF}_{k+1}(t) = I^{-1} \sum_{i=1}^I E_1 \{ r_k(t) + \varepsilon_k E_k [wn^i(t)] \} \quad \text{Eq. 5-5}$$

Repeat **Eq. 5-4** until the residue component no longer satisfies the decomposition condition. Finally, the original signal $d(t)$ is decomposed into

$$d(t) = \sum_{i=1}^K \overline{IMF}_i(t) + R(t) \quad \text{Eq. 5-6}$$

where R represents final residue.

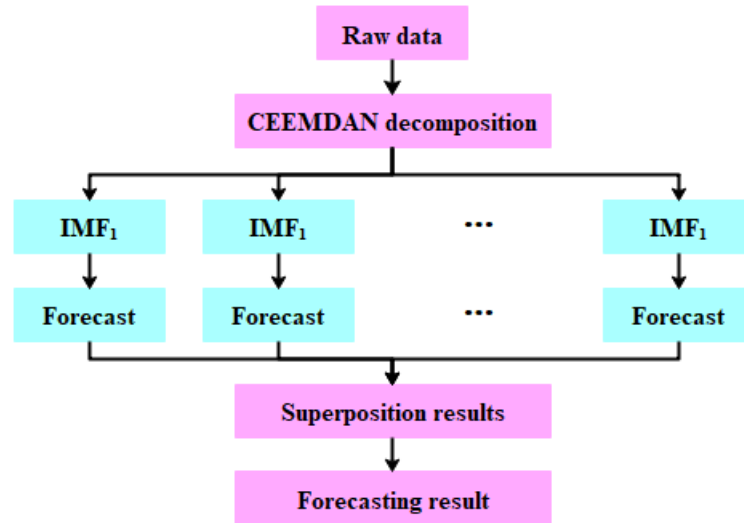


Figure 5-1: Prediction process based on CEEMDAN (Lu et al., 2020c).

5.2.2 Prediction Models

5.2.2.1 Prediction model 1: RBFNN

RBFNN is a feedforward neural network with the unique best approximation (Dhanalakshmi et al., 2009). RBFNN usually has only three layers, including the input layer, hidden layer, and output layer, as shown in **Figure 5-2**. The prediction of RBFNN firstly maps the low-dimensional input to the high-dimensional space of the middle layer.

Secondly, the hidden layer chooses the radial basis function for conversion, and then classifies the output layer and calculates the linear combination, to realize the mapping relationship between input and output.

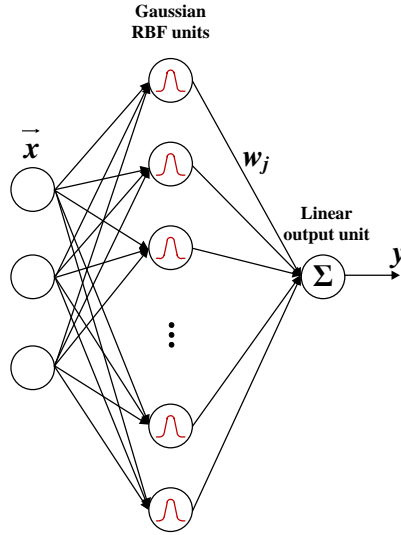


Figure 5-2: The architecture of the RBFNN (Lu et al., 2020d).

The commonly used radial basis function uses Euclidean distance and Gaussian function, which is expressed as follows (Halali et al., 2016)

$$\vartheta(\|x - \mu_i\|) = \exp\left(-\frac{\|x - \mu_i\|^2}{2\sigma^2}\right) \quad \text{Eq. 5-7}$$

where μ_i represents center point of the Gaussian function of the i -th node of the hidden layer; σ_i represents the width parameter of the i -th node.

The network output is

$$y_j = \sum_{i=1}^M w_{ij} \vartheta(\|x - \mu_i\|^2), j = 1, 2, \dots, P \quad \text{Eq. 5-8}$$

where w_{ij} represents the hidden to output weight corresponding to the i -th hidden node;

M represents the total number of hidden nodes

5.2.2.2 Prediction model 2: WOA-SVM

WOA-SVM is a hybrid prediction model, in which SVM is the main forecasting model, and WOA as an optimization algorithm, it can improve the forecasting accuracy of SVM. Therefore, WOA and SVM need to be introduced separately in this section.

5.2.2.2.1 Whale optimization algorithm (WOA)

WOA is a meta-heuristic algorithm proposed by Seyedali Mirjalili and Andrew Lewis in 2016 based on whale predation (Mirjalili and Lewis, 2016). The predation method of whales is the bubble net predation method. First, the whales sneak into the deep water, move upwards in a spiral path, and constantly spit out bubbles of different sizes. A series of bubbles form a bubble net and surround the small fish or shrimp. Finally, the prey is eaten by the whale.

Through practice, WOA algorithm has the advantages of simple operation and few parameters. In this algorithm, there are three stages: search for prey, encircling prey and bubble-net predation. Suppose the best candidate solution is the target prey or close to the optimal solution. Therefore, after defining the best whale position, other whales will swim towards the whale's position to update their position. The distance between the whale individual and the optimal whale position is

$$\vec{D} = |\vec{C} \cdot \vec{X}^*(t) - \vec{X}(t)| \quad \text{Eq. 5-9}$$

where t represents current iteration; $\vec{X}^*(t)$ represents the location of the best whale in the t generation; $\vec{X}(t)$ represents the position of the individual whale in the t generation; \vec{C} represents the oscillation factor, its expression is

$$\vec{C} = 2 \cdot \vec{r} \quad \text{Eq. 5-10}$$

Whales are updated according to the location of humpback whales

$$\vec{X}(t + 1) = \vec{X}^*(t) - \vec{A} \cdot \vec{D} \quad \text{Eq. 5-11}$$

where \vec{A} represents convergence factor, its expression is

$$\vec{A} = 2\vec{a} \cdot \vec{r} - \vec{a} \quad \text{Eq. 5-12}$$

where \vec{r} represents a random number between [0,1].

There are two strategies for whale local search stage. The first strategy is the shrinking encircling mechanism, in which the location updating of whales is achieved by **Eq. 5-11**. The range of \vec{A} at this stage is realized from 2 to 0 as \vec{a} decreases linearly. \vec{A} represents a random number between $[-a, a]$. The second strategy is spiral updating position. The whale first calculates its distance to its prey, then spirals up and spits out bubbles. The mathematical expression of the predatory behavior is

$$\vec{D}' = |\vec{X}^*(t) - \vec{X}(t)| \quad \text{Eq. 5-13}$$

$$\vec{X}'(t + 1) = \vec{D}' \cdot e^{bl} \cdot \cos 2\pi l + \vec{X}^*(t) \quad \text{Eq. 5-14}$$

where \vec{D}' represents the distance from the i -th whale to the prey (optimal solution), l represents a random value between $[-1,1]$, and b represents a spiral constant.

Since whales have two predation strategies, assuming that the probability of adopting one of them is 50%, the mathematical model is

$$\vec{X}(t + 1) = \begin{cases} \vec{D}' \cdot e^{bl} \cdot \cos 2\pi l + \vec{X}^*(t) & p \geq 0.5 \\ \vec{X}^*(t) - \vec{A} \cdot \vec{D} & p < 0.5 \end{cases} \quad \text{Eq. 5-15}$$

where p represents a random number between [0,1].

In order to avoid local optimum, the whale will also enter the global search phase, the mathematical model of this phase is

$$\begin{cases} \vec{D} = |\vec{C} \cdot \vec{X}_{rand}(t) - \vec{X}| \\ \vec{X}(t + 1) = \vec{X}_{rand} - \vec{A} \cdot \vec{D} \end{cases} \quad \text{Eq. 5-16}$$

where \vec{X}_{rand} represents the location of a random whale in the current population.

5.2.2.2.2 Support vector machine (SVM)

The SVM is a machine learning method widely used in statistical classification and regression analysis (see **Figure 5-3**). It has a solid theoretical foundation and good generalization performance, and it is often used to solve nonlinear problems with small amount of data (Vapnik, 2010).

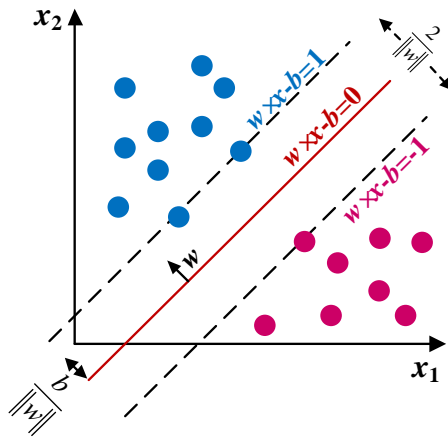


Figure 5-3: Support vector machine.

In regression analysis, assume that the training set is

$$\{(x_i, y_i) | x_i \in R^n, y_i \in R, i = 1, \dots, m\} \quad \text{Eq. 5-17}$$

where x_i represents the input vector; y_i represents the output vector.

The optimal linear decision function constructed in high-dimensional space is

$$f(x) = \omega^T \varphi(x) + b \quad \text{Eq. 5-18}$$

where $\varphi(x)$ represents nonlinear mapping function; ω represents weighted vector; b represents deviator.

Based on the principle of structural risk minimization, introducing the slack variables ξ_i, ξ_i^* , then the linear regression function can be expressed as

$$\min \left[0.5 \|\omega\|^2 + C \sum_{i=1}^m (\xi_i + \xi_i^*) \right] \quad \text{Eq. 5-19}$$

$$\text{s. t. } \begin{cases} y_i - \omega^T \varphi(x) - b \leq \varepsilon + \xi_i \\ \omega^T \varphi(x_i) - y_i + b \leq \varepsilon + \xi_i^* \\ \xi_i, \xi_i^* \geq 0 \end{cases} \quad \text{Eq. 5-20}$$

where C represents penalty factor; ε represents insensitive loss function.

The Lagrange function is introduced and converted into dual form

$$\max \left[-0.5 \sum_{i=1}^n \sum_{j=1}^n (\alpha_i - \alpha_i^*)(\alpha_j - \alpha_j^*) K(x_i, x_j) \right. \\ \left. + \sum_{i=1}^n \alpha_i (y_i - \varepsilon) - \sum_{i=1}^n \alpha_i^* (y_i - \varepsilon) \right] \quad \text{Eq. 5-21}$$

$$\text{s. t. } \begin{cases} \sum_{i=1}^n \alpha_i = \sum_{i=1}^n \alpha_i^* \\ 0 \leq \alpha_i \leq C, 0 \leq \alpha_i^* \leq C \end{cases} \quad \text{Eq. 5-22}$$

where $K(x_i, x_j)$ represents kernel function.

Assume that the optimal solutions obtained by **Eq. 5-21** are α_i and α_i^* , then the regression function can be expressed as

$$f(x) = \sum_{i=1}^n (\alpha_i - \alpha_i^*) K(x_i, x_j) + b \quad \text{Eq. 5-23}$$

The selection of kernel functions is a key issue of the SVM model, and different kernel functions can lead to different generalization and learning ability of prediction models. Three kinds of kernel functions that are used more: polynomial kernel function, radial basis function (RBF), and Sigmoid kernel function. Because the characteristic space corresponding to the RBF is infinite, it is sure that the sample can be linearly

separable under the condition of the finite sample, so the RBF is used in this dissertation (Lu et al., 2019)

$$K(x_i, x_j) = e\left(-\frac{\|x_i - x_j\|^2}{2\sigma^2}\right) \quad \text{Eq. 5-24}$$

where σ represents the width of Gaussian radial basis function.

5.2.2.2.3 Hybrid model

According to the introduction of the SVM model, the model contains two hyperparameters: the penalty factor C and the width of the Gaussian radial basis function σ . These two parameters directly determine the accuracy of the prediction. Therefore, in the hybrid model, the role of the WOA is to seek the optimal or superior values of the two hyperparameters at a faster speed. Note that since the optimization process is random, the optimal or better hyperparameters obtained each time are also random, so the prediction results are also random, but the prediction results will only change within a small range. **Figure 5-4** is a flow chart of the WOA-SVM.

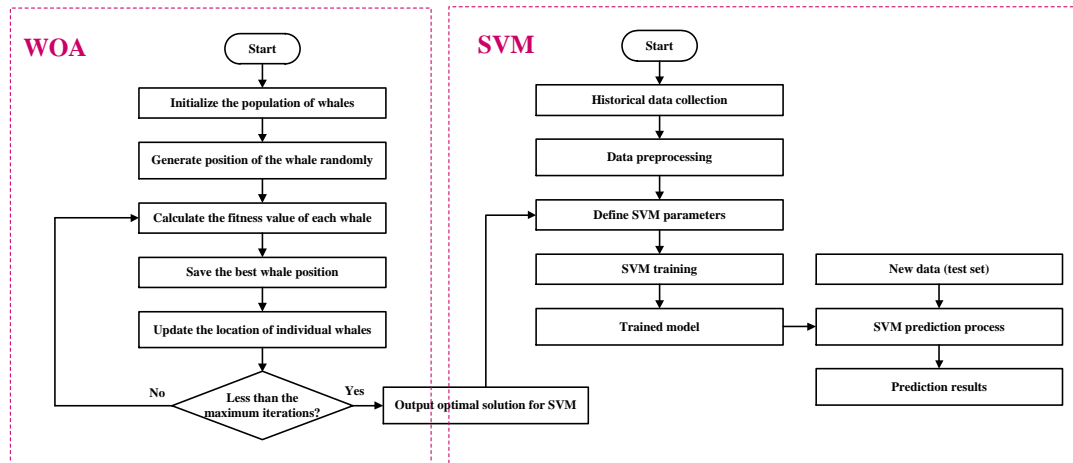


Figure 5-4: Flow chart of WOA-SVM.

5.2.2.3 Prediction model 3: Random forest (RF)

RF is an ensemble machine learning algorithm emerged in 2001 (Breiman, 2011), which integrates multiple decision trees to form forests to get results. RF is composed of multiple unrelated classification and regression trees (CART), in which each tree can vote, and the prediction result is the average prediction value of multiple decision trees.

Figure 5-5 gives flowchart of RF (Lu and Ma, 2020).

The CART decision tree uses Gini coefficient to select optimal feature and determine optimal binary segmentation point of the feature. The Gini coefficient is defined as (Huang et al., 2019)

$$Gini(p) = 2p - 2p^2 \quad \text{Eq. 5-25}$$

where *Gini* represents Gini coefficient.

According to the feature *A* on a certain value *a* ($A = a$ or $A \neq a$), the dataset *D* is split into two datasets, i.e., D_1 and D_2 . With the condition of feature $A = a$, the Gini coefficient is

$$Gini(D, A) = \frac{D_1 Gini(D_1) + D_2 Gini(D_2)}{D} \quad \text{Eq. 5-26}$$

where $Gini(D, A)$ represents uncertainty of set *D*; $Gini(D_1)$, $Gini(D_2)$ represent uncertainty of sets D_1 and D_2 , respectively.

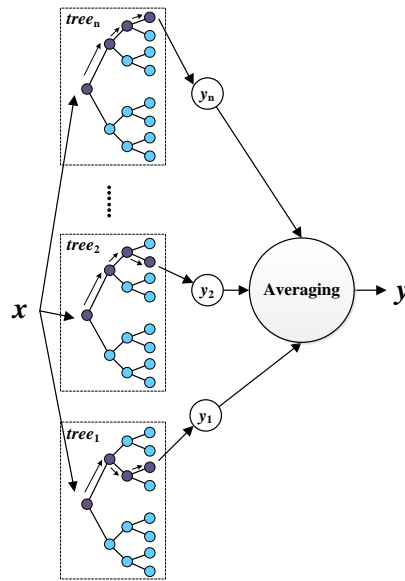


Figure 5-5: Basic flowchart of RF (Safari et al., 2017).

5.3 Applications

5.3.1 Project Overview and Data Description

In this dissertation, two HDD projects crossing the Yangtze River in China's Sichuan-East Gas Project are taken as examples, and the prediction models are validated through the monitoring data of the construction site. One project crosses the main channel of the Yangtze River on the Nanjing branch (referred to as Project 1), and the other crosses the Jiujiang River (referred to as Project 2). Their design crossing curves are shown in **Figure 5-6**, and their engineering design parameters are shown in **Table 5-1**. The pullback force data of two HDD projects were collected from field monitoring. 216 pullback force data are collected from Project 1, the maximum value is 276 tons, the minimum value is 89 tons, the average value is 172.51 tons, and the standard deviation is 52.44 tons. The dataset obeys the Johnson SB distribution with the parameters of $\gamma = -0.17286$, $\delta = 0.63753$, $\lambda = 190.54$, $\xi = 68.325$. 235 pullback force data are collected

from Project 2, the maximum value is 148 tons, the minimum value is 69 tons, the average value is 101.66 tons, and the standard deviation is 20.64 tons. The dataset obeys the Gen. Pareto distribution with the parameters of $k = -0.4091, \sigma = 39.104, \mu = 73.908$.

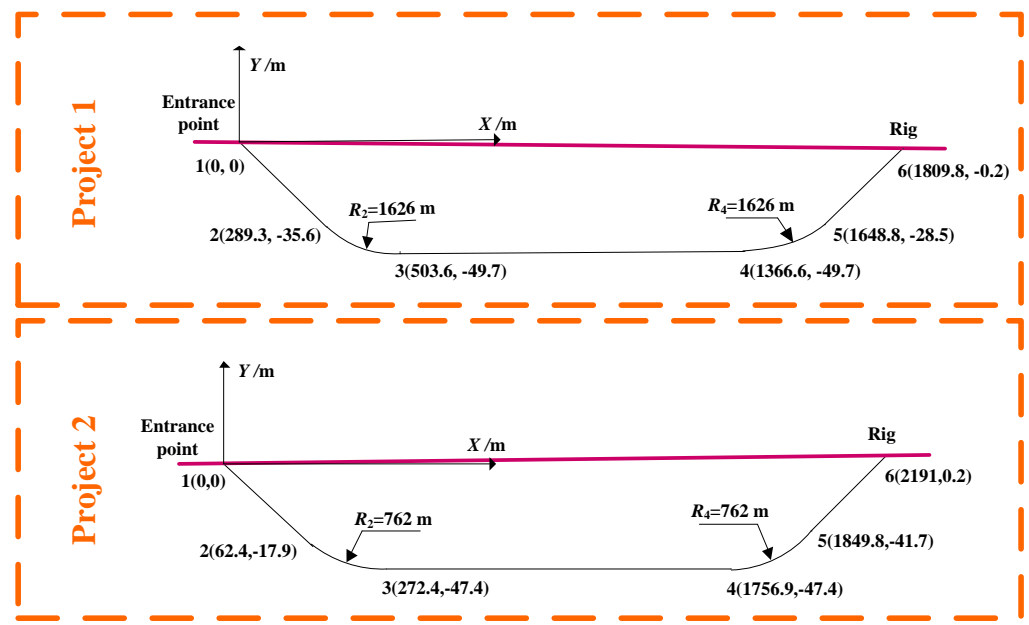


Figure 5-6: Design crossing curves for two HDD projects.

Table 5-1: Design parameters of two HDD projects.

Parameters	Project 1	Project 2
Diameter (mm)	813	508
Thickness (mm)	15.9	11.9
Borehole diameter (mm)	1219.5	762
Pipe density (kg/m³)	7800	7800
Pipe elastic modulus (GPa)	200	200
Consistency coefficient (Pa Sⁿ)	6.4366	6.4366
Fluidity index	0.3063	0.3063
Mud flow (L/min)	380	265
Mud density (kg/m³)	1200	1200
Pipeline pullback speed (m/s)	0.026	0.052
Friction coefficient between pipeline and ground	0.2	0.3
Friction coefficient between pipe and borehole wall	0.3	0.2

5.3.2 Prediction Steps

(1) Data decomposition

The CEEMDAN is used to decompose the raw data so that each decomposed dataset is smoother than the raw data. In other words, the data in the same dataset has

more obvious similar features. As can be seen from **Figure 5-7**, the raw data of Project 1 is decomposed into seven datasets, and the raw data of Project 2 is decomposed into nine datasets. Two sets of data are decomposed into different number of datasets because the fluctuation degree of the two sets of raw data is different and the same final residue⁸ is set.

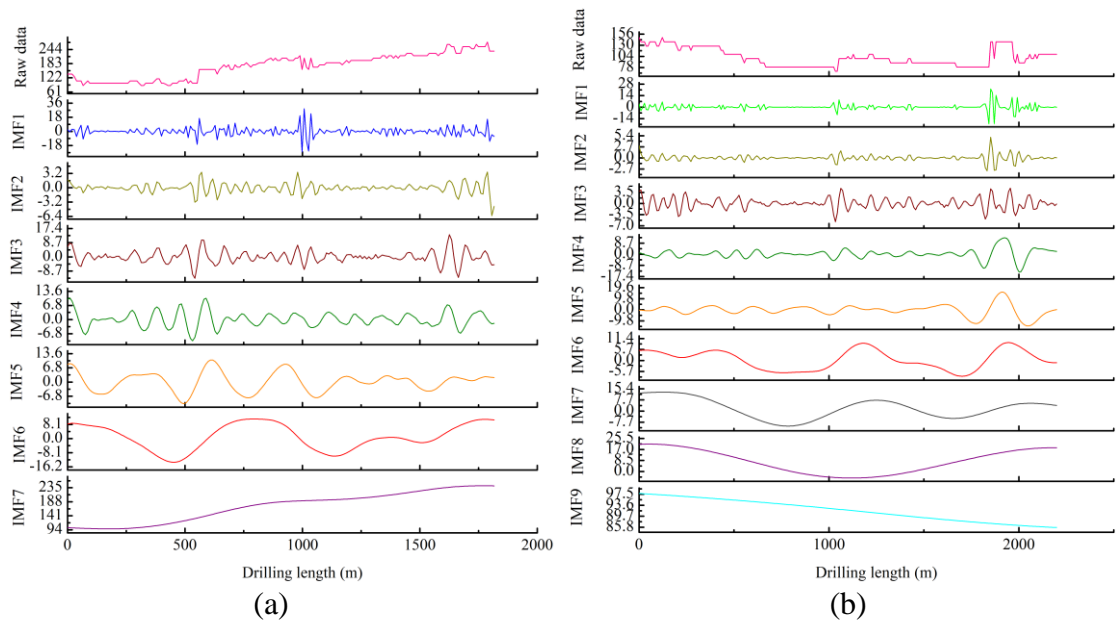


Figure 5-7: Decomposition of raw data by CEEMDAN. (a) Project 1; (b) Project 2.

(2) Data normalization

In order to eliminate the dimensional influence of the data indicators, the data after the decomposition is normalized and limited to the range of [0,1] (see **Figure 5-8**), using the following equation

$$Z_n = \frac{Z_i - Z_{min}}{Z_{max} - Z_{min}} \quad \text{Eq. 5-27}$$

⁸ The final residual settings are usually based on the original authors' default settings.

where n represents size of the sample; z_n represents normalized data; z_i represents raw data; z_{min} and z_{max} represent minimum and maximum of the raw data, respectively.

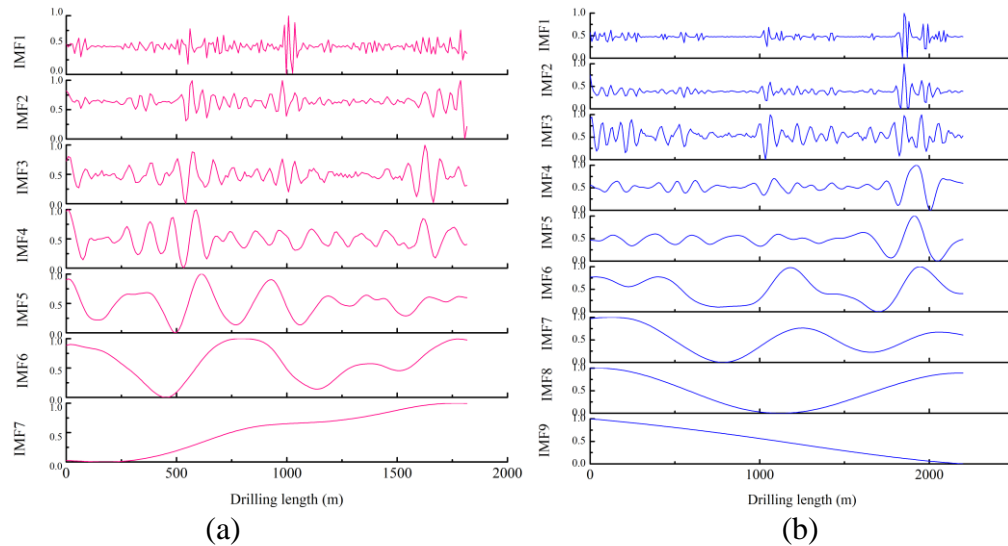


Figure 5-8: Normalized data. (a) Project 1; (b) Project 2.

(3) Divide data into the training set and test set

In this dissertation, decomposed datasets are divided into the training sets and test sets, and their ratios are 9:1. The sliding window length is four, that is, the first three data is used to predict the next data, as shown in **Figure 5-9**. In addition, the input and output content are different from the conventional time series prediction. The input is the historical pullback force and the drilling length, and the output is the pullback force.

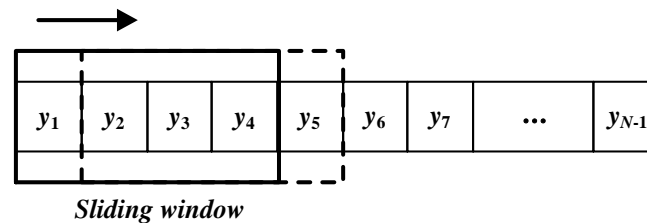


Figure 5-9: Predictive sliding window schematic.

(4) Prediction

The forecasting model is used to make the prediction in the denoised datasets, the prediction results are summarized, then denormalize the summarized data to get the ultimate result, as shown in **Figure 5-10**.

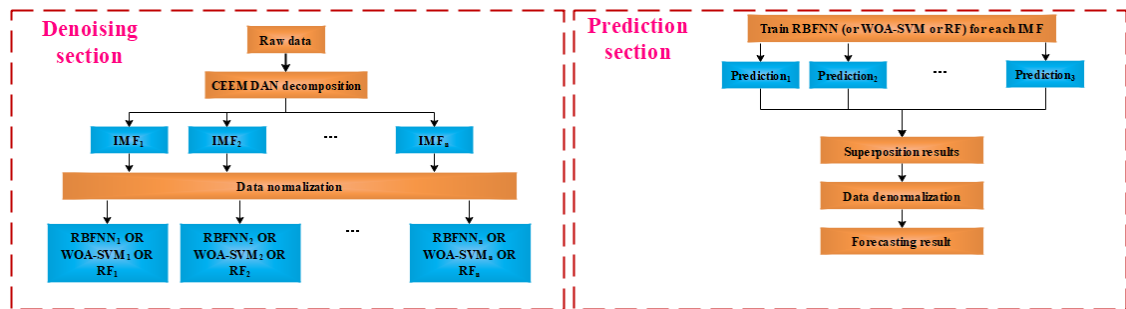


Figure 5-10: Data denoising and prediction processes.

(5) Prediction error analysis

After the prediction results are obtained, the error needs to be analyzed. Six error metrics are used to evaluate the accuracy of the prediction, including mean absolute error (MAE), root mean square error (RMSE), mean absolute percentage error (MAPE), root mean squared percentage error (RMSPE), Theil U statistic 1 (U1), and Theil U statistic 2 (U2), their expressions can be found from **Eq.5-28** to **Eq.5-33**. Among them, MAE, RMSE, MAPE, and RMSPE indicate the error of the prediction result, U1 indicates the overall accuracy of the prediction, and U2 indicates the overall quality of the prediction. The smaller the value of the six metrics, the higher the prediction accuracy.

$$\text{MAE} = \frac{1}{n} \sum_{t=1}^n |O_t - P_t| \quad \text{Eq. 5-28}$$

$$\text{RMSE} = \sqrt{\frac{1}{n} \sum_{t=1}^n (O_t - P_t)^2} \quad \text{Eq. 5-29}$$

$$\text{MAPE} = \frac{100\%}{n} \sum_{t=1}^n \left| \frac{O_t - P_t}{O_t} \right| \quad \text{Eq. 5-30}$$

$$\text{RMSPE} = \sqrt{\frac{1}{n} \sum_{t=1}^n \left(\frac{O_t - P_t}{O_t} \right)^2} \quad \text{Eq. 5-31}$$

$$\text{U1} = \frac{\sqrt{\frac{1}{n} \sum_{t=1}^n (O_t - P_t)^2}}{\sqrt{\frac{1}{n} \sum_{t=1}^n O_t^2 + \frac{1}{n} \sum_{t=1}^n P_t^2}} \quad \text{Eq. 5-32}$$

$$\text{U2} = \frac{\sqrt{\sum_{t=1}^n (O_t - P_t)^2}}{\sqrt{\sum_{t=1}^n O_t^2}} \quad \text{Eq. 5-33}$$

where O_t represents actual value at time t ; P_t represents the prediction value at time t ; n represents the sample size.

5.3.3 Results and Discussions

5.3.3.1 Prediction results

In this dissertation, the prediction results of the models are compared with the actual monitoring data. In addition, the predicted results are compared with a commonly used analytical method (improved Polak method). The Polak model systematically studies the pullback force prediction method from a theoretical perspective, which is representative in the current research in this field. Since the Polak model simplifies the mud flow in the pilot hole to a stable flow of Newtonian fluid in the concentric annular space, the mud drag resistance is small. Therefore, using the steady flow assumption of

the power law fluid in the concentric annular space, the Polak model is modified, and the following three equations can be used to solve the mud drag resistance

$$v(r) = \begin{cases} v_p + \int_{R_p}^r \left[\frac{1}{2K} \left(-\frac{dp}{dz} \right) \right]^{\frac{1}{j}} \left(\frac{R_I^2}{r} - r \right)^{\frac{1}{j}} dr & R_p \leq r \leq R_I \\ \int_r^{R_B} \left[\frac{1}{2K} \left(-\frac{dp}{dz} \right) \right]^{\frac{1}{j}} \left(r - \frac{R_I^2}{r} \right)^{\frac{1}{j}} dr & R_I \leq r \leq R_B \end{cases} \quad \text{Eq. 5-34}$$

$$Q = \int_{R_p}^{R_B} 2\pi r \cdot v(r) \cdot dr \quad \text{Eq. 5-35}$$

$$(T_d)_i = K \left(\left. \frac{dv(r)}{dr} \right|_{r=R_p} \right)^j \cdot \pi D_p \sum_{k=1}^{i-1} L_k \quad \text{Eq. 5-36}$$

where v_p represents pipeline pullback speed; $\frac{dp}{dz}$ represents pressure gradient of mud along the axis of the pipe; R_I represents radius at the maximum velocity of the mud in the annulus; R_B represents radius of the pilot hole; Q represents mud flow; K represents consistency coefficient; j represents flow property number; R_p and D_p represent radius and diameter of the pipe, respectively; $v(r)$ represents velocity distribution law of mud.

5.3.3.1.1 RBFNN and CEEMDAN-RBFNN

From **Figure 5-11**, it indicates that the pullback force in the HDD construction process predicted by CEEMDAN-RBFNN and RBFNN models can be better matched with the real value in detail. For Project 1, the maximum pullback force occurs near the end point, about 249 tons, the pullback force shows an upward trend as a whole. For Project 2, the maximum pullback force occurs near the entrance, which is about 148 tons. In addition, the overall fluctuation range of Project 2 is significantly higher than that of Project 1. The use of the improved Polak model to predict the pullback force can only be

consistent in the overall trend (increase or decrease). However, it is difficult for CEEMDAN-RBFNN and RBFNN to see their prediction accuracy in **Figure 5-11**. Therefore, their error indicators are compared, as shown in **Table 5-2**. It suggests that for Project 1, the MAE, RMSE, MAPE, RMSPE, U1 and U2 of CEEMDAN-RBFNN model's prediction (test set) are 7.67 tons, 10.10 tons, 3.15%, 4.21%, 0.0201 and 0.0405, respectively. Compared with the corresponding indicators of RBFNN model, they are reduced by 48.83%, 47.01%, 49.19%, 47.44%, 46.26%, and 46.99%, respectively. For Project 2, the MAE, RMSE, MAPE, RMSPE, U1, and U2 of CEEMDAN-RBFNN model's prediction (test set) are 7.11 tons, 8.70 tons, 7.13%, 9.04%, 0.0421, 0.0844, respectively. Compared with the corresponding indicators of RBFNN prediction results, they are reduced by 34.04%, 42.73%, 36.40%, 44.78%, 40.28%, 42.74%, respectively. In conclusion, the prediction accuracy of the original RBFNN model can be greatly improved by using CEEMDAN.

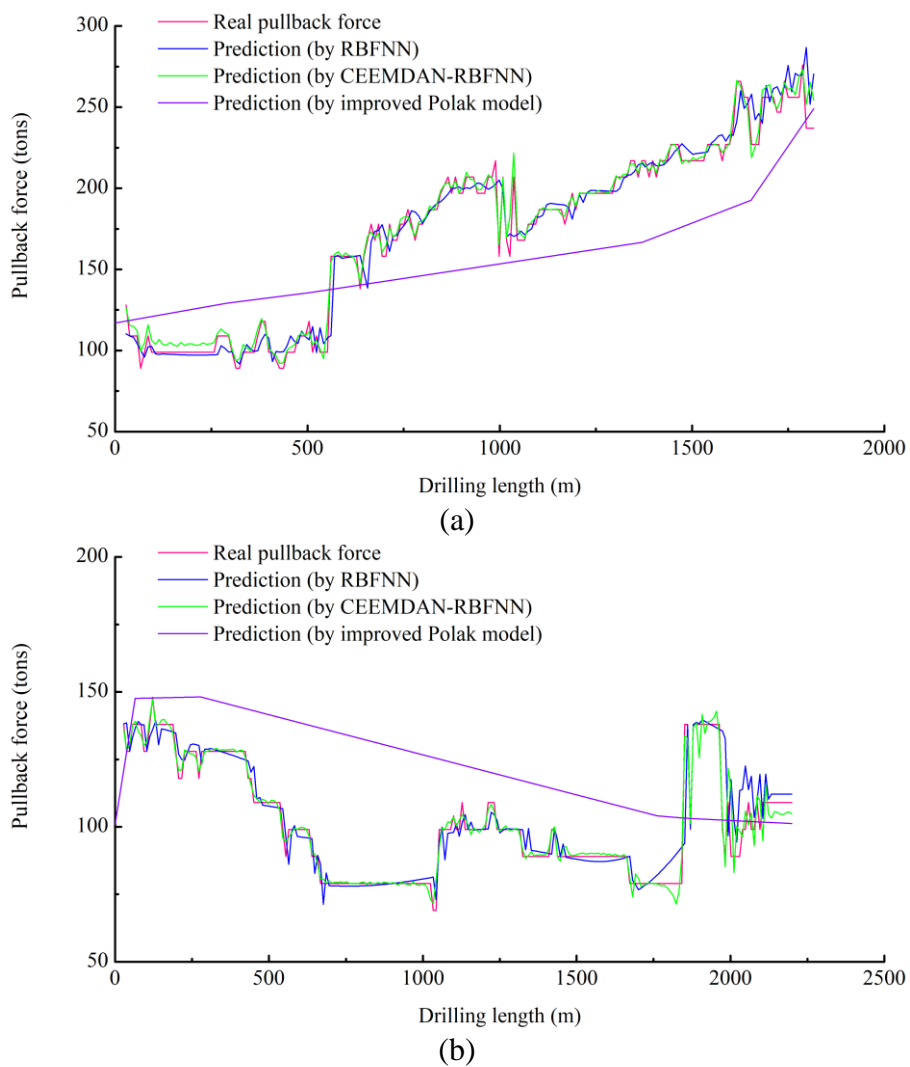


Figure 5-11: Prediction results by RBFNN-based models. (a) Project 1; (b) Project 2.

Table 5-2: The prediction errors of CEEMDAN-RBFNN and RBFNN in the two HDD projects.

Dataset	Project	Model	Error metrics					
			MAE (t)	RMSE (t)	MAPE (%)	RMSPE (%)	U1	U2
Training set	Project 1	CEEMDAN-RBFNN	3.17	4.54	2.35	3.55	0.0132	0.0265
		RBFNN	6.10	9.37	4.00	6.15	0.0273	0.0547
	Project 2	CEEMDAN-RBFNN	1.51	2.36	1.52	2.52	0.0115	0.0229
		RBFNN	3.05	5.75	3.09	5.58	0.0278	0.0557
Test set	Project 1	CEEMDAN-RBFNN	7.67	10.10	3.15	4.21	0.0201	0.0405
		RBFNN	14.99	19.06	6.20	8.01	0.0374	0.0764
	Project 2	CEEMDAN-RBFNN	7.11	8.70	7.13	9.04	0.0421	0.0844
		RBFNN	10.78	15.19	11.21	16.37	0.0705	0.1474

5.3.3.1.2 WOA-SVM and CEEMDAN-WOA-SVM

Similarly, by observing **Figure 5-12**, it implies that for both projects, the prediction results of WOA-SVM are closer to the actual values than the results of CEEMDAN-WOA-SVM. From **Table 5-3**, it reveals that for Project 1, the MAE, RMSE, MAPE, RMSPE, U1 and U2 of CEEMDAN-WOA-SVM model's prediction (test set) are 21.74 tons, 24.50 tons, 8.52%, 9.44%, 0.0512 and 0.0982, respectively. Compared with the corresponding indicators of WOA-SVM model, they are reduced by 4.19%, 7.55%, 6.48%, 10.78%, 6.23%, and 7.53%, respectively. For Project 2, the MAE, RMSE, MAPE, RMSPE, U1, and U2 of CEEMDAN-WOA-SVM model's prediction (test set) are 6.14 tons, 7.62 tons, 6.12%, 7.88%, 0.0371, 0.0735, respectively. Compared with the corresponding indicators of WOA-SVM model, they are reduced by 6.97%, 3.18%, 9.20%, 7.08%, 1.85%, 3.29%, respectively. In conclusion, the prediction accuracy of the original RBFNN model can be greatly improved by using CEEMDAN.

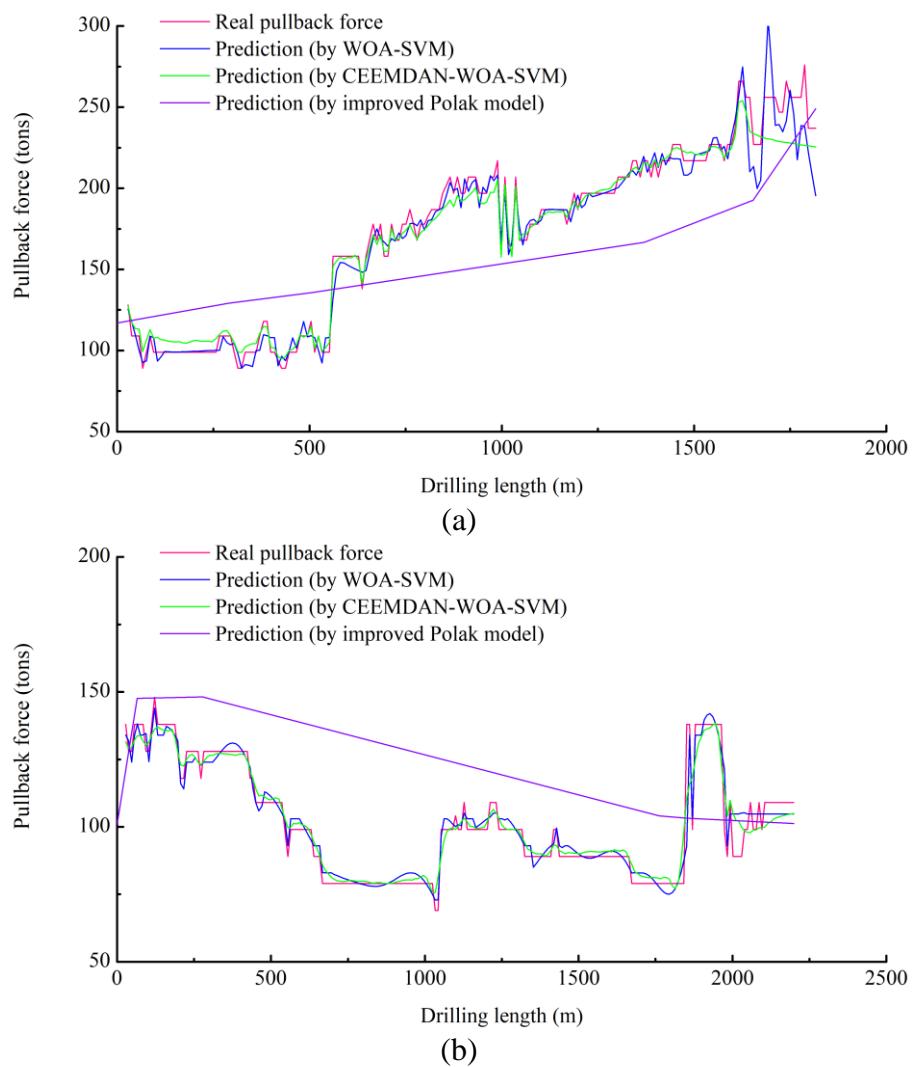


Figure 5-12: Prediction results by WOA-SVM-based models. (a) Project 1; (b) Project 2.

Table 5-3: The prediction errors of CEEMDAN-WOA-SVM and WOA-SVM in the two HDD projects.

Dataset	Project	Model	Error metrics					
			MAE (t)	RMSE (t)	MAPE (%)	RMSPE (%)	U1	U2
Training set	Project 1	CEEMDAN-WOA-SVM	4.26	5.26	2.95	3.86	0.0154	0.0306
		WOA-SVM	5.20	6.42	3.39	4.40	0.0188	0.0374
	Project 2	CEEMDAN-WOA-SVM	2.87	4.74	2.84	4.60	0.0230	0.0460
		WOA-SVM	3.04	4.69	3.01	4.21	0.0227	0.0455
Test set	Project 1	CEEMDAN-WOA-SVM	21.74	24.50	8.52	9.44	0.0512	0.0982
		WOA-SVM	22.69	26.50	9.11	10.58	0.0546	0.1062
	Project 2	CEEMDAN-WOA-SVM	6.14	7.62	6.12	7.88	0.0371	0.0735
		WOA-SVM	6.60	7.87	6.74	8.48	0.0378	0.0760

5.3.3.1.3 RF and CEEMDAN-RF

Table 5-4 lists the prediction errors in the test set of Project 1 and Project 2 using RF and CEEMDAN-RF. It can be seen that the prediction accuracy of CEEMDAN-RF in project 1 is higher, and the MAPE is 7.74%. However, the prediction accuracy of the hybrid model in project 2 is lower than that of the original RF model. It shows that data denoising sometimes cannot get better prediction performance.

Table 5-4: The prediction errors of CEEMDAN-RF and RF in the two HDD projects.

Project	Model	Error metrics					
		MAE (t)	RMSE (t)	MAPE (%)	RMSPE (%)	U1	U2
Project 1	CEEMDAN-RF	19.69	23.45	7.74	9.19	0.0488	0.1398
	RF	32.40	34.92	12.75	13.57	0.0748	0.0939
Project 2	CEEMDAN-RF	16.99	21.82	17.13	22.83	0.1034	0.2117
	RF	17.54	21.92	16.63	21.18	0.1024	0.2127

5.3.3.2 *Stability of prediction*

Stability is a considerable significance index for a prediction model because sometimes although a prediction model can have high accuracy on the whole, there will be significant errors at some key points, which is very inconvenient for engineering guidance. According to the results in **Section 5.3.3.1**, it implies that the prediction accuracy of the RBFNN-based models is higher by comparing the prediction errors, so this chapter takes the RBFNN-based model as the research object. The percentage error is utilized to measure the deviation of each predicted point from the actual value. The

standard deviation of the percentage error is used to measure the overall prediction stability because it can measure the degree of deviation of the error as a whole. The smaller the standard deviation, the higher the stability of the prediction model. As shown in **Figure 5-13(a)**, for Project 1, the overall percentage error of the CEEMDAN-RBFNN model is small, only a few points have a large degree of deviation, and the percentage error is in the interval of $[-19.27\%, 7.98\%]$. For Project 2 (see **Figure 5-13(b)**), the percentage error of the CEEMDAN-RBFNN model prediction results is still small, ranging from -28.82% to 13.08% . It can be seen from **Figure 5-14** that the standard deviations of the percentage error of the CEEMDAN-RBFNN model in Project 1 and Project 2 are 3.22% and 3.76% , respectively, which are lower than RBFNN, indicating that the proposed model has higher prediction stability.

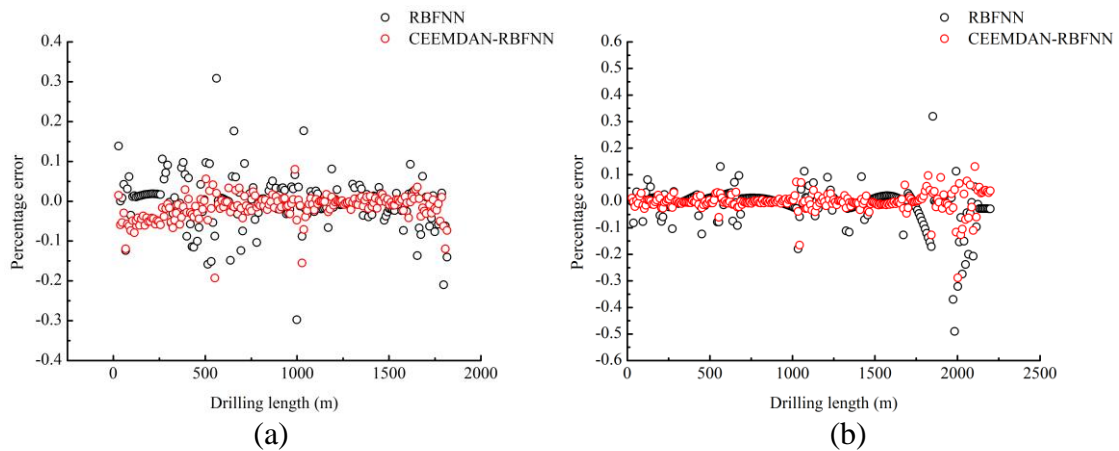


Figure 5-13: Percentage error at each prediction point. (a) Project 1; (b) Project 2.

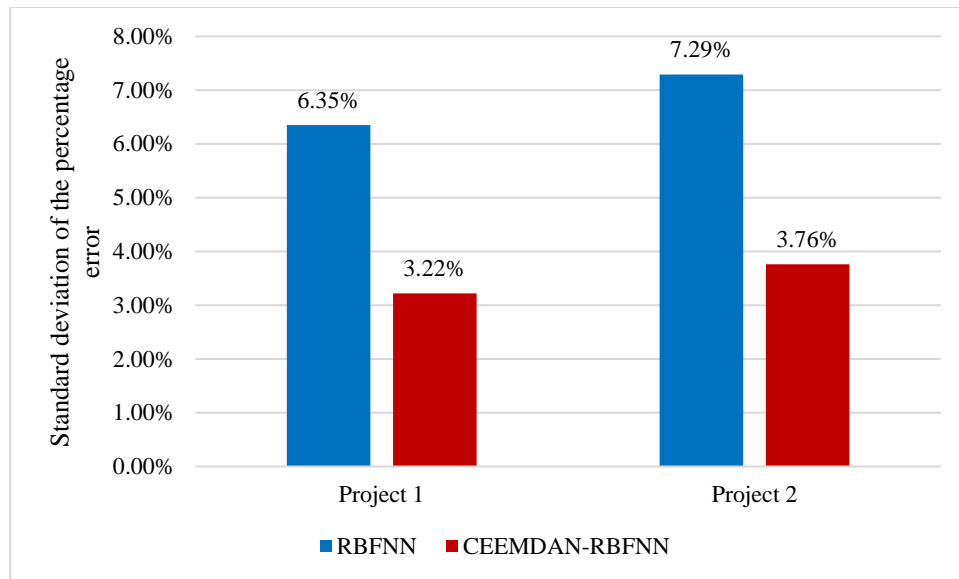


Figure 5-14: Standard deviation of the percentage error of two models in Project 1 and Project 2.

5.3.3.3 *Sliding window length*

In the prediction of pullback force in HDD construction, a long data series will bring much inconvenience when extracting vital information, and the information description of the sequence may be inaccurate. If the length of the sliding window is too long, the amount of calculation may increase, and the ill-conditioned matrix caused by the multi-collinearity problem may occur, so the determination of the length of the sliding window is crucial. The length of the sliding window used in the case study is four, that is, the first three data is used to predict the next one. Thus, the effect of sliding window lengths of 2, 4, 6, 8, and 10 on prediction results is discussed in this section. The MAPEs of the test set are shown in **Table 5-5**. It indicates that for the Project 1, when the sliding window length is 6, the prediction performance is the best. For the Project 2, when the sliding window length is 8, the prediction performance is the best.

Table 5-5: The prediction MAPEs of test sets corresponding to different sliding window lengths.

Project	Sliding window length	MAPE (%)
Project 1	2	6.13
	4	3.15
	6	2.17
	8	2.55
	10	2.32
Project 2	2	7.03
	4	7.13
	6	5.94
	8	3.57
	10	6.08

5.3.4 Feasibility of Near Real-time Prediction

Because the HDD construction process is a short-term behavior, the short time spent is very important for a near real-time prediction. Therefore, in this section, the time complexity of the prediction model is analyzed. In general, time complexity can be measured by the time required for the prediction process. The lower the time complexity, the faster the model is calculated, and the higher the efficiency. Taking CEEMDAN-RBFNN as an example, the model is implemented in MATLAB R2017b using a Workstation with an Inter(R) Core (TM) i7-7700HQ CPU @ 2.8 GHz and Windows 10

with 64 bits and an 8.00 GB RAM environment. Run the program ten times and take the average of the calculation time⁹. It can be known that the average time spent by Project 1 is 0.71 seconds, and the average time spent by Project 2 is 0.57 seconds. It shows that the prediction work with a data volume of about 200 can be completed in less than 1 second, which proves the feasibility of near real-time prediction of the pullback force during HDD construction using machine learning models.

5.4 Summary

Aiming at the calculation of the pullback force in the HDD construction process, in this dissertation, three novel machine learning-based hybrid models are proposed, which jumps out of the original analytical method and is based on the data-driven method. In the hybrid model, the original prediction models (RBFNN, WOA-SVM, and RF) are used for model training and prediction, and CEEMDAN is introduced to decompose the original data into multiple smoother datasets. In order to verify the prediction accuracy of the model, two river-crossing pipeline projects installed by HDD method in the Sichuan-East China Gas Project are taken as examples to predict their pullback force. The original data set is divided into a training set and a test set according to a ratio of 9:1, and the sliding window length is set to 4. Through experiments, it can be concluded that: (1) If the CEEMDAN-RBFNN model is adopted, the MAPE of Project 1's prediction is 3.15%, and that of Project 2 is 7.13%. Compared with the improved Polak model, the prediction accuracy is greatly improved. (2) The prediction accuracy of the CEEMDAN-RBFNN model is higher than other models.

⁹ Add “tic” and “toc” to Matlab code to record the operation time.

The standard deviation of percentage error is also examined to measure the predictive stability of the model. The results show that the standard deviations of percentage error of CEEMDAN-RBFNN model in Project 1 and Project 2 are 3.22% and 3.76% respectively, which are smaller than RBFNN, indicating that the predictive stability of the new model is higher. Also, the influence of sliding window length on prediction results is discussed. The results show that for Project 1, when the sliding window length is 6, the prediction performance is the best. For Project 2, when the sliding window length is 8, and the prediction performance is the best.

Note that although the proposed method has higher prediction accuracy than the traditional analytical method, it can only be used as an auxiliary method, not as an alternative method because it is a data-based model. The model can realize near real-time prediction after collecting a small amount of data in the field, thus providing more detailed data for the project.

Furthermore, based on the large amount of measured engineering data, the proposed model will have a broader application prospect and higher prediction accuracy because the model can be trained in advance. Therefore, in the context of big data, engineering companies can establish corresponding databases to train more data-driven models to achieve more intelligent construction, which is one of the future development directions.

CHAPTER 6

CONCLUSIONS AND FUTURE WORKS

6.1 Conclusions

The primary research of this dissertation is distributed in three chapters, of which two chapters (Chapters 3 and 4) analyze the pipeline stress during the operation. When the high-pressure natural gas pipeline crosses the river by HDD method, the stress of the pipeline is larger and more dangerous when it is just completed (filled with mud between the pipeline and the borehole). In addition, under the same conditions, compared with open-cut method, the stress of the pipeline installed by HDD method is lower. Through the influencing factor analysis and stress sensitivity analysis, it is concluded that the sensitivity order (from high to low) of five factors (diameter, thickness, pressure, drilling fluid density, buried depth) to pipeline stress is as follows: diameter, thickness, pressure, drilling fluid density, buried depth.

Another study in this dissertation (Chapter 5) is related to the prediction of pullback force during HDD construction. To the best of author's knowledge, this is the first time that the machine learning model is introduced into the pullback force prediction of HDD projects. Three new hybrid models are proposed to predict pullback force: CEEMDAN-RBFNN, CEEMDAN-WOA-SVM, and CEEMDAN-RF. These models have been verified in two projects across the Yangtze River in China. It implies that the

prediction accuracy has been greatly improved compared with the original analytical models (or empirical models).

6.2 Future Works

On the one hand, the research on pipeline stress analysis in this dissertation is carried out on the premise that the borehole has not been destroyed. However, in practical engineering, due to construction defects, changes in soil properties and other reasons, the borehole may collapse and so on. Therefore, in future work, for different crossing projects, more complex working conditions can be considered, which can provide more design and management basis for HDD projects. In addition, the mechanical behavior of pipelines during HDD construction is also worth studying, which involves complex contact issues.

On the other hand, it can be seen from the research of HDD pullback force prediction that large amounts of data will be generated in trenchless installation construction. Therefore, it is necessary to better manage the data in trenchless installation. In the context of big data, it is necessary to make better use of collected data to assist engineering.

APPENDIX A

PROGRAM FOR DRUCKER-PRAGER MODEL IN WORKBENCH

mat1=matid

!

et,mat1,45

!

TB,dp,mat1,,

tbmodif,1,1,29300

tbmodif,1,2,18.4

tbmodif,1,3,28.7

BIBLIOGRAPHY

- Adedapo, A. (2007). Pavement Deterioration and PE Pipe Behaviour Resulting from Open-cut and HDD Pipeline Installation Techniques. *Doctoral Dissertation*. Waterloo, Ontario, Canada: University of Waterloo.
- Alejano, L. R., & Bobet, A. (2012). Drucker–Prager Criterion. *Rock Mechanics & Rock Engineering*, 45(6), 995-999.
- Alzabeebee, S. (2019). Seismic response and design of buried concrete pipes subjected to soil loads. *Tunnelling and Underground Space Technology*, 93, 103084.
- American Society of Civil Engineers (ASCE). (2017). ASCE Manuals and Reports on Engineering Practice No. 108. Pipeline Design for Installation by Horizontal Directional Drilling. Second Edition 2017.
- American Society for Testing and Materials (ASTM). (2011). Standard guide for use of maxi-horizontal directional drilling for placement of polyethylene pipe or conduit under obstacles, including river crossings. ASTM F1962, West Conshohocken, PA.
- Bai, Y., & Wierzbicki, T. (2009). Application of extended Mohr–Coulomb criterion to ductile fracture. *International Journal of Fracture*, 161(1), 1–20.
- Banushi, G., & Weidlich, I. (2018). Seismic analysis of a district heating pipeline. *Energy Procedia*, 149, 216-225.
- Baumert, M. E., & Allouche, E. N. (2002). Methods for estimating pipe pullback loads for horizontal directional drilling (HDD) crossings. *Journal of infrastructure systems*, 8(1), 12-19.
- Bradley, K. (2016). Q&A With Gabe’s Construction: HDD and the Oil and Gas Pipeline Sector. *Trenchless Technology*. <https://trenchlesstechnology.com/trenchless-technology-hdd-q-and-a-gabes-construction/> (accessed 15 December 2019)
- Breiman, L. (2001). Random forests. *Machine learning*, 45(1), 5-32.
- British Petroleum (BP), 2019. BP Energy Outlook 2019 edition. <https://www.bp.com/content/dam/bp/business-sites/en/global/corporate/pdfs/energy-economics/energy-outlook/bp-energy-outlook-2019.pdf/> (accessed 15 April 2019).

- Cai, L., & Polak, M. A. (2019). A theoretical solution to predict pulling forces in horizontal directional drilling installations. *Tunnelling and Underground Space Technology*, 83, 313-323.
- Cai, L.X., He, L.M., Lv, Y.L., Wang, B.K., Yu, D.J. (2012). Prediction model of backtow loads in horizontal directional drilling installation. *Oil Gas Storage Transp*, 31(2), 147-151.
- Chen, X. (2015). *Engineering Fluid Mechanics*. Beijing: Petroleum Industry Press.
- China National Petroleum Corporation. (1997). GB/T 9711.1-1997 Petroleum and natural gas industries—Steel pipe for pipelines—Technical delivery conditions—Part 1: Pipes of requirements class A.
- Cousens, P., & Jandu, C. (2008). Stress Analysis of a Gas Pipeline Installed Using HDD and Auger Bore Techniques. *Proceedings of the 2008 7th International Pipeline Conference*. 2008 7th International Pipeline Conference, Volume 1. Calgary, Alberta, Canada. September 29–October 3, 2008. ASME.
- Dhanalakshmi, P., Palanivel, S., & Ramalingam, V. (2009). Classification of audio signals using SVM and RBFNN. *Expert Systems with Applications*, 36(3), 6069-6075.
- Díaz-Díaz, L. M., Omer, J., & Arias, D. (2018). Finite elements analysis of an underground collector installed by pipe-jacking method. *International Journal of Geotechnical Engineering*, 12(1), 66-75.
- Driscopipe, P. (1993). Technical expertise application of Driscopipe in directional drilling and river-crossings. *Technical Note*, 41.
- Eraslan, A. N. (2002). Inelastic deformations of rotating variable thickness solid disks by Tresca and von Mises criteria. *International Journal of Computational Engineering Science*, 3(01), 89-101.
- Fan, X., Dai, Z., Song, F., Liu, D. (2019). Simulation Analysis of Buried Pipeline under Multiple Wheel Loads of Vehicle. *Journal of Qingdao University (Engineering & Technology Edition)*, 34(2), 78-84.
- Francis, M., Kwong, J., Kalani, J., & Nakayama, D. (2004). Comparison of calculated and observed pipeline pullback forces during horizontal directional drilling. *NASTT No-Dig*, New Orleans, Louisiana.
- Goltabar, A. M., & Shekarchi, M. (2010). Investigation of traffic load on the buried pipeline by using of real scale experiment and Plaxis-3D software. *Research Journal of Applied Sciences, Engineering and Technology*, 2(2), 107-113.
- Halali, M. A., Azari, V., Arabloo, M., Mohammadi, A. H., & Bahadori, A. (2016). Application of a radial basis function neural network to estimate pressure gradient in water–oil pipelines. *Journal of the Taiwan Institute of Chemical Engineers*, 58, 189-202.

Huang, G., Wu, L., Ma, X., Zhang, W., Fan, J., Yu, X., Zeng, W., & Zhou, H. (2019). Evaluation of CatBoost method for prediction of reference evapotranspiration in humid regions. *Journal of Hydrology*, 574, 1029-1041.

Huey, D. P., Hair, J. D., & McLeod, K. B. (1996). Installation loading and stress analysis involved with pipelines installed by horizontal directional drilling (No. CONF-9603151-). North American Society for Trenchless Technology, Chicago, IL, United States.

Iseley, D. T., & Gokhale, S. B. (1997). Synthesis of highway practice 242: trenchless installation of conduits beneath roadways. Transportation Research Board, National Academy Press, Washington, DC.

Kershenbaum, N. Y., Mebarkia, S. A., & Choi, H. S. (2000). Behavior of marine pipelines under seismic faults. *Ocean Engineering*, 27(5), 473-487.

Lan, G., Zhao, X., Sun, A. (2012). Research on Influencing Factors on Mechanical Properties of Road Crossing Gas Pipeline. *Journal of Chengdu University (Natural Science Edition)*, 31(3), 290-294.

Lan, H., Ma, B., Zhang, Y., & Shu, B. (2014). Buried pipe affected by river erosion when crossing the Yangtze River. *Journal of Pipeline Systems Engineering and Practice*, 6(3), A4014002.

Li, J., Chu, F., Tang, D. (2014). Stress Analysis of River-crossing Pipeline in Seismic Belt. *Science Technology and Engineering*, 14(22), 17-22.

Liu, X., Zhang, H., Xia, M., Chen, Y., Wu, K., & Wang, B. (2018). Numerical Analysis and Strength Evaluation of an Exposed River Crossing Pipeline with Casing Under Flood Load. *Periodica Polytechnica Civil Engineering*, 62(4), 911-920.

Lu, H., Behbahani, S., Azimi, M., Matthews, J., Han, S., Iseley, T. (2020a). Trenchless Construction Technologies for Oil and Gas Pipelines: State-of-the-Art Review. *Journal of Construction Engineering and Management*, 146(6), 03120001.

Lu, H., Wu, X., Ni, H., Azimi, M., Yan, X., & Niu, Y. (2020b). Stress analysis of urban gas pipeline repaired by inserted hose lining method. *Composites Part B: Engineering*, 183, 107657.

Lu, H., Ma, X., Huang, K., & Azimi, M. (2020c). Carbon trading volume and price forecasting in China using multiple machine learning models. *Journal of Cleaner Production*, 249, 119386.

Lu, H., Ma, X., & Azimi, M. (2020d). US natural gas consumption prediction using an improved kernel-based nonlinear extension of the Arps decline model. *Energy*, 194, 116905.

Lu, H., Ma, X., Huang, K., & Azimi, M. (2020e). Prediction of offshore wind farm power using a novel two-stage model combining kernel-based nonlinear extension of the Arps

decline model with a multi-objective grey wolf optimizer. *Renewable and Sustainable Energy Reviews*, 127, 109856.

Lu, H., Matthews, J., & Iseley, T. (2020f). How does trenchless technology make pipeline construction greener? A comprehensive carbon footprint and energy consumption analysis. *Journal of Cleaner Production*, 261, 121215.

Lu, H., & Ma, X. (2020). Hybrid decision tree-based machine learning models for short-term water quality prediction. *Chemosphere*, 249, 126169.

Lu, H., Azimi, M., & Iseley, T. (2019). Short-term load forecasting of urban gas using a hybrid model based on improved fruit fly optimization algorithm and support vector machine. *Energy Reports*, 5, 666-677.

Luo, X., Lu, S., Shi, J., Li, X., & Zheng, J. (2015). Numerical simulation of strength failure of buried polyethylene pipe under foundation settlement. *Engineering Failure Analysis*, 48, 144-152.

Lyu, D. (2012). *Modal Analysis of Chevrolet 350 V8 Engine Crankshaft System*. Master Degree Thesis. Chengdu, Sichuan, China: Xihua University.

Matsuoka, H., & Nakai, T. (1985). Relationship among tresca, mises, mohr-coulomb and matsuoka-nakai failure criteria. *Soils and Foundations*, 25(4), 123-128.

Mirjalili, S., & Lewis, A. (2016). The whale optimization algorithm. *Advances in Engineering Software*, 95, 51-67.

Najafi M. (2010). *Trenchless Technology Piping: Installation and Inspection*. Columbus: McGraw-Hill Education.

Noor, M. A., & Dhar, A. S. (2003). Three-dimensional response of buried pipe under vehicle loads. *Pipeline Engineering and Construction International Conference 2003*, July 13-16, 2003, Baltimore, Maryland, United States.

O'Rourke, M. J., & Liu, X. (1999). Response of buried pipelines subject to earthquake effects. MCEER Technical Reports (public).

özgün. (2018). *Contact Types and Behaviours in Ansys*.
<http://www.mechead.com/contact-types-and-behaviours-in-ansys/> (accessed 15 December 2019)

Rabiei, M., Yi, Y., Bayat, A., & Cheng, R. (2016). General method for pullback force estimation for polyethylene pipes in horizontal directional drilling. *Journal of Pipeline Systems Engineering and Practice*, 7(3), 04016004.

Sinopec. (2010). *Research Report on Construction Technology of Sichuan-East Gas Pipeline Project*. (unpublished)

Song, J., Wang, J., & Lu, H. (2018). A novel combined model based on advanced optimization algorithm for short-term wind speed forecasting. *Applied Energy*, 215, 643-658.

Sun, C. (2006). Study on Applying the ANSYS Software to Service Pipe and Drainpipe Laying by Trenchless Technology. Master Degree Thesis. Chengdu, Sichuan, China: Southwest Jiaotong University.

Sun, H. (2017). Quantitative Research on Risk Acceptance of Gas Pipeline. Master Degree Thesis. Chengdu, Sichuan, China: Southwest Petroleum University.

Safari, N., Chung, C. Y., & Price, G. C. D. (2017). Novel multi-step short-term wind power prediction framework based on chaotic time series analysis and singular spectrum analysis. *IEEE Transactions on Power Systems*, 33(1), 590-601.

Tang, S., Li, Y. (2006). Analysis of a driven pile by ANSYS. *Rock and Soil Mechanics*, 27(6), 973-976.

Torres, M. E., Colominas, M. A., Schlotthauer, G., & Flandrin, P. (2011). A complete ensemble empirical mode decomposition with adaptive noise. *Proceedings of the IEEE International Conference on Acoustics, Speech, and Signal Processing, ICASSP 2011, May 22-27, 2011, Prague Congress Center, Prague, Czech Republic. IEEE.*

Toupin, R. A. (1965). Saint-Venant's principle. *Archive for Rational Mechanics and Analysis*, 18(2), 83-96.

Tsung, N., Zheng, M., Najafi, M., & Mehraban, S. (2016). A Comparative Study of Soil Pressure and Deformation of Pipes Installed by the Open-Cut Method and Trenchless Technology. *Pipelines 2016, July 17–20, 2016, Kansas City, Missouri, United States.*

Underground Construction. (2019). 21st Annual Horizontal Directional Drilling Survey. *Underground Construction Magazine*, 74(6).
<https://ucononline.com/magazine/2019/june-2019-vol74-no-6/features/uc-exclusive-21st-annual-horizontal-directional-drilling-survey>

United States Government Accountability (USGA) Office. (2014). Oil and gas transportation: department of transportation is taking actions to address rail safety, but additional actions are needed to improve pipeline safety. *Neuroscience & Behavioral Physiology*, 27(4), 347.

Vapnik, V. N. (2010). *The nature of statistical learning theory*. New York, NY: Springer.

Vazouras, P., Karamanos, S. A., & Dakoulas, P. (2010). Finite element analysis of buried steel pipelines under strike-slip fault displacements. *Soil Dynamics and Earthquake Engineering*, 30(11), 1361-1376.

Wang, Z. (2006). Study on Mechanical Behaviors of Buried Pipelines Under Traffic Loads. Doctoral Dissertation. Hangzhou, Zhengjiang, China: Zhejiang University.

Wang, Z., Zhao, Y., Yang, X. (2018). Analysis and application of the vector form intrinsic finite element based on the hexahedral grid. *Chinese Journal of Computational Mechanics*, 35(4), 480-486.

Wu, X., Lu, H., Huang, K., Wu, S., & Qiao, W. (2015). Frequency spectrum method-based stress analysis for oil pipelines in earthquake disaster areas. *PLoS One*, 10(2), e0115299.

Wu, X., Lu, H., Yu, X., & Shu, H. (2017). Stress analysis method for the large excavation of a river-crossing oil pipeline--A case study of Baiyang river oil pipeline. *Journal of Engineering Research*, 5(1), 105-123.

Wu, Z., & Huang, N. E. (2009). Ensemble empirical mode decomposition: a noise-assisted data analysis method. *Advances in Adaptive Data Analysis*, 1(1), 1-41.

Xu, G., Cai, L., Ji, R., & Wang, Z. (2018). Numerical simulation of pipe-soil interaction during pulling back phase in horizontal directional drilling installations. *Tunnelling and Underground Space Technology*, 76, 194-201.

Yan, X., Ariaratnam, S. T., Dong, S., & Zeng, C. (2018). Horizontal directional drilling: State-of-the-art review of theory and applications. *Tunnelling and Underground Space Technology*, 72, 162-173.

Yang, C. J., Zhu, W. D., Zhang, W. H., Zhu, X. H., & Ren, G. X. (2014). Determination of pipe pullback loads in horizontal directional drilling using an advanced computational dynamic model. *Journal of Engineering Mechanics*, 140(8), 04014060.

Yao, A., Xu, T., Zeng, X., & Jiang, H. (2013). Numerical analyses of the stress and limiting load for buried gas pipelines under excavation machine impact. *Journal of Pipeline Systems Engineering and Practice*, 6(3), A4014003.

Zayed, T., & Mahmoud, M. (2013). Data acquisition and factors impacting productivity of horizontal directional drilling (HDD). *Tunnelling and Underground Space Technology*, 33, 63-72.

Zhang, T., Shao, Y. (2007). Dynamic analyses of pipes in saturated soil under traffic loads. *Journal of Zhejiang University (Engineering Science)*, 41(1), 48-51.

Zhao, C. (2018). Research on deformation control of ground and excavation face for pipe-jacking. Master Degree Thesis. Zhengzhou, Henan, China: Zhengzhou University.

Zhao, J. Q., & Doherty, I. J. (2003, April). Behavior and performance of liner pipe in trenchless and trenched portions of sliplining rehabilitation. In *No-Dig 2003 Conference*, Las Vegas, NV.

Zheng, M., Tsung, N., Oh, I. E., Jiang, G., & Sun, P. (2016). A Preliminary Study of the Earth Pressure Exerted on Pipelines Installed By the Open-Cut Method and Trenchless Technology. *Electronic Journal of Geotechnical Engineering*, 21, 6451-6468.

Zhou, L., Xu, C., Yuan, Z., Lu, T. (2019). Dam Deformation Prediction Based on CEEMDAN-PSR-KELM Model. *Yellow River*, 41(6), 138-142.

Zhou, W., Ma, B., Zhang, H. (2015). Comparison of calculation models of soil pressure for trenchless pipe in the standards at home and abroad. *Water & Wastewater Engineering*, 41 (4), 98-103.

Zhu, Q. Z., Wu, C., Li, Q. Y., Zhang, X. Q., Zeng, L. B., Gao, S. B. (2017). Development status and trend of global oil and gas pipelines. *Oil & Gas Storage and Transportation*, 36(4), 375-380.

Zienkiewicz, O. C., Taylor, R. L., Nithiarasu, P., & Zhu, J. Z. (1977). *The finite element method* (Vol. 3). London: McGraw-hill.